INFORMATION TO USERS

This manuscript has been reproduced from the microfilm master. UMI films the text directly from the original or copy submitted. Thus, some thesis and dissertation copies are in typewriter face, while others may be from any type of computer printer.

The quality of this reproduction is dependent upon the quality of the copy submitted. Broken or indistinct print, colored or poor quality illustrations and photographs, print bleedthrough, substandard margins, and improper alignment can adversely affect reproduction.

In the unlikely event that the author did not send UMI a complete manuscript and there are missing pages, these will be noted. Also, if unauthorized copyright material had to be removed, a note will indicate the deletion.

Oversize materials (e.g., maps, drawings, charts) are reproduced by sectioning the original, beginning at the upper left-hand corner and continuing from left to right in equal sections with small overlaps.

Photographs included in the original manuscript have been reproduced xerographically in this copy. Higher quality 6" x 9" black and white photographic prints are available for any photographs or illustrations appearing in this copy for an additional charge. Contact UMI directly to order.

ProQuest Information and Learning
300 North Zeeb Road, Ann Arbor, MI 48106-1346 USA
800-521-0600

ANALYTICAL AND FINITE ELEMENT INVESTIGATION OF INITIAL CLEARANCE EFFECT ON TUBE-TO-TUBESHEET JOINT STRENGTH

BY

Ali Dhaif Al-Zayer

A Thesis Presented to the

DEANSHIP OF GRADUATE STUDIES

KING FAHD UNIVERSITY OF PETROLEUM & MINERALS

DHAHRAN, SAUDI ARABIA

In Partial Fulfillment of the
Requirements for the Degree of

MASTER OF SCIENCE

In

Mechanical Engineering

December 2001

(Ramadan 1422 H)

KING FAHD UNIVERSITY OF PETROLEUM & MINERALS
DHAHRAN, SAUDI ARABIA

DEANSHIP OF GRADUATE STUDIES

This thesis, written by

ALI DHAIF AL-ZAYER

under the direction of his thesis advisor and approved by his thesis committee, has been presented to and accepted by the Dean of Graduate Studies, in partial fulfillment of the requirements for the degree of

MASTER OF SCIENCE IN MECHANICAL ENGINEERING

Thesis Committee

Dr. Nesar Merah (Chairman)

Dr. Abdel Rahman N. Shuaib (Member)

Dr. Abul Fazal Arif (Member)

Dr. Abdulghani A. Al-Farayedhi
Chairman, Mechanical Engineering

Prof. Osama A. Jannadi
Dean, College of Graduate Studies

13/1/2002
Date

TO

MY WIFE

SONS

BROTHERS

AND

SISTERS

ACKNOWLEDGEMENTS

I am extremely grateful to Allah, who alone made this accomplishment possible.

Acknowledgement is due to King Fahd University of Petroleum and Minerals (KFUPM) for the support in carrying out this research.

I would like to express my deepest gratitude to my thesis advisor, Dr. Nesar Merah for his constant help and guidance during the course of this work. The experience that I got while working with him is going to influence my future life. Thanks are due to members of my thesis committee, Dr. Abdel Rahman N. Shuaib and Dr. Abul Fazal Arif for their cooperation and valuable suggestions.

I would like to thank Dr. Al-Farayedhi, Chainman ME, faculty members and graduate students of the department.

Finally, I am grateful to my family for their extreme moral support, encouragement and patience during the course of my studies. Thanks also to all my friends who had a role in making this work possible.

TABLE OF CONTENTS

LIST OF FIGURES

LIST OF TABLES

NOMENCLATURE

c	:	Initial radial clearance
E_s	:	Tubesheet modulus of elasticity
E_t	:	Tube modulus of elasticity
E_{tt}	:	Tube tangent modulus
f	:	Coefficient of friction
F	:	Pull out force
L	:	Original tube length
L'	:	Final tube length
L_e	:	Expanding length
p	:	Pitch
P_{con}	:	Residual contact pressure
P_e	:	Expanding pressure
P_{emax}	:	Maximum limiting pressure
P_{e-p}	:	Elastic-plastic interface pressure
r_{e-p}	:	Elastic-plastic interfacial radius
r_i	:	Tube inner radius
$r_{i,f}$	:	Final tube inner radius
r_o	:	Tube outer radius
SI_{max}	:	Maximum stress intensity
U_{ri}	:	Tube's inner surface radial deformation
U_{ro}	:	Tube's outer surface radial deformation
R_i	:	Equivalent sleeve inner radius
R_o	:	Equivalent sleeve outer radius

t	:	Original tube wall thickness
t'	:	Final tube wall thickness
TT	:	Tube thinning
w	:	Groove's width
WR	:	Wall reduction
z	:	Reduction factor
σ_r	:	Radial stress
σ_y	:	Yield stress
σ_{ys}	:	Tubesheet yield stress
σ_{yt}	:	Tube yield stress
ρ	:	Yield stresses ratio
ρ_L	:	Limiting yield stresses ratio
υ	:	Poisson's ratio
η	:	Ligament efficiency

ABSTRACT

Name:	Ali Dhaif Al-Zayer
Thesis Title:	Analytical and Finite Element Investigation of Initial Clearance Effect on Tube-to-Tubesheet Joint Strength
Major Field:	Mechanical Engineering
Date of Degree:	December 2001

The tube-to-tubesheet joints in the shell-tube heat exchangers are usually made by expanding the tube into the tubesheet. Tube rolling is the most popular form of expansion. However, uniform pressure expansion has been often assumed in the studies of the joint strength. The joint strength is influenced by many factors such as the method of attachment, material properties, geometry and dimensions. To simplify the analysis, researchers have assumed zero initial radial clearance and elastic-perfectly-plastic material in the study of the joint strength.

In this thesis, finite element analysis is conducted on axisymmetric, plane stress and plane strain models to investigate the effect of initial radial clearance and tube strain hardening on the residual contact pressure between the tube and tubesheet hole after expanding the tube by applying uniform pressure. Results show that the radial clearance has a negative effect on the joint strength. The effect becomes more significant with increasing the level of tube strain hardening. A practical equation to calculate the reduction factor due to the initial radial clearance and tube strain hardening, which could be used with the closed-form solution of the residual contact pressure available in the literature, is proposed. Other equations for calculating the tube's inner and outer surfaces radial deformation, which are used to calculate the tube wall reduction and tube thinning, are also proposed. The results obtained from the finite element analysis are compared with the experimentally measured results, which were conducted on roller-expanded tubes into a nine-holes square block. Because of the low level of tube strain hardening, experimental results show that the joint strength seems to be unaffected by the initial radial clearance.

Master of Science Degree

King Fahd University of Petroleum and Minerals

Dhahran, Saudi Arabia

December 2001

الـخـــلاصـــــة

الاســـــــــــم: عـلـــــــي ضـيـــــف الـــزايـــــــر

عنوان الرسالة: دراسة تأثير الخلوص القطري الأولي على قوة وصلات الأنابيب بالصفائح عبر التحليل وباستخدام أسلوب العنصر المحدود

التـــخـــصـص: هـنـدســـة ميـكـانـيـكـيـــة

تـاريـخ الشـهـادة: رمضـــــــان ١٤٢٢ هـ

تثبت غالبا وصلات الأنابيب بالصفائح في المبدلات الحرارية بواسطة التوسيع، وتجري معظم عمليات التوسيع بواسطة الدلفنة. ولكن افترض الباحثون الضغط المنتظم بدلا من الدلفنة لدراسة قوة الوصلات، كما افترضوا أيضا عدم وجود أي خلوص قطري أولي ومواد مثالية اللدونة لتبسيط التحليل حيث أن قوة الوصلات تتأثر بعوامل كثيرة مثل طريقة الوصل، خواص المواد، الشكل والمقاس.

في هذا البحث، تم تطبيق تحليل العنصر المحدود على ثلاثة نماذج: متماثل محوري، إجهاد مستوي وانفعال مستوي لدراسة تأثير الخلوص القطري الأولي و مستوى التقسية الانفعالي على الضغط التلامسي المتخلف بين الأنابيب وثقوب الصفائح بعد توسيع الأنابيب بواسطة الضغط المنتظم. أظهرت النتائج أن الخلوص القطري يؤثر سلبا في قوة الوصلات وأن هذا التأثير يزداد مع زيادة مستوى التقسية الانفعالي للأنابيب. تم اقتراح معادلة عملية لحساب عامل الخفض بسبب الخلوص القطري الأولي و مستوى التقسية الانفعالي للأنابيب والتي يمكن استخدامها مع المعادلات المطروحة في الدراسات المنشورة لحساب الضغط التلامسي المتخلف. تم أيضا اقتراح معادلات أخرى لحساب الإزاحة القطرية لأسطح الأنابيب الداخلية والخارجية والتي يمكن من خلالهما حساب مستوى الخفض في جدار الأنابيب ومستوى ترقيق الأنابيب. بالإضافة إلى ذلك، تم مقارنة نتائج تحليل العنصر المحدود مع نتائج التجربة التي أجريت على أنابيب تم توسيعها في صفائح مربعة تحوي تسعة ثقوب بواسطة الدلفنة والتي أظهرت أن قوة الوصلات لم تتأثر بمقدار الخلوص القطري الأولي بسبب انخفاض مستوى التقسية الانفعالي للأنابيب.

درجة الماجستير في العلوم

جامعة الملك فهد للبترول والمعادن

الظهران، المملكة العربية السعودية

رمضان ١٤٢٢ هـ

CHAPTER 1

INTRODUCTION

1.1 INTRODUCTION

The tube-to-tubesheet joint is a very critical element of the shell-tube heat exchangers. It separates the two fluids and thus its strength level has a direct effect on the safety of the process plant. This joint is made by either expansion, welding or a combination. However, tube expansion is mostly used in the industry, since Tubular Exchanger Manufacturer Association (TEMA) standard [1] call for tube expansion joints. Tube expansion is done by rolling, uniform (hydraulic) pressure, bladder, rubber, explosive or hybrid expansion. Among all these kinds of expansion, rolling is the most common kind since it is the easiest and cheapest. In the expansion process, the tube deforms plastically and the tubesheet deforms elastically after which tubesheet reverse deformation is more than that of the tube and causes permanent contact.

To get a strong tube-tubesheet joint, certain limitations specified by TEMA have to be applied. Among these limitations is the maximum allowable initial radial clearance between the tube and tubesheet, which is specified in terms of over tolerance. Table RCB-7.41 in the TEMA standards [1] lists this limitation for each tube size. Tube expansion into tubesheet holes having more than the allowable radial clearance (over tolerance) may stretch the tubes beyond their strain limit or may cause tube wall reduction to be more than a pre-specified acceptable limit. According to Yokell [2], roller-expanded joints are generally rejected when tube wall reductions approach 12%, since resultant joint would be weak and may fail under working pressure.

The tube-to-tubesheet joint strength is measured by the residual contact pressure between the tube's outer surface and tubesheet's hole surface or by the pull or push out force needed to draw the tube apart from the tubesheet. Both measures are directly related, as will be seen later. Several studies to estimate this joint strength and how it is affected by changing different parameters involved are already published. However, the effect of initial radial clearance on the joint strength was not thoroughly addressed.

The objective of this thesis is to study the effect of initial radial clearance and material strain hardening on the strength of the expanded tube-to-tubesheet joint by using finite element method (FEM). The study involves numerical estimation of the residual contact pressure through the use of a general finite element code (ANSYS) [3]. It also involves analytical calculation of the residual contact pressure through the use of already developed equations. This study will use the same model geometry and base line data

presented in the experimental work conducted by Shuaib et al [4]. In this experimental work, test blocks of nine holes representing the tubesheet design of the Stabilizer Feed/Bottom Exchanger were manufactured. To establish a range of initial radial clearances, each test block has its own set of hole sizes which are different from the other test blocks. To include the ligament effect, tubes were then roller-expanded into the nine-hole block. The pull out force was measured on the center hole only. The residual contact pressure will be calculated from the experimentally measured pull out force by using the correlation published in the literature. This pressure will then be compared with the results of the analytical and numerical analyses.

1.2 PROBLEM DEFINITION

The Tubular Exchanger Manufacturer Association (TEMA) standard [1] specifies the maximum limit of the initial radial clearance between the tube and tubesheet for each tube size, above which tube-tubesheet assembly is rejected when more than 4% of the total holes exceed this limit. During maintenance, tubes may need to be removed and then a new set of tubes is expanded into the same tubesheet. Frequent processes of removing old tubes and expanding new tubes during the life of the heat exchanger enlarge the hole of the tubesheet. This may result in hole sizes beyond those of the TEMA limit. When new tubes are roller expanded in enlarged holes, tubes wall reduction may exceed 12%, which is the maximum allowable limit above which the joints are generally rejected [2]. This results in a low residual contact pressure, which leads to a weak tube-tubesheet joint. In general, a strong joint is one that is formed by applying an optimum expanding force,

which creates a maximum residual contact pressure between the tube and the hole after its release.

1.3 OBJECTIVES

The main goal of this research is to study the effect of initial radial clearance between tube and tubesheet hole on the residual contact pressure. The specific objectives are:

1. Use the existing analytical and numerical solutions to estimate the residual contact pressure.

2. Develop a finite element model that will incorporate the variation of initial radial clearance and strain hardening of tube material.

3. Estimate the residual contact pressure using commercial computer software (ANSYS); the effect of initial radial clearance on the contact pressure will be determined.

4. Compare the analytically estimated residual contact pressure and that obtained from the finite element analysis with the experimental results.

1.4 APPROACH TO THE PROBLEM

The stated objectives will be achieved by analyzing the tube-to-tubesheet joint strength using existing analytical solutions described in Chapter 2. In addition, finite element analysis will also be conducted by using a commercial code (ANSYS). More attention

will be paid to the later method. Comparison between the results obtained from the finite element analysis and those measured in the experimental program will then be presented. Attempts will be made to evaluate the relative merits and shortcomings of each approach.

1.4.1 Analytical Approach

The analytical investigation will be conducted using the approaches outlined in the open literature. Equations for calculating the equivalent sleeve radius, residual contact pressure, pull out force and the reduction factor caused by initial radial clearance developed by different researchers and discussed in Chapter 2 will be used in the analysis. The effect of the sleeve radius and the initial radial clearance were ignored in the proposed closed-form equations for calculating the residual contact pressure and thus the pull out force. However, a modified approach for calculating the residual contact pressure, in which the effect of the sleeve radius is accounted for, will be presented. So, an equivalent sleeve radius that will produce the same end results as the real tubesheet would have to be calculated first. Different approaches for calculating the equivalent sleeve are outlined in the literature. Among those, the closest approach to the objective of this study will be selected. Finally, the reduction on the residual contact pressure due to the initial radial clearance will be investigated.

1.4.2 Finite Element Approach

Finite element analysis will involve the evaluation of the residual contact pressure between the tube and tubesheet and how it changes with the initial radial clearance and tube's material properties. For this purpose, axisymmetric, plane stress and plane

strain models are generated and analyzed. In addition, tube's inner and outer surfaces radial deformations will be reported. Using these results, the effect of initial radial clearance and tube's material properties on the tube wall reduction will be analyzed. Furthermore, clearance effect on the tube retraction obtained from the axisymmetric model will be investigated. Finite element method computer code (ANSYS) [3] will be used in this approach.

1.4.3 Experimental Approach

The earlier experimental investigation [4] dealt mainly with the pull out force and percentage wall reduction measurements. The results obtained from the experimental work will be compared with those obtained from the finite element analyses. To do so, the experimentally measured pull out force and final tube inner radius are used to calculate the residual contact pressure and tube wall reduction, respectively. The equations published in the open literature will be utilized for these calculations.

1.5 THESIS LAYOUT

The thesis has been divided into six chapters. The first chapter describes the objectives of the study and the approaches to attain these objectives. The second chapter will present the relevant research work in the area. The third will describe the model used in the study. The fourth chapter will illustrate the results obtained from the analytical solution, finite element analysis and the experimental work. The fifth chapter will present an analysis of the effect of the initial radial clearance and tube strain hardening level on the expanded

tube-to-tubesheet joint strength. The last chapter presents the conclusions and recommendations of this research work.

CHAPTER 2

LITERATURE REVIEW

2.1 INTRODUCTION

Tube-to-tubesheet joints in the tubular heat exchangers are made by expanding the tube into the tubesheet's hole or by welding them together. Some manufacturers combine these two methods to create the joint. That is, they expand the tube into the tubesheet first and then seal-weld the tube to the front face of the tubesheet. However, in the industry, the tube-to-tubesheet joints are built by tube expansion only in the majority of tubular exchanger, since Tubular Exchanger Manufacturer Association (TEMA) standard [1] calls for tube expansion joints. Tube expansion is performed by rolling, uniform (hydraulic) pressure, bladder, rubber, explosive or hybrid expansion. Rolling is the most practical and commonly used method to create the joints. However, rolling is more difficult to simulate

and analyze when compared to the uniform pressure expansion. That is why most of the researchers had assumed uniform pressure in their studies.

This literature review will present a description of the uniform pressure, roller and hybrid expansions. It will then summarize the studies performed on the tube-to-tubesheet joint strength in three distinct parts: analytical, numerical or finite element and experimental. The study of the effect of initial radial clearance will be treated in a separate section. In addition, the effect of grooves and surface finish of holes on the joint strength will be included in the subsequent sections.

2.2 UNIFORM PRESSURE EXPANSION

Most of the published articles on the theoretical and numerical analyses of tube-to-tubesheet joint strength consider uniform (hydraulic) expansion. Less attention was paid to other types of joint (roller expansion, welding, and any combination). Uniform pressure expansion is performed by applying hydraulic pressure directly over a certain length contained within the tubesheet. As pressure is applied inside the tube, the tube deforms elastically. Increasing the pressure increases the deformation until the tube makes contact with the tubesheet's hole. At contact, the deformation may be fully elastic, fully plastic or elastic-plastic interface may exist on the tube depending on its material, size and initial radial clearance. At contact, a thick walled, high-yield stress tube may be full elastic, while a thin walled, low-yield stress may be fully plastic. Increasing the applied pressure more will then elastically deform the tubesheet. To finish the expansion process, the

pressure is released to zero that causes both the tube and tubesheet to spring back. To create residual contact pressure between the tube and tubesheet: 1- tube deformation must be fully plastic; 2- tubesheet must deflect; 3- tubesheet recovery must be greater than tube recovery.

The applied pressure should not exceed the plastic limit of the tube (limiting stress), which is $(2/\sqrt{3})\sigma_{yt}$, referred to as P_{max}. This is simply because the tube metal will extrude if a pressure grater than P_{max} is applied. At this pressure, the elastic-plastic interface zone is at a radius (r_{e-p}) equal to $1.75r_i$ [2]. So, when the ratio of the tube's outer radius to its inner radius (r_o/r_i) is less than 1.75, the tube material will be fully plastic when P_{max} is applied. Otherwise, elastic-plastic interface will exist in the tube.

2.3 ROLLER EXPANSION

The subject of rolling has received less attention in the published technical papers compared with the uniform expansion. Nevertheless, roller expansion is the most popular form of expansion. Roller expanded joints are generally stronger than hydraulically expanded joints [5]. On the other hand, Roller expansion causes a higher tube wall reduction than hydraulic expansion [2]. In the roller expansion process, rolls apply pressure far greater than the plastic limit on an infinitesimally small contact surface that creates depression in the inner shells and pushes a wave of metal ahead and cause tube-end extrusion. The tube-end shortening is overcome by this extrusion. If the tubes are not fixed before rolling, rolls may twist the tubes creating torsion along the length. Rolling

should be done in steps if the tube length to be expanded is more than 2 in. In this case, all the steps must overlap, otherwise, there will be a serious transition between the rolled and unrolled lengths, which creates another region that can fail [2].

Uniform wall reduction is achieved by controlling the rolling torque. There are no correlations between the wall reduction and the residual contact pressure or the pull out force established yet. Residual contact pressure is not measurable and wall reduction is difficult to measure. Consequently, direct correlation between joint strength and rolling torque would be more feasible [2].

2.4 HYBRID EXPANSION

Uniform expansion increases the tube outside diameter and decreases the length. The decrease in length develops tensile stress in tubes. To minimize the tensile stress in the tubes caused by the shortening of its length, the tube could be rolled after the uniform expansion to set its length back to original. Rolling in this case is done at about half the usual torque [6]. The tube length after uniform expansion (L') can be expressed as:

$$L' = L\frac{(2r_o - t)t}{(2r_o - t')t'} \tag{2-1}$$

where, L = Original tube length

t = Original tube wall thickness

t' = Tube wall thickness after expansion

In their experiment, Jawad et al [7] found that, after performing uniform expansion, rolling the tube to 3% wall reduction will set the tube back to its original length. They found that the pull out force for the case of uniformly expanded tube and then 3% roller expanded is higher than that for the case of uniformly expanded only. In fact, it is even higher than the theoretical pull out force. This is due to the fact that roller expansion increases the pre-compression pressure between the tubes and tubesheet. Also, roller expansion substantially fills the grooves on the tubesheet hole surface with extruded material from the tubes.

2.5 TUBE-TO-TUBESHEET JOINT STRENGTH

The tube-to-tubesheet joint strength is measured in terms of the residual contact pressure between the tube's outer surface and the tubesheet hole's surface or the force required to pull or push the tube out of the tubesheet. Both of which are linearly related. The residual contact pressure, and thus the pull out force, is directly proportional to the expansion pressure and the contact surface area. The joint strength is also influenced by initial clearance, material strain hardening, static coefficient of friction, Poisson's constant, grooving, seal-weld, surface finish, etc.

Many researchers studied how these different parameters affect the strength of the tube-to-tubesheet joint strength. Each one had looked at it from a different angle. The studies performed can be categorized into three sections: analytical, finite element and experimental approaches.

2.5.1 Analytical Approach

Yokell [2] had performed analytical analysis on the tube-to-tubesheet joint strength. He assumed that the tube is uniformly expanded into an infinitely large tubesheet and the axial stress is zero. With respect to the relative values of the tube and tubesheet yield strength, he analyzed the three possible cases, namely: yield stresses of tube and tubesheet are the same, yield stress of tubesheet is greater or yield stress of tube is greater. He was able to find the appropriate expanding pressure for different ratios of tube outside to inside radius. The optimum contact pressure when P_{emax} was applied was found to occur when $r_o/r_i = 1.45$.

For single hole models, the greatest residual contact pressure is achieved by applying a pressure equal to the plastic limit of the tube (P_{emax}). However, if the elastic-plastic interfacial radius (r_{e-p}) lies beyond tangency with adjacent holes, they may be plastically deformed out of round, and may loosen the tube. So, it is advisable to apply pressure at which the elastic-plastic interfacial radius will just be tangent to the adjacent holes.

For the usual drilling pitch of 1¼ tube diameters ($p = 2.5r_o$), as per Yokell [2], the expanding pressure (P_e) that will produce the elastic-plastic interfacial radius to be just tangent to the adjacent holes for the case of equal tube and tubesheet yield stresses ($\sigma_{yt} = \sigma_{ys} = \sigma_y$), could be approximated by

$$P_e = \sigma_y(1.945 - 1.384 r_i / r_o) \qquad (2\text{-}2)$$

For this case, Yokell [2] used a closed-form solution proposed earlier by Kasraie et al [8] for calculating the residual contact pressure (P_{con}) directly:

$$P_{con} = P_e\left[1-\left(\frac{r_i}{r_o}\right)^2\right]-\frac{2}{\sqrt{3}}\sigma_y\left[\ln\left(\frac{r_o}{r_i}\right)\right] \tag{2-3}$$

For the case of tubesheet yield stress (σ_{ys}) higher than tube yield stress (σ_{yt}), the elastic-plastic interface radius ($r_{e\text{-}p}$) moves inward. When $\sigma_{ys} = 2\sigma_{yt}$, tubesheet will always remain fully elastic. Here, for $r_{e\text{-}p}$ to be just tangent to next holes, P_e is given by:

$$P_e = \sigma_{yt}\frac{1+r_o\rho}{t+r_o}(1.945-1.384\frac{r_i}{r_o}) \tag{2-4}$$

where $\rho = \sigma_{ys}/\sigma_{yt}$

In the last possible case, that is for tubesheet yield stress lower than tube yield stress, P_e is limited to a value such that the pressure on the hole equals to the plastic limit of the tubesheet.

$$P_e = \sigma_{yt}(1.945-1.384r_i/r_o)\rho/\rho_L \tag{2-5}$$

where ρ_L is the limiting ratio when $P_e = P_{emax} = (2/\sqrt{3})\sigma_{yt}$ produces the plastic limit on the tubesheet.

Jawad et al [7] had analyzed the behavior of the tubes during uniform expansion based on four steps. First, tube behavior up to yield stress, where the tube follows the

stress-strain relationship given by the theory of elasticity. Then, they looked at the deformation of tube until contact with tubesheet. In this step, the tube is plastically deformed. Third, partial yielding of tubesheet in which elastic and plastic regions are developed in the tubesheet. Stresses in the elastic and plastic regions were calculated using the theory of plasticity. Last step is the reduction of pressure to zero in which the elastic theory can be applied again to find the stresses.

It is important to note that thin walled, high strength tubes may remain fully elastic up to and beyond the point of contact with the tubesheet hole. This may happen when the modulus of elasticity of the tube is significantly smaller than that of the tubesheet and the yield stress of the tube is significantly higher than that of the tubesheet. Also, tubesheets with yield stress significantly higher than the tubes may remain fully elastic.

To find the force (F) required to pull the tube out of the tubesheet, Goodier and Schoessow [9] treated the tube-tubesheet assembly as a tube in a thick sleeve with its outside radius at the elastic-plastic interface and came up with the following equation:

$$F = P_{con}\frac{2\pi r_o}{\gamma}\left(L_e - e^{-\gamma L_e}\right) \qquad (2\text{-}6)$$

where $\gamma = \upsilon\dfrac{r_{e-p}^2 - r_i^2}{r_o\left(r_{e-p}^2 - r_o^2\right)}$

L_e = Expanded length of tube

f = Coefficient of friction

υ = Poisson ratio.

As stated by Yokell [2], the coefficient of friction (f) is usually assumed to range from 0.3 to 0.7, with the average value of 0.5 used for most estimates. But, it actually may be as big as 1.0. With this regard, he proposed a simplified equation for the pull out force in which he neglected the Poisson effect and considered unity for the coefficient of friction:

$$F = 2\pi d P_{con} r_o L_e \tag{2-7}$$

However, Jawad et al [7] stated that the coefficient of friction for steel to steel is about 0.74, and they used this value in their proposed equation for the pull out force:

$$F = 2\pi f P_{con} r_o L_e \tag{2-8}$$

The coefficient of friction is directly related to the pull out force and its value will greatly influence the result. Since it is very difficult to determine the coefficient of friction, a precise answer of the pull out force can not be attained.

2.5.2 Finite Element Approach

A number of researches [5, 10-15] have investigated the tube-to-tubesheet joints with special emphasis on the residual contact pressure by using the finite element method. The axisymmetric or plane stress finite element models have been often considered to simulate the nonlinear behavior of the tube-to-tubesheet joint expansion. Various nonlinearities are generated from three particular sources:

1- Material non-linearity as a result of the elastic-plastic behavior of the tube and tubesheet materials.

2- Boundary condition non-linearity due to the contact interaction between the tube outer surface and the hole inner bore.

3- Geometrical non-linearity due to the large strain occurring during the expansion process.

2.5.2.1 Finite Element Models

In their paper, Allam et al [11] studied the influence of several parameters by the use of axisymmetric finite element model. Figure 2-1 shows the equivalent single-tube axisymmetric model they used in their study. The elements used in this model are 2-D axisymmetric 8-node quadrilateral isoparametric elements. 2-D interference axisymmetric elements were also used to simulate the initial clearance between the tube and the tubesheet as well as the contact state, when it occurs. In order to provide stability to the numerical solution, the front ends of the tube and the tubesheet at the tubesheet primary side are restrained in the axial direction. A uniform internal pressure is applied over the portion of the tube that lies within the tubesheet, as shown in Figure 2-1, and as specified by TEMA [1]. The pressure is applied incrementally up to its maximum value and then fully released.

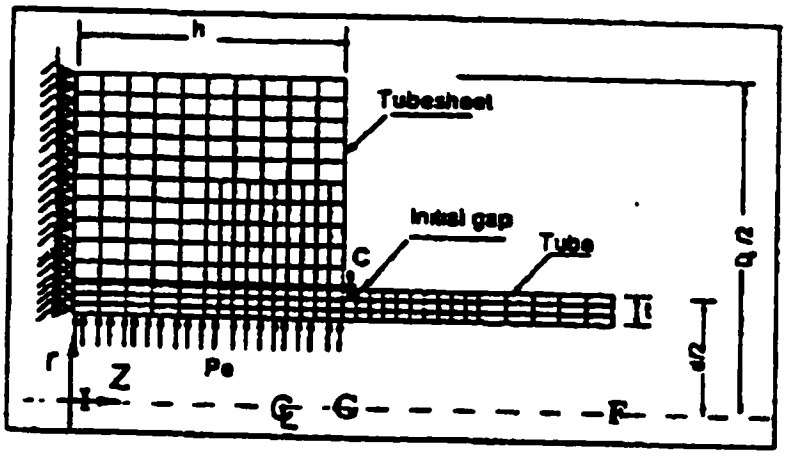

Fig. 2-1: Equivalent Single-Tube Axisymmetric Model

Allam et al [11] used the ABAQUS finite element code [16] with the appropriate types of elements together with suitable options. The incremental load technique is available in this code, which provided an acceptable tool for solving the problem. Other softwares were used by different researchers. MARC general-purpose finite element code was used by Scott et al [5] and Thiel et al [17] used SYSTUS computer code [18] for analyzing their axisymmetric model.

Kohlpaintner [12] used a different model for his finite element analysis to determine the effective tubesheet zone from which the equivalent sleeve diameter is derived, which was necessary in his computation of the residual contact pressure. The effective tubesheet zone is the extent of the tubesheet area that must be considered to get results very close to the full tubesheet. In a tubesheet design having each hole be surrounded by six other holes, he found that the effective tubesheet zone must contain 19 holes (centered hole surrounded by two

circular layers of holes). A 7 holes tubesheet (centered hole surrounded by one circular layers of holes) will not give accurate results, while 37 holes tubesheet (centered hole surrounded by three circular layers of holes) will give very close results to those given by the 19 holes tubesheet. Because of symmetry, only tubesheets with triangular hole patterns were considered. Therefore, only a sector of 30 deg was modeled with finite elements. Figure 2-2 shows the structural model of a tubesheet with 37 holes. The outer diameter was taken to be four times the pitch.

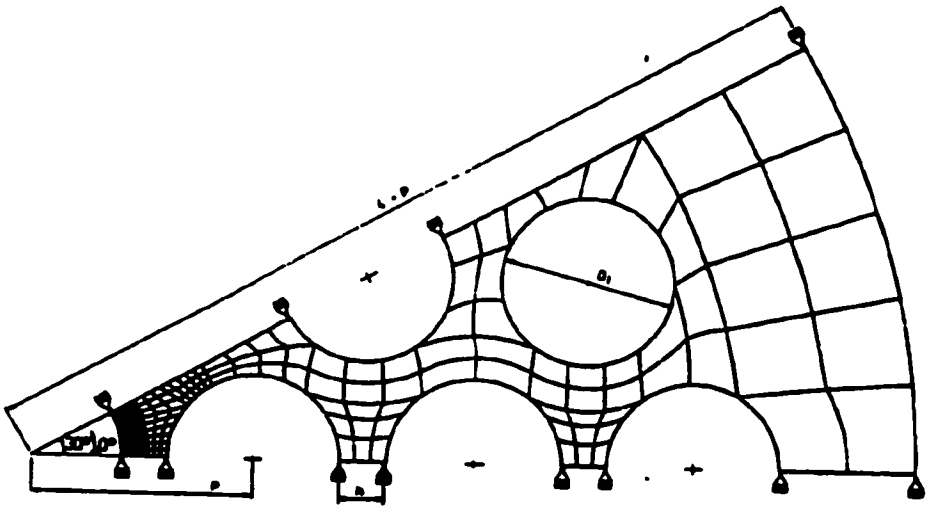

Fig. 2-2: 30 Deg. Sector of a Tubesheet With 37 Holes Model

To evaluate the equivalent sleeve diameter, Kohlpaintner equated the average radial deformation of the centered hole boundary in the effective tubesheet zone to the radial displacement at the inner radius of a single hole sleeve when the

same pressure is applied into both cases. His analysis resulted in the following equation:

$$\frac{2R_o}{p} = 12.55009\eta^5 - 16.21818\eta^4 + 10.88288\eta^3 - 2.43388\eta^2 + 1.94683\eta + 0.98034 \quad (2\text{-}9)$$

where R_o = Equivalent sleeve outer radius

P = Pitch

η (ligament efficiency) is defined as:

$$\eta = \frac{p - 2R_i}{p}$$

where R_i = Equivalent sleeve inner radius

Chaaban et al [13] used a different approach to find the equivalent sleeve diameter. Instead of equating the radial deformation, they equated the residual contact pressure around the centered hole as a result of any applied pressure to that of the equivalent sleeve under the application of the same pressure. To do so, they used the two models similar to those described above. First, they used plane stress seven-tube model to find the average residual contact pressure at the outer surface of the central tube. Then, they used the axisymmetric single-tube model to find the equivalent sleeve diameter by adjusting the outer diameter of the sleeve until the residual contact pressure comes out to be equal to that found in the first step. They performed the analysis for two cases: simultaneous and sequential expansions. In the simultaneous expansion, the pressure is applied in

all the seven tubes and then released at the same time. On the other hand, sequential expansion is done by applying a pressure in one tube only and then released. It is then repeated for the other holes one by one. They proposed the following equation to calculate the equivalent sleeve radius (R_o) that can be used for the two cases:

$$\frac{R_o}{r_o} = e^{a0}\left(\frac{t}{2r_o}\right)^{a1}\left(\frac{p}{2r_o}\right)^{a2}\left(\frac{P_e}{\sigma_{yt}}\right)^{a3}\left(\frac{E_t}{\sigma_{yt}}\right)^{a4}\left(\frac{E_s}{E_t}\right)^{a5}\left(\frac{\sigma_{ys}}{\sigma_{yt}}\right)^{a6} \qquad (2\text{-}10)$$

where the constants a0, a1, a2, a3, a4, a5 and a6 are as follows:

	a0	a1	a2	a3	a4	a5	a6
Sequential Case	-1.3538	0.0140	1.3147	0.3404	0.3244	-0.2457	-0.2885
Simultaneous Case	-1.6277	-0.1909	1.0552	0.2153	0.2307	-0.0214	-0.1607

Reinhardt et al [15] reported that this is the best approach if the intent of the study is to find the stress distribution in the expanded tube. However, if the optimum expansion pressure was to be determined, a slightly different approach is more advantageous. For this purpose, their approach for finding the equivalent sleeve diameter was based on the definition of the maximum stress intensity (SI_{max}), which is:

$$SI_{max} = 2P_e \frac{R_o^2}{R_o^2 - R_i^2} \qquad (2\text{-}11)$$

They carried out a plane strain analysis on a section of tubesheet having a center hole surrounded by a full set of holes to find the maximum stress intensity around the circumference of the center hole when an arbitrary pressure is applied. Having known SI_{max} and P_e with a pre-specified equivalent sleeve inner radius (R_i), the equivalent sleeve outer radius (R_o) is calculated from the above equation.

2.5.2.2 Finite Element Analysis

Allam et al [11] used the 2-D axisymmetric finite element model to study the effect of seven different parameters on the residual stresses in the contact zone. They applied three levels for each parameter, namely: lower, intermediate (reference) and upper values of the parameters, which cover many tube-to-tubesheet joints practical applications. The residual stress profiles on the tube inner and outer surfaces as well as the residual contact pressure were computed as a function of the hydraulic expansion pressure for the different parameter combination. Their attention was focused on how the residual contact pressure varies with each parameter. It must be mentioned here that the residual contact pressure was taken as the average value over the entire surface of contact between the tube and tubesheet.

They found that the effects of tubesheet yield strength and strain hardening are relevant only if the tubesheet is plastically deformed during the expansion process. For the cases of no high plastic deformation in the tubesheet, the residual contact pressure becomes independent of those parameters. However, the tubesheet modulus of elasticity (E_s) to tube modulus of elasticity (E_t) ratio and tube strain hardening have a direct effect on the residual contact pressure.

Allam et al [11] also found that the effect of the tube wall thickness on the residual contact pressure is not significantly noticeable. However, the residual contact pressure seems to increase almost linearly with increasing expansion pressure. The residual contact pressure is significantly affected at lower values of the sleeve diameter. For higher values of sleeve diameter, the sleeve behaves as an infinite plate for which the external diameter has no effect on the joint characteristics. In addition, the level of the residual contact pressure was found to be affected by the initial radial clearance. For strain hardening tube material, the residual pressure decreases as the clearance increases.

Chaaban et al [13] proposed an empirical equation for calculating the residual contact pressure based on finite element analysis of the axisymmetric model shown in Figure 2-1. Just like their work on the equivalent sleeve diameter described above, they calculated the residual contact pressure for the two cases: simultaneous and sequential expansions. They proposed the following equation,

which has the same general form as equation (2-10), to calculate the residual contact pressure (P_{con}) that is applicable for the two cases:

$$\frac{P_{con}}{\sigma_{yt}} = e^{a0}\left(\frac{t}{2r_o}\right)^{a1}\left(\frac{p}{2r_o}\right)^{a2}\left(\frac{P_o}{\sigma_{yt}}\right)^{a3}\left(\frac{E_t}{\sigma_{yt}}\right)^{a4}\left(\frac{E_s}{E_t}\right)^{a5}\left(\frac{\sigma_{ys}}{\sigma_{yt}}\right)^{a6} \qquad (2\text{-}12)$$

where the constants a0, a1, a2, a3, a4, a5 and a6 are as follows:

	a0	a1	a2	a3	a4	a5	a6
Sequential Case	2.7290	-0.1804	-0.6592	6.7358	-0.6752	-3.4445	0.8230
Simultaneous Case	2.9596	-0.0982	-0.8182	6.0719	-0.6357	-3.1539	0.6639

Reinhardt et al [15] studied the stresses and strains on the surface of the expanded tubes using an axisymmetric model with the ANSYS finite element software [3]. They used node-to-surface contact element between the tube outside surface and the sleeve inside surface with a friction coefficient of 0.13 at the contact surface. The nodes at the free end of the tube were coupled in longitudinal direction. A multi-linear kinematic hardening material model was used for the tube and a bilinear isotropic hardening material was specified for the tubesheet. Later, they reported that isotropic hardening material yielded no appreciable difference in the results when compared with kinematic hardening material.

They noticed a small depth of crevice between tube and tubesheet hole at the secondary face. They claim that this crevice is regarded as beneficial to prevent hideout of impurities that could promote stress corrosion cracking. A small crevice depth is achieved by applying the expansion pressure up to the secondary face of the tubesheet or a small distance below. If the crevice is very small, the tube develops a slight bulge at the point where it comes in contact with the tubesheet hole. The bulge indicates a change in the residual stress field.

2.5.3 Experimental Approach

Jawad et al [7] conducted tests on titanium and carbon steel tubes inserted into a carbon steel tubesheet. They compared the analytical calculated pull out force to the experiment test performed on titanium and carbon steel tubes expanded in carbon steel tubesheet. Table 2-1 shows a summary of their results.

Table 2-1: Theoretical And Experimental Pull Out Forces

	Theoretical Pull out Force	Experimental Pull out Force	Percentage Difference
Titanium Tube	2490	1840	26.10%
Carbon Tube	13140	7330	44.22%

In their study of the residual stresses in the transition zone, Reinhardt et al [15] experimentally measured the stresses and strains on the surface of the expanded tubes by the use of X-Ray diffraction technique. In their experiment, the tube was expanded

into a cylindrical single hole sheet having a diameter equal to the equivalent sleeve diameter rather than into a section of the actual tubesheet. By doing so, it eliminates the circumferential variability of the stress states and thus simplifies the measurements. Furthermore, it allows a direct comparison with the finite element results, which were obtained using the same technique. The stress distribution on the outer surface of the tube measured experimentally was found to be of very similar shape to that found in the finite element analysis. However, in the expanded part of the tube and in the transition zone, the experimental hoop stresses are generally more tensile than the finite element hoop stresses, while the experimental axial stresses are generally more compressive than the finite element ones.

They noticed that the hoop stress has its maximum in the middle of the transition zone between the expanded and unexpanded parts of tube. The peaks of the axial stress coincide roughly with the points of maximum curvature in the transition region where the largest tube wall bending would be expected. They had also reported that a variation of the coefficient of friction between 0.13 and 0.3 showed no difference in the results. They concluded that sticking occurs immediately after the tube wall attaches to the hole because the radial load due to the applied pressure dominates over the axial load that derives from the Poisson effect.

Beside the X-Ray diffraction technique, Scott et al [5] also used stress corrosion tests and strain gage measurements to evaluate the residual stresses and strains on the expanded tube surface. In the stress corrosion tests, the expanded joints are exposed

to a corrosive environment for specific periods of time. If tensile stresses exist, cracks will form on the surface. The longer the test, the lower is the stress required to initiate cracking. Therefore, by timing the test until the first cracks are observed, and by comparing this time to that required to form cracks in calibrated samples, the maximum stress in the expanded joints can be deduced. The other technique Scott et al used is the strain gage measurements. In this technique, they used a strain gage tool that is inserted into the tube after expansion. Three strips spaced at 120 degrees were installed in each tube, one to measure axial strain and two to measure circumferential strains.

Thiel et al [17] also used the strain gage measurements technique. They, however, mounted two strain gages (one for axial and the other for hoop strains) on the outside surface of the tube just above the top of the sleeve. They had also mounted two other strain gages on the outside wall of the sleeve.

2.6 EFFECT OF INITIAL RADIAL CLEARANCE

The residual contact pressure is very sensitive to the initial radial clearance. The initial clearance plays a negative role regarding the level of the residual contact pressure obtained when strain hardening tube material is considered. However, when the elastic perfectly plastic tube material is assumed, a constant horizontal line results between the initial clearance and the level of the residual contact pressure. Neglecting the effect of the initial clearance on the residual contact pressure when the tube material has zero strain

hardening is just justified [11]. This assumption was considered in developing equations (2-3) and (2-12) discussed earlier.

Allam et al [11] had showed that residual contact pressure deceases when the tube tangent modulus (E_t) and/or the initial radial clearance (c) increase. The residual contact pressure (P_{con}) given above for an elastic perfectly plastic material must thus be modified by a reduction factor (z), which accounts for the effect of the material strain hardening and initial radial clearance. Based on their study, they proposed the following factor:

$$z = 0.91745 - 5559\left(\frac{c}{2r_o}\right)\left(\frac{E_n}{E_t}\right) - 1.48397\frac{E_n}{E_t} \qquad (2\text{-}13)$$

This work, to the best of the proponents' knowledge, is the only available work in open literature that studied the effect of initial radial clearance with strain hardening material. Since elastic perfectly plastic material is not common and since initial radial clearance may significantly affect the level of the residual contact pressure on the strain hardened material, Allam et al [11] found it surprising that many analytical analyses [8, 9, 19-21] did not consider the effect of the initial clearance with the level of strain hardening.

2.7 EFFECT OF GROOVES

Grooves tend to improve the strength of tube-to-tubesheet joints. In particular, the width and the number of grooves have an effect on the strength of the roller-expanded joints. This is due to the additional locking mechanism, which is produced by deforming the tube into the grooves during the rolling process [22]. According to Scott et al [5], the joint

strength may be 13 times stronger if the tubes are expanded into grooved tubesheets. Grooves are required by the TEMA standard [1]. The TEMA standard grooves of two 1/8 in wide x 1/64 in deep are adequate for most rolled joints. However, for thin-walled, high strength tubes, a series of smaller, shallower grooves of the same width produce better results.

Wider than TEMA standard grooves are desirable for hydroexpanding. Assuming Poisson's ratio (υ) of 0.3, an ideal width (w) would be [2]:

$$w = 1.1\sqrt{(r_i + r_o)t} \tag{2-14}$$

where w = Groove's width

r_i = Tube inner radius

r_o = Tube outer radius

t = Tube wall thickness

However, Jawad et al [7] conducted tests on steel and titanium tubes expanded in steel tubesheet and found that the grooves showed an opposite effect on the titanium tubes. This is due to the fact that the 1/8" grooves tend to reduce the surface area of the contact pressure and thus reduce the pull out force. Tests on different groove widths indicated that a groove width of $1.56\sqrt{rt}$ for titanium tube would give the best result.

2.8 EFFECT OF HOLES' SURFACE FINISH

Jawad et al [7] conducted tests on steel and titanium tubes expanded in steel tubesheet at different surface conditions: burnished and unburnished holes. They found the pull out force for each condition and concluded that there is no major effect of surface roughness on the titanium tube. However, joint strength for the steel tube improves with the surface roughness and with burnishing the smooth holes.

To conclude this part, it is worth mentioning that due to the complexity in dealing with the elastic-plastic behavior of the real materials, most of the researchers assumed elastic-perfectly-plastic behavior of the tube and tubesheet material [8, 9, 19-21] to simplify the analysis of tube-to-tubesheet joint. Updike et al [23] simplified the elasto-plastic behavior of the tube and tubesheet materials by a linear strain hardening. If an elastic-perfectly-plastic material behavior is assumed, the initial radial clearance would not affect the joint strength. However, initial radial clearance has a negative effect on the joint strength when a level of strain hardening is assumed. The effect becomes more significant as the level of strain hardening increases.

CHAPTER 3

MODEL

3.1 INTRODUCTION

In the industry, most of the tube-to-tubesheet joints in the tubular heat exchanger are formed by means of roller expansion. However, due to the difficulty associated with the analytical analyses and numerical simulation of the roller expansion, uniform pressure expansion has been usually assumed in most of the studies performed on the tube-tubesheet joints. In addition, each joint is actually surrounded by six or eight joints, depending on the design. The neighboring joints have an effect on each other during the expansion process. Nevertheless, an equivalent simplified single hole model has been already established and often used in the existing literature. The equivalent model has the same stiffness that will produce the same end results as the real assembly would. Furthermore, the material's elastic-plastic behavior is usually simplified by assuming a linear or multi-linear strain hardening relation.

In the current work, all these simplifications will be utilized in the investigation of the effect of initial radial clearance on the tube-tubesheet joint strength. Although the investigation was experimentally performed on roller expanded tube-tubesheet joints, uniform pressure expansion will be assumed in the finite element analyses. Equivalent axisymmetric and single hole planar models are formed and bilinear elastic-plastic behavior is assumed.

This chapter will illustrate the model used in this work and how previous results are implemented to generate it. Descriptions of the models' geometry used to perform the experiment and that used in the finite element analysis are presented first. Details of the finite element meshing options selected are then introduced. The material specifications of the tubes and tubesheets used in the experiment and the finite element analysis are then outlined. Boundary conditions specified on the finite element model are then prescribed and finally the loading procedure is illustrated.

3.2 GEOMETRY OF THE MODEL

A test block simulating the tubesheet hole design configuration of the stabilizer feed/bottom exchanger was used in the experimental work. In this exchanger type, the holes on the tubesheet are arranged in a rotated square pattern with 1-inch tube pitch. The tubesheet hole is 0.76 ± 0.002 in. in diameter and has two grooves on the channel, each 1/8 in. wide by 1/64 in. deep. The thickness of the tubesheet is 2 7/16 in. The tube has a nominal diameter of ¾ in. Based on this, a 4.5 × 4.5 in., 2 7/16 in. thick square steel block

containing nine holes with dimensions as shown in Figure 3-1 was used in the experiment. This is similar to the test block for shear load testing of the tube-to-tubesheet joints given in Appendix A of Section VIII of the ASME standard [24]. The test assembly consists of an array of tubes expanded in the tubesheet such that the tube of the test joint is in the geometric center of the array and is completely surrounded by one row of adjacent tubes. This is to ensure that the effect of ligament on the test joint (the center hole) is accounted for. At the same time, the assembly reflects the same configuration as the real tubesheet. Also, the test block extends three times the thickness of the tubesheet ligament (0.75 in.) beyond the edge of the peripheral holes in the assembly to reduce the edge effect. Each block was cut and machined to size from a carbon steel type, ASTM A516 G70 tubesheet plate. Nine ¾ in. holes were drilled through the block and then bored to the required diameter, as will be explained later. Just like the real tubesheet, two grooves, each 1/8 in. wide by 1/64 in. deep, were then machined in each bored hole of the test block. A 1/16 in. radius chamfer was made on both ends of the machined holes. A standard ¾ nominal diameter tubes with an average outer radius (r_o) of 0.3745 in. and inner radius (r_i) of 0.2863 in. were finally roller expanded in each hole. The tube expanded in the test joint (central joint) was 6 in. long and the tubes expanded in all the other eight surrounding joints were 3 in. long. This is to ease grapping the tube of test joints in the pull out machine afterward. All the tubes were cut from the seamless cold-drawn low carbon steel type, ASTM 179. To simulate the real expansion process, rolling was done on a row by row of holes basis. By this order, half of the surrounding holes will be expanded before the test joint and the other half will be after.

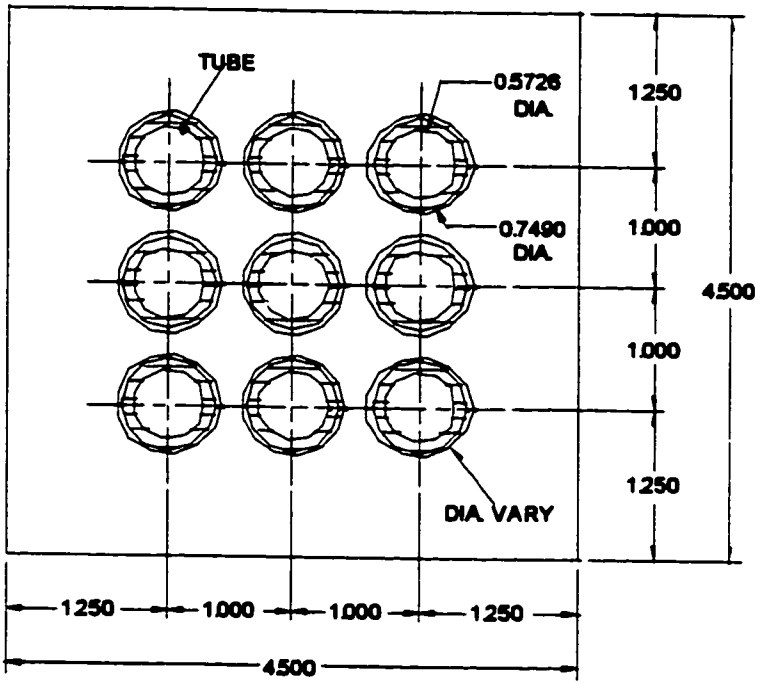

Fig. 3-1: Test Block Model

For performing finite element analyses, the equivalent sleeve diameter has found its way in most of the previous studies [5, 11, 15, 17]. In fact, this concept has even been implemented in some experimental work [5, 15]. The equivalent sleeve is a single hole model that will produce contact pressure, stress distribution or deflection, depending on the objective of the study, around the hole equivalent to the average of those around the test hole on the real tubesheet configuration. This eliminates the fluctuation of results around the test joint and yields a major simplification of the model. The equivalent sleeve concept will be implemented in this study where finite element code (ANSYS) is used to

predict the effect of initial radial clearance on the residual contact pressure. For this purpose, equation (2-10) proposed by Chaaban et al [13] for calculating the equivalent sleeve diameter will be utilized to find an equivalent sleeve diameter. This equation was based on equating the contact pressure resulting on the equivalent sleeve to that on the real tubesheet, as explained in Chapter 2. Because rolling is sequentially carried out during the experimental work, the constants of the sequential case will be substituted in the equation.

Using the above dimensions together with the material specifications described below into equation (2-10) would yield an equivalent sleeve radius (R_o) of 1.4165 in. The resulting equivalent single hole axisymmetric model dimensions are shown in Figure 3-2. As mentioned in Chapter 2, the only work that addressed initial radial clearance and material strain hardening was that by Allam et al in 1998 [11]. They found that the residual contact pressure decreases as initial radial clearance and/or tangent modulus increase. Assuming bilinear stress-strain relation material, they proposed equation (2-13) for calculating the reduction in contact pressure caused by these two parameters. To get a better estimate of the residual contact pressure between the tube and tubesheet, the reduction factor (z) of equation (2-13) needs to be multiplied by the residual contact pressure given by equation (2-3) or any other equation that is not considering the initial radial clearance and material strain hardening.

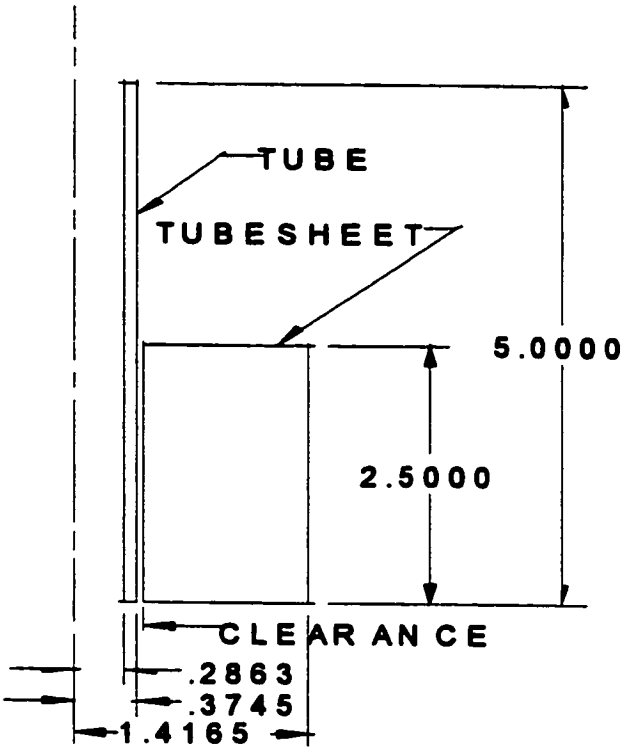

Fig. 3-2: Axisymmetric Model Showing Clearance

Besides the single hole axisymmetric model, a single hole planar model is developed using the same radial dimensions. Due to the all around symmetry and to reduce the computational time, only a sector included between any angle needs to be analyzed. In this study, a quarter circle was chosen as shown in Figure 3-3. This model is a simplified planar model where a symmetrical sector of a multiple holes circular plate, like that shown in Figure 2-2, was usually used in the literatures [5, 12]. It is used to perform both plane stress and plane strain analyses.

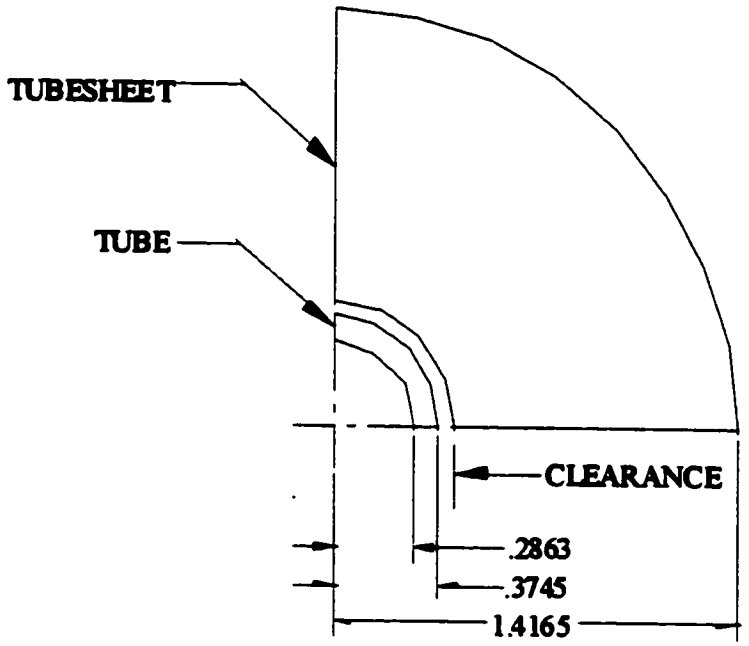

Fig. 3-3: Planar Model

The planar single hole model is smaller, easier to analyze and requires less computational time than the axisymmetric model. However, the planar model does not show the fluctuation in the contact pressure, stress and strain through the longitudinal direction. This might be very critical in the transition zone between the expanded and unexpanded portions of the tube. Also, the planar model does not show the changes that may occur in the tube length as a result of the expansion process. For validation, the results obtained from the usually used axisymmetric model will be compared with the relative results obtained from the plane stress and plane strain analyses of the simplified single hole model.

To establish a range of initial clearances simulating different hole enlargement levels during maintenance process of the heat exchangers, tubesheet hole's diameter is changed while keeping tube's outer diameter fixed. For a ¾ nominal tube outside diameter, TEMA requires that at least 96% of the joints must be within an over tolerance of 0.002 in. Remaining joints might go over this but must not exceed 0.01 in. [1]. Practically, this means that the initial radial clearance between the tube and tubesheet should be between 0.002 in. and 0.006 in. In the experimental work, radial clearances up to 0.0132 in. were introduced in the tubesheet to evaluate the effect of the clearance on the strength and integrity of the tube-to-tubesheet joint. However, in this numerical study, where tube's tangent modulus was allowed to be changed within the range discussed below, an initial radial clearance of 0.004 in. was found to be the maximum clearance that could be introduced, especially with high tube's tangent modulus. Initial radial clearances above 0.004 in. will not yield any contact when an expansion pressure equal to the tube's yield strength is applied inside a tube having tangent modulus equal to 3.33% of its modulus of elasticity. Since it is not the intent of this work to study the effect of expansion pressure level and over-expansion, all the analyses were done with a fixed value of expansion pressure, equal to the yield strength of the tube material. Consequently, initial radial clearance values were limited to 0.004 in. only. Table 3-1 shows the range of tubesheet's hole sizes and corresponding initial radial clearances covered in this study.

Table 3-1: Initial Radial Clearances

	1	2	3	4	5	6	7	8	9
Tubesheet Hole Rad. (in)	0.3745	0.3750	0.3755	0.3760	0.3765	0.3770	0.3775	0.3780	0.3785
Radial Clearance (in)	0.0000	0.0005	0.0010	0.0015	0.0020	0.0025	0.0030	0.0035	0.0040

3.3 MESH

A higher order quadrilateral two-dimensional eight-nodes element (PLANE82) was selected. This type of element provides more accurate results than the four-nodes quadrilateral element and can tolerate irregular shapes without much loss of accuracy. This 8-nodes element is well suited to model curved boundaries. It is defined by eight nodes having two degrees of freedom at each node, i.e. translations in the nodal x and y directions. This element can be used as a planar element or as an axisymmetric element. It has plasticity, stress stiffening, large deflection, and large strain capabilities.

CONTA172 and TARGE169 elements are used to represent flexible-to-flexible surface-to-surface contact between the deformable surfaces on the tube and tubesheet. These elements have two degrees of freedom at each node: translations in the nodal x and y directions. CONTA172 elements overlay the solid elements describing the boundary of the deformable tube surface and TARGE169 elements overlay the solid elements describing the boundary of the deformable tubesheet surface. These elements have the

same geometric characteristics as the solid elements with which they are connected. Tube and tubesheet boundary surfaces are discretized by a set of contact and target segment elements, CONTA172 and TARGE169 respectively. Contact occurs when CONTA172 element surface penetrates TARGE169 element surface.

CONTA172 and TARGE169 are paired via a shared real constant set. ANSYS uses a set of 11 real constants to control contact behavior of these surface-to-surface contact elements. Out of the 11 real constants, two are used to define the geometry of the target surface elements and the remaining nine are used by the contact surface elements. These real constants were tested and found that only three constants affect our model for the type of analysis we are seeking. They are the normal contact stiffness factor (FKN), the initial closure factor (ICONT) and the positive or negative offset value (CNOF).

FKN real constant control the solution convergence and the contact penetration. When convergence difficulties or too much penetration are encountered, the stiffness factor can be adjusted. If the value for FKN is too small, too much penetration can occur. If the value for FKN is too large, the problem may not converge. The optimum value of FKN is the value that minimizes contact penetration while avoiding excessive iterations. This real constant has been tested on our model and found that as FKN value increases, both the final residual contact pressure and penetration decreases while the total cumulative iterations needed for the solution to converge increases. Another observation on this real constant is that there is a value above which the final residual contact pressure remains almost constant while the contact penetration keeps dropping down more and more with

increasing FKN. An FKN value of 300 has been fixed for all types of the models. This value was found to be satisfactory, it gives the finest contact pressure value with a reasonable cumulative iteration. Contact penetration is too small at this value of FKN even though it may drop down more when FKN value is increased.

The initial closure factor (ICONT) real constant is a tolerance value between the contact and target elements. If the initial clearance is less than this tolerance, ANSYS considers the model to be in initial contact. Since the main objective of the current work is to study the effect of the initial clearance on the residual contact pressure, the model to be built must not be in initial contact. So, a value smaller than the initial clearance under investigation has to be specified for the code to consider a negligible initial contact closure. Trial runs on the model with different values of ICONT real constant show that the final residual contact pressure does not change, no matter how small ICONT is as far as it is smaller than the clearance. However, care should be taken when specifying a value just smaller than the clearance. It may still fall in the clearance range. This is because of the numerical round off due to geometry modeling and mesh generation, especially on curved surfaces. Since the clearances to be investigated in this study are in the order of 10^{-4}, a value of 1.0×10^{-6} has been fixed for ICONT on all the analyses.

The contact surface offset (CNOF) real constant defines an offset value applied to the contact surface. This offset value can be either positive or negative. A positive offset means that the entire contact surface is internally offset towards the target surface (that is, to decrease the clearance). A negative offset means that the entire contact surface is

internally moved away from the target surface (that is, to increase the clearance). This means that the model can be generated initially with no clearance and then specifying a negative CNOF value equal to the initial radial clearance to be investigated. Trials on our model proves that either this way or the traditional way, that is building the model geometry with initial radial clearance, would give the same results as far as the residual contact pressure is concerned. The difference between CNOF and ICONT real constants is that the former shifts the entire contact surface with the distance value CNOF, the latter moves all initially open contact points which are inside of adjustment band ICONT onto the target surface.

A regular meshing pattern was created in the models. The level of refining was tested to establish effective meshed models. It has been found that as the model is refined more and more, the final results are very slightly changed in a way that it does not justify having refined meshed model taking into consideration the computational time it will require. For example, an axisymmetric model having 990 nodes was compared with a 6908 nodes model. The difference in the final residual contact pressure was 0.45 % only, while the computational time consumed by the 6908 nodes model was about 20 times more than the computational time needed for the 990 nodes model. Similarly, the final residual contact pressure on the planar model would vary by only 0.94% if a 962 nodes model was used instead of a 7966 nodes model. For this reason, a 990 nodes axisymmetric model and a 962 nodes planar model, as shown in Figures 3-4 and 3-5 respectively, were used in the analyses.

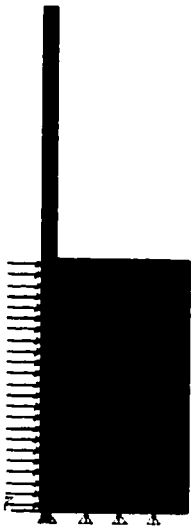

Fig. 3-4: Meshed Axisymmetric Model

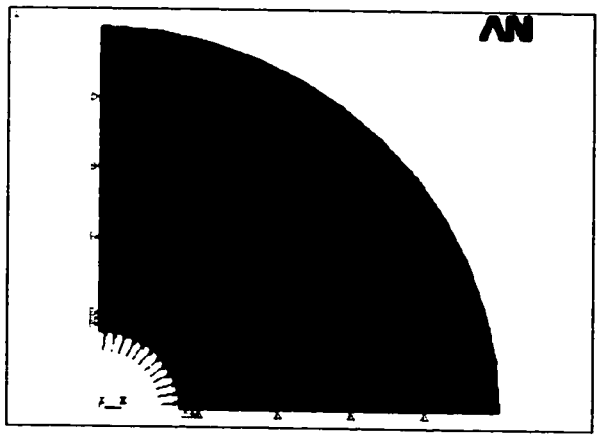

Fig. 3-5: Meshed Planar Model

3.4 MATERIAL

In the experimental work, the tube used was seamless cold-drawn low carbon steel type ASTM 179 and the tubesheet material was carbon steel type ASTM A516 G70. Their mechanical properties were obtained from ASTM standards and were measured in the lab by performing tensile tests. The true stress-strain curve of the tube as measured in the lab is shown in Figure 3-6. Measurements results show that the tube's yield stress is about 37.7 ksi and that for tubesheet ranges from 35.1 to 37.3 ksi. So, both materials have nearly the same yield stress with an average value of 36 ksi. This value was specified for the tube and tubesheet materials in the finite element analysis as illustrated in Table 3-2.

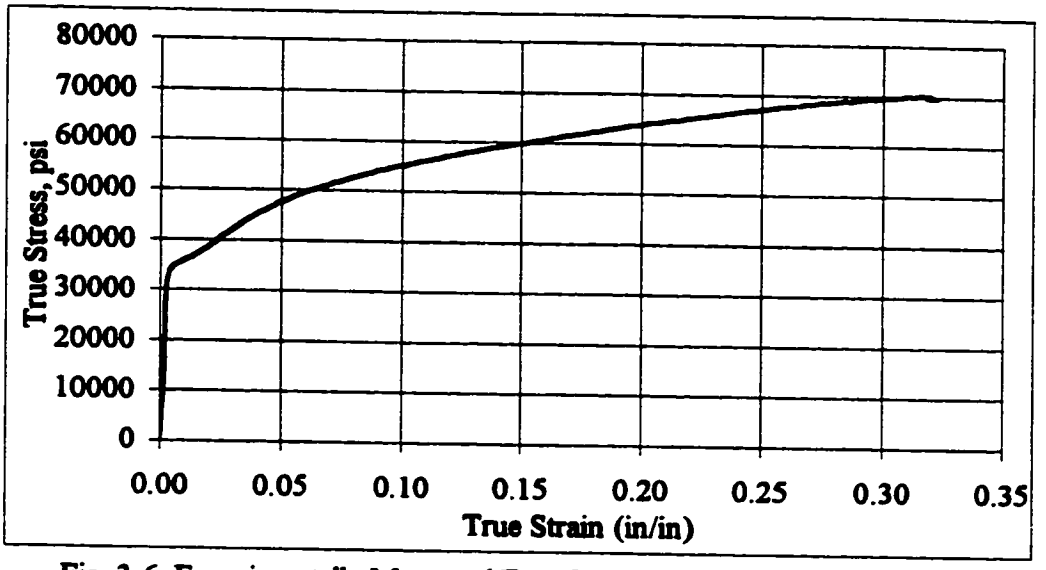

Fig. 3-6: Experimentally Measured True Stress-Strain Curves of The Tube

Measurements results also show that the modulii of elasticity of the tube and tubesheet materials are about 30×10^6 psi, which is typical for most of the steel material. This value is fixed for the tube and tubesheet materials in this study. In the plastic region, i.e. beyond the yield stress, stress-strain relationship is not linear anymore. However, it can be approximated by a linear or multi-linear relationship. The slope of the approximated line (or lines) in the plastic region of the true stress-strain diagram defines the tangent modulus. An elastic-perfectly-plastic material is that having zero tangent modulus (Figure 3-7). To illustrate how critical the tangent modulus on the analyses and how its values of both the tube and tubesheet affecting the resultant residual contact pressure, trial runs on the axisymmetric model were performed in the following order. First, a different tangent modulus value was specified for the tube on each run while keeping that for the tubesheet fixed. Secondly, the tube's tangent modulus value was kept fixed while changing that for

the tubesheet on each run. Thirdly, both the tube and tubesheet's tangent modulus values were changed on each run. Results show that the tube-to-tubesheet residual contact pressure decreases with increasing the tube's tangent modulus value, keeping every thing else the same. The tubesheet's tangent modulii values have no effect on the residual contact pressure. This is due to the fact that the tubesheet's hole surface does not yield under the application of expansion pressure equal to the tube's yield stress. This is in agreement with the work reported by Allam et al [11]. So, a zero tangent modulus was specified for the tubesheet, in other words, elastic-perfectly-plastic material was assumed.

The true stress-strain curve of the tube in the plastic region (Figure 3-6) can be approximated by a line having a slope of 127,000 psi. This means that the material of the tubes used in the experiment have an approximate tangent modulus of 0.127×10^6 psi. However, to generalize the study, tube's tangent modulus (E_a) was varied to take these values, 0.1×10^6, 0.5×10^6 and 1.0×10^6 psi. These values were chosen to cover most of the tangent modulii of steel materials. Furthermore, the material behavior was modeled in ANSYS assuming a bilinear curve and isotropic hardening. The assumed true stress-strain curve for the tube and tubesheet is shown in Figure 3-7.

The other material properties that need to be specified in the finite element code are the Poisson's ratio and the frictional coefficient. The first is usually taken as 0.3 for most of the steel material. Moreover, since it is very difficult to precisely determine the coefficient of friction between any two materials in this type of application, an average value of 0.74 [7] is specified in this study. Nevertheless, the effect of coefficient of friction on the

resultant residual contact pressure will be investigated by changing its value in a certain range. Table 3-2 illustrates a summary of the material properties specified for the tube and tubesheet.

Table 3-2: Tube And Tubesheet Material Properties

	Material Property				
	Yield Stress (psi)	Modulus of Elasticity (psi)	Tangent modulus (psi)	Poisson's Ratio	Frictional Coefficient
Tube	36×10^3	30×10^6	Varies (3 levels)	0.3	0.74
Tubesheet	36×10^3	30×10^6	0	0.3	0.74

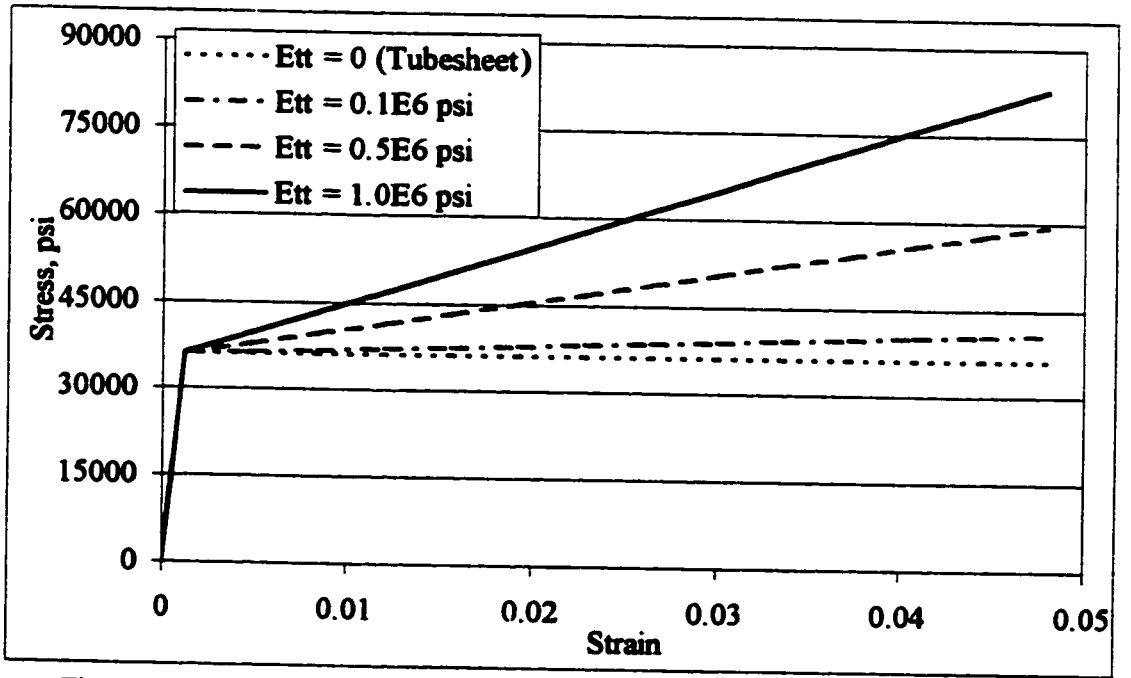

Fig. 3-7: Assumed True Stress-Strain Curves For Tube And Tubesheet Materials

3.5 BOUNDARY CONDITIONS

To stabilize the model for finite element analysis, boundary conditions have to be specified. As mentioned in the literature [11, 15], for the axisymmetric model, the front ends of the tube and the tubesheet at the tubesheet primary side, through which rolling or uniform pressure is conducted, are constrained in the axial direction (y-direction). As shown in Figure 3-4, all other surfaces are not constrained.

In the planar model, symmetry lines are specified on the tube and tubesheet at both edges of the 90° sector used (Figure 3-5). In fact, if the whole round tube and tubesheet areas were modeled (360°), a problem in specifying a boundary condition may arise. If one node on the outer surface of the tubesheet was constrained, results will not be symmetrical all around as it should be. If more than one node or all the outer tubesheet line were constrained, the model then will not closely represent the actual physical system, since the outer tubesheet radius (sleeve radius) was originally calculated by the equation proposed by Chaaban who considered this surface to be free, as explained in Chapter 2.

3.6 LOADING

Specifying the proper loading conditions is a key step in the finite element analysis. Load application becomes very critical in nonlinear models, such as the model under investigation in this study. Nonlinearities in this model are generated from three sources: material nonlinearity as a result of the elastic-plastic behavior of the tube material, boundary condition nonlinearity due to the contact interaction between the tube outer

surface and the tubesheet's hole and geometric nonlinearity due to the large strain occurring during the expansion process. For all these reasons and to ease convergence, a uniform pressure of 36000 psi, which is equal to the tube and tubesheet yield stress, was gradually applied on the internal surface of the tube forming multiple load steps. Each load step is automatically divided into many sub-steps in which the pressure increases gradually at each sub-step, with the full value occurring at the end of the load step. When the applied pressure on a certain load step reaches the required expansion pressure (36000 psi), the subsequent load step will be that of releasing the pressure to zero. Pressure release can be done in one load step divided into multiple sub-steps.

It has been noticed that the planar model converges much faster than the axisymmetric model. The latter is more sensitive to the way loading was applied and requires more load steps. Very refined load steps need to be specified just before and after the value of the pressure at which initial contact may occur. A way to find this pressure is to build a model consisting of the tube only with the same dimensions and properties and then applying a pressure on the inside surface of the tube. The radial displacement of the tube's outer surface is recorded with respect to the applied pressure. The expansion pressure at which initial contact will take place is the applied pressure that will give the tube's outer surface a radial displacement equal to the initial clearance. For instance, in an axisymmetric model having a tube tangent modulus of 0.5×10^6 psi and radial initial clearance of 0.001 in., the tube outer surface will initially come into contact with tubesheet when a pressure of 10500 psi is applied. This means that the first load step may go all the way to a value just below this pressure without any convergence problems. Subsequent load steps should

be refined in terms of the increase in the applied pressure value. To avoid convergence problems, pressure increments as little as 50 psi are added each time until the tube comes totally in contact with the tubesheet. In the next load steps, pressure addition is gradually increased. The last pressure application load step may go from 20000 psi, to the full expansion pressure of 36000 psi. Schematic drawing of the load history for this example is shown in Figure 3-8. This load history will differ as the material specification or initial clearance changed. The only way to master the most effective load history is by trial and error.

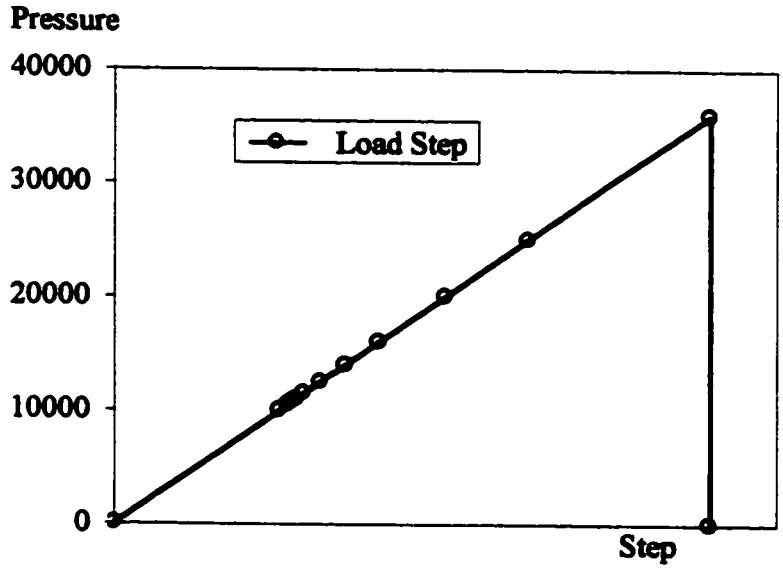

Fig. 3-8: Load History

The loading scheme described above is necessary for the axisymmetric model to have a convergent solution. Conversely, for the convergence of the planar model, refined loading is not necessary. A very coarse way of loading will still do the job without any

difficulties. In fact, pressure can be applied in one load step only. The second load step will be dropping the pressure to zero. So, a total of two (2) load steps is enough to solve the planar model, while the axisymmetric model needs between ten (10) to eighteen (18) load steps depending on the initial radial clearance and tube's tangent modulus.

On the axisymmetric model, the pressure is applied all through the portion embedded in the tubesheet, as shown in Figure 3-4. Pressure is applied all around the tube's inside surface on the planar model, as shown in Figure 3-5.

Finally, it is worth to mention that the models detailed above are built in the code (ANSYS) by writing a subroutine text file and letting the code read from this file. For hundreds of runs that may be performed throughout the study, using a subroutine to make out geometry dimensions, material specification, meshing options, boundary conditions, loading, solution options, ... etc will be very effective. On each subsequent run, a line or so may be adjusted to get a new data. A sample subroutine is given in Appendix A. This subroutine is for building an axisymmetric model with all dimensions, material specification, meshing, contact and boundary conditions, as described above. It specifies a tube's tangent modulus of 0.5×10^6 psi and initial radial clearance of 0.001 in. It solves the model by applying the required expansion pressure in thirteen (13) load steps and releases the pressure in the fourteenth load step. Listing and/or viewing the important results may be also added in the subroutine. In the above sample, the commands for plotting the contour of the contact pressure and listing their values are included at the end of the subroutine.

CHAPTER 4

ANALYTICAL, FINITE ELEMENT AND EXPERIMENTAL RESULTS

4.1 INTRODUCTION

In this chapter, analytical calculation of the residual contact pressure between the tube and tubesheet after releasing the uniformly applied expansion pressure for the model configurations described in Chapter 3 is presented. In the analytical calculation, the initial radial clearance and the material strain hardening are ignored. The effect of these two parameters on the joint strength will be accounted for later by introducing a reduction factor using the results published by Allam et al [11]. The results of the residual contact pressure, tube's inner and outer radial deformation and tube retraction obtained from the finite element analysis for all the cases covered in this study, as described in Chapter 3,

will then be presented. Investigation of the effect of the coefficient of friction on the joint strength is then outlined. In addition, for comparison purposes, the results of the residual contact pressure and tube's inner and outer surfaces radial deformation obtained from analyzing the original multi holes model are included. Finally, the measured tube's inner surface radial deformation and the pull out force for all the range of initial radial clearance covered in the experiment program are illustrated.

4.2 ANALYTICAL APPROACH AND RESULTS

Closed-form solutions for estimating the tube-to-tubesheet joint strength are available in the open literature. The strength is measured in terms of either the residual interfacial contact pressure between the tube and tubesheet or the pull out force, which is the force needed to draw the tube apart from the tubesheet. Equation (2-3) derived by Kasraie et al [8] will be employed in this study to estimate the residual contact pressure of the configuration described in Chapter 3. In deriving this equation, a zero initial radial clearance and elastic-perfectly-plastic material were assumed. Also, the effect of adjacent holes was neglected by assuming an infinitely large single hole tubesheet.

A correction to the calculated residual contact pressure from equation (2-3) has been developed by Allam et al [11] using finite element analysis. The authors have accounted for the material strain hardening and initial radial clearance by introducing a reduction (correction) factor to be multiplied with the residual contact pressure calculated from equation (2-3). This factor will be discussed in Section 4.2.2. In addition, an alternative

approach for calculating the residual contact pressure while accounting for the effect of adjacent holes will be developed in Section 4.2.1. This will be done by considering the equivalent sleeve dimension in the calculation, since the equivalent sleeve diameter was calculated using equation (2-10) proposed by Chaaban et al [13] who accounted for the effect of adjacent holes in deriving this equation.

4.2.1 Residual Contact Pressure Calculation

In order to estimate the tube-tubesheet's residual contact pressure using Kasraie and Yokell approach, the actual tube radii and its yield strength together with the expansion pressure are entered into their proposed equation. As described in Chapter 3, the tube inner radius (r_i) for the case under study is 0.2863 in., tube outer radius (r_o) is 0.3745 in., tube yield strength (σ_{yt}) is 36000 psi and the expansion pressure (P_e) is 36000 psi. By entering all these variables into equation (2-3), an estimated pressure of 3797 psi is found to be the residual contact pressure between the tube and tubesheet after releasing the expansion pressure. As mentioned earlier, this result was based on the assumption of zero radial clearance, elastic-perfectly-plastic material and the equivalent sleeve is infinitely large. Hereafter, an alternative approach for calculating the contact pressure while considering the equivalent sleeve dimension is developed.

In the beginning, it is worth reminding that the residual contact pressure is the difference between the radial stresses in the loading and unloading stages. So, the approach for determining the contact pressure while considering the sleeve dimensions will be by calculating the radial stresses during loading and unloading

stages. A zero initial radial clearance and elastic-perfectly-plastic material are assumed in this calculation approach. As mentioned above, they will be taken into consideration later by introducing a correction factor, which will be explained in Section 4.2.2.

During the loading process, the radial stress is partially plastic and partially elastic, since the tube is stressed beyond its yield point. An elastic-plastic interfacial radius ($r_{e\text{-}p}$) will exist at some radius. Neglecting the initial radial clearance at this stage, the tube and tubesheet can be considered as a thick cylindrical shell. The shell will have an inner radius equal to the tube's inner radius (r_i) and an outer radius equal to the equivalent sleeve radius (R_o), see Figure 4-1.

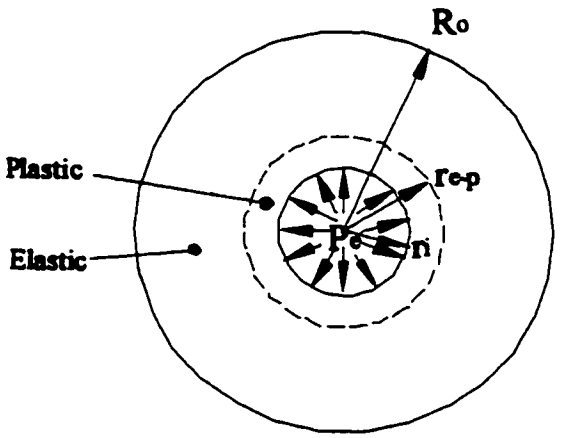

Fig. 4-1: Elastic-Plastic Interface in a Cylindrical Shell

Jawad et al [7] had derived the equations for hoop, radial and longitudinal stresses in the elastic and plastic regions during the expansion process. From the plasticity theory, they showed that the radial stress in the plastic portion at any radius (r) between r_i and r_{e-p} is:

$$\sigma_r = \left(\frac{\sigma_y}{\sqrt{3}}\right)\left(-1 + \frac{r_{e-p}^2}{R_o^2} + 2\ln\frac{r}{r_{e-p}}\right) \tag{4-1}$$

and the radial stress in the elastic portion at any radius (r) between r_{e-p} and R_o is:

$$\sigma_r = \left(\frac{\sigma_y}{\sqrt{3}}\right)\left(\frac{r_{e-p}^2}{R_o^2}\right)\left(1 - \frac{R_o^2}{r^2}\right) \tag{4-2}$$

where the elastic-plastic interfacial radius can be found from the following expression:

$$P_e = \left(\frac{\sigma_y}{\sqrt{3}}\right)\left(1 - \frac{r_{e-p}^2}{R_o^2} - 2\ln\frac{r_i}{r_{e-p}}\right) \tag{4-3}$$

By combining equations (4-1) and (4-3) to eliminate the elastic-plastic interfacial radius (r_{e-p}), the radial stress in the plastic portion can be expressed as:

$$\sigma_r = -P_e + \frac{2}{\sqrt{3}}\sigma_y \ln\frac{r}{r_i} \tag{4-4}$$

This equation gives the residual radial stress at any radius while the expansion pressure is still applied (loading stage). The contact pressure between the tube and tubesheet at this stage is calculated by letting r equal to the tube's outer radius (r_o).

For the present case, with the expansion pressure taken equal to the yield stress of the tube material (i.e. $P_e = \sigma_y = 36000$ psi), inner radius (r_i) = 0.2863 in. and tube's outer radius (r_o) = 0.3745 in., the residual contact pressure (P_{con}) was calculated to be -24837 psi.

During the unloading stage, the stresses can be found from the elasticity theory. When the pressure begins to fall, the elastic-perfectly-plastic material which was at the yield stress will have its stress level reduced, and will thus immediately re-enter the elastic range. Because of the permanent plastic deformation in the contained plastic zone, the elastic stress relations will refer to the changes in the residual stresses. So, all the material can be considered to behave elastically [25]. The elastic radial stress for a thick cylinder under internal pressure is given by:

$$\sigma_r = P_e \frac{r_i^2}{R_o^2 - r_i^2}\left(1 - \frac{R_o^2}{r^2}\right) \qquad (4\text{-}5)$$

This equation gives the reduction amount in the residual radial stress at any radius while releasing the expansion pressure (unloading stage). Again, the contact pressure decrease between the tube and tubesheet at this stage is calculated by letting r equal to the tube's outer radius (r_o) in equation (4-5). Using the figures given above with the equivalent sleeve radius (R_o) = 1.4165 in., the reduction in the residual contact pressure (P_{con}) after unloading was calculated to be -20403 psi.

The residual contact pressure between the tube and tubesheet at the end of the expansion process (loading and then unloading) will basically be the difference

between the elastic-plastic radial stress and the radial stress which would have occurred at the same pressure if the material had remained elastic, that is for the present case:

$$P_{con} = (-24837) - (-20403) = -4434 \text{ psi} \tag{4-6}$$

To visualize the radial stress distributions through the shell, equations (4-1) and (4-2) are used to plot the radial stress distribution during the loading stage in the plastic and elastic regions respectively. This is done by substituting the model's parameters involved while letting r be the independent variable changing from the tube's inner radius (r_i) to the equivalent sleeve radius (R_o). But the elastic-plastic interfacial radius ($r_{e\text{-}p}$) has to be determined first. Equation (4-3) is used to find $r_{e\text{-}p}$ for a specified expansion pressure (P_e), which is equal to the tube's yield stress (36000 psi) for the present case. When substituting these values and those of r_i and R_o, given above, into equation (4-3), the elastic-plastic interfacial radius ($r_{e\text{-}p}$) is found to be 0.43255 in. The calculated $r_{e\text{-}p}$ is then substituted into equations (4-1) and (4-2) together with the other model's parameters to calculate and plot the radial stress distribution during the loading stage. On the other hand, equation (4-5) is used to calculate and plot the radial stress distribution during the unloading stage. The difference between the loading and unloading stresses gives the residual radial stress at each value of the radius r.

Radial stress distributions through the thick cylindrical wall in the loading and unloading stages and the residual radial stresses afterward are plotted in Figure 4-2

for the present case. A line is drawn at r = 0.3745 in., which correspond to the tube's outer radius. This line crosses the loading, unloading and residual radial stresses distribution curves at the values -24837, -20403 and -4434 psi respectively, which were calculated above.

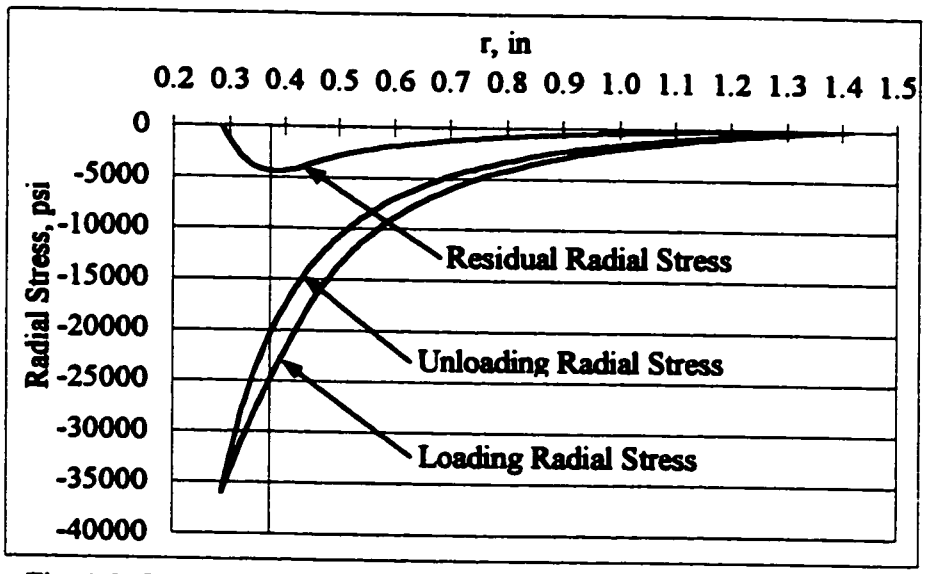

Fig. 4-2: Radial Stresses Distribution Through a Thick Cylindrical Wall

Recall that the calculated contact pressure using equation (2-3) proposed by Kasraie was 3797 psi; a difference of about 14.4% exists between the results obtained from the two approaches. This difference is due to the fact that Kasraie had assumed an infinite sleeve radius while the modified approach had taken the sleeve radius into consideration. Both approaches have assumed zero initial radial clearance and elastic-perfectly-plastic material. In addition, an axisymmetric model of the same case under study was generated in the finite element code (ANSYS), the residual contact pressure obtained from the code was 4494 psi. This result is very close to the result

obtained from the modified approach. The difference is about 1.35% only. Furthermore, the residual contact pressure calculations for a list of arbitrarily chosen model's dimensions were performed by using equation (2-3), the modified approach and ANSYS. The results obtained from the modified approach and ANSYS were always very close to each other, while a significant difference existed when compared to that found from equation (2-3).

4.2.2 Initial Radial Clearance And Strain Hardening Effect

As stated earlier in Chapter 2, to the best of the author's knowledge, the only published study of the effect of the initial radial clearance and material strain hardening on the tube-tubesheet joint strength is that accomplished by Allam et al [11]. They conducted a parametric study using ABAQUS finite element code [16] and proposed a reduction factor (z) given by equation (2-13) that accounts for the effect of the initial radial clearance and material strain hardening. This factor is then multiplied with the residual contact pressure calculated above where a zero initial radial clearance and elastic-perfectly-plastic material were assumed. Result will be a closer estimate of the residual contact pressure between the tube and tubesheet.

Equation (2-13) is employed here to express the effect of the radial clearance and tube's strain hardening on the residual contact pressure calculated above (4434 psi). As explained in Section 3.4, the material strain hardening is denoted by the tangent modulus, which is the slope of the approximated line (or lines) in the plastic region of the true stress-strain diagram, see Figure 3-7. Tubesheet's strain hardening is not

considered since, as was discussed in Section 3.4, its value has no effect on the residual contact pressure on the model under study.

The reduction factor calculated from equation (2-13) for each pair of initial radial clearance (c) and tube's tangent modulus (E_{tt}), covered in this study, is presented in Table 4-1. The final residual contact pressure, which results by multiplying the reduction factor by the residual contact pressure calculated earlier (4434 psi), is also shown in the table.

Table 4-1: Reduction Factor And Final Contact Pressure

Radial Clearance (in)	E_{tt} = 100000 psi		E_{tt} = 500000 psi		E_{tt} = 1000000 psi	
	Reduction Factor	Contact Pressure (psi)	Reduction Factor	Contact Pressure (psi)	Reduction Factor	Contact Pressure (psi)
0.0000	0.9125	4046	0.8927	3958	0.8680	3849
0.0005	0.9001	3991	0.8309	3684	0.7443	3300
0.0010	0.8878	3936	0.7690	3410	0.6206	2752
0.0015	0.8754	3881	0.7072	3136	0.4969	2203
0.0020	0.8630	3827	0.6453	2861	0.3732	1655
0.0025	0.8507	3772	0.5835	2587	0.2495	1106
0.0030	0.8383	3717	0.5216	2313	0.1258	558
0.0035	0.8259	3662	0.4598	2039	0.0021	9
0.0040	0.8135	3607	0.3979	1764	-0.1216	-539

A plot of final residual contact pressure versus the initial radial clearance for each tube's tangent modulus as shown in Table 3-1 is presented in Figure 4-3. This figure clearly shows that the residual contact pressure decreases linearly with initial radial clearance increase. The slope of the line is steeper for the larger tube's tangent

modulus (E_{tt}) and it reaches zero as E_{tt} approaches to zero. This means that for an elastic-perfectly-plastic material, the residual contact pressure will be constant regardless of the initial radial clearance. The effect of the initial radial clearance and tube's tangent modulus will be explained in the next chapter.

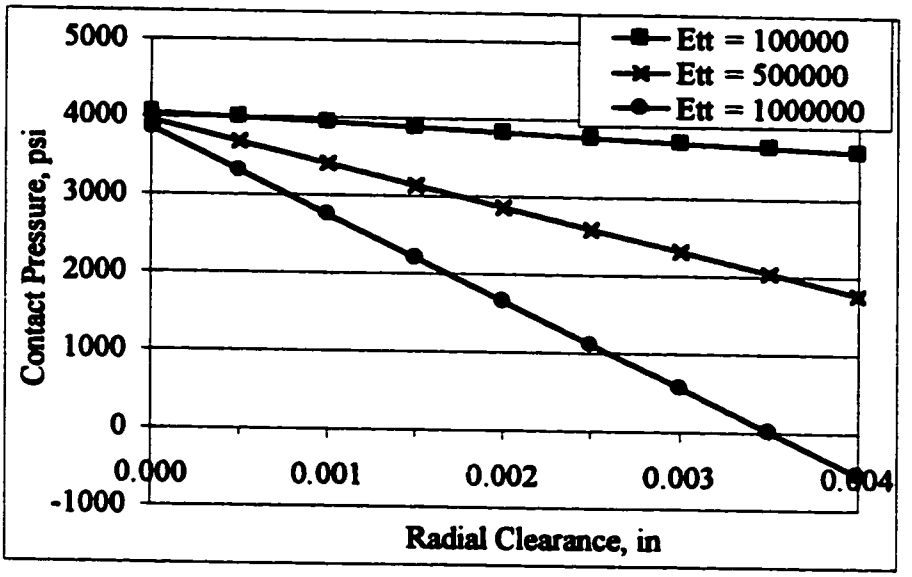

Fig. 4-3: Residual Contact Pressure

4.3 FINITE ELEMENT ANALYSIS AND RESULTS

The finite element computer code (ANSYS) has been used to analyze the model described in Chapter 3. The simplified axisymmetric and planar models are used to compute the residual contact pressure and tube's inner and outer radial deformations results. The axisymmetric model has been also used to illustrate the tube retraction with the initial radial clearance and the effect of the coefficient of friction on the tube-tubesheet joint strength. In addition, a planar analysis of the original multi holes model is used to

compute the residual contact pressure and tube's inner and outer radial deformations for selected cases. The results will be compared with those obtained from the axisymmetric model to find how realistic the simplified single hole models are.

4.3.1 Residual Contact Pressure

The main objective of this study is to investigate the effect of the initial radial clearances on the tube-to-tubesheet joint strength. As stated earlier, one way to look at the joint strength is by estimating the residual contact pressure between the tube and tubesheet. A typical residual contact pressure distribution at the end of expansion process along longitudinal direction as obtained from the axisymmetric analysis for the case of 0.002 in. initial radial clearance and tube's tangent modulus (E_t) of 500,000 psi is shown in Figure 4-4. This case was selected for demonstration because it falls in middle of the ranges of the initial radial clearances and tube's tangent modulus covered in this study.

Recall from Chapter 3 that the expansion pressure is applied into the tube through the entire portion embedded into the tubesheet, which is 2.5 in. for the present case. In other words, the pressure is applied from the tubesheet's primary side (y = 0 in.) to the secondary side (y = 2.5 in.). The contact pressure shown in Figure 4-4 is constant, with a value of about 3300 psi, through out the tube length extending from y = 0 in. to y = 1.73 in. This length corresponds to about 70% of the expanded tube portion. The contact pressure then starts to decrease very slightly before it shots up to its maximum of 6304 psi at the approximate location of y = 2.28 in. Then it falls down

to zero just below the secondary side (y = 2.5 in.) where the expansion pressure ended.

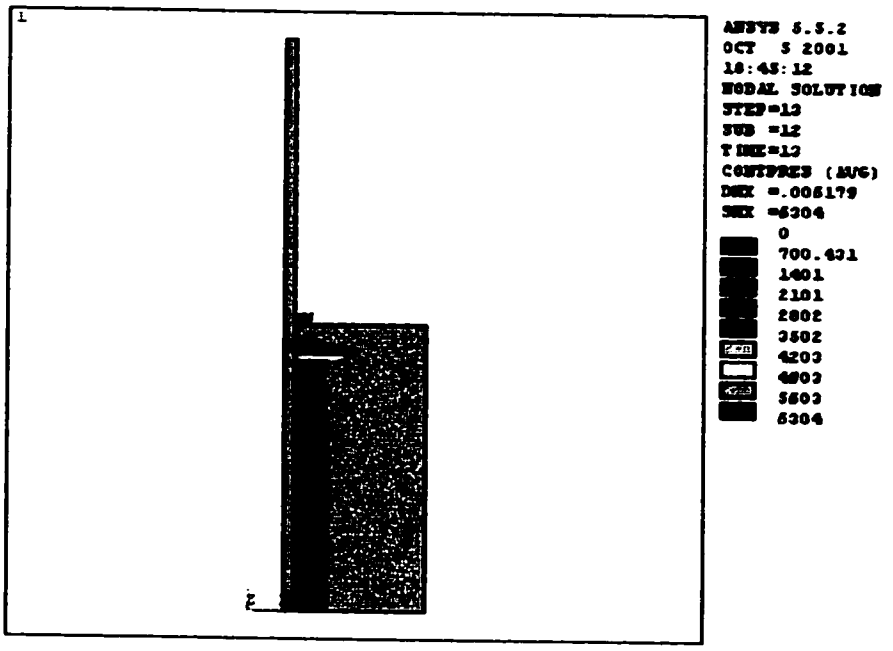

Fig. 4-4: Longitudinal Contact Pressure Distribution For The Case c = 0.002 in., E_{tt} = 500000 psi

The above described residual contact pressure distribution is common for all the cases covered in this study that have an initial radial clearance other than zero. However, an axisymmetric model with zero initial radial clearance did not have a maximum contact pressure value below the secondary face of the tubesheet. In this case, the contact pressure is constant through out the section extended from the tubesheet's primary side to a point just below the secondary side where it starts to drop down gradually to a small value (not even zero) at the secondary side. Figure 4-5 shows a typical residual contact pressure distribution in the longitudinal direction for the case

of zero initial radial clearance. It is important to note that the residual contact pressure, to be illustrated later for all the cases covered in this study, is the uniform pressure that takes place in the major part of the expanded tube length. This is the pressure extending from the primary side (y = 0 in.) to the point below the secondary side at which the pressure starts to drop down.

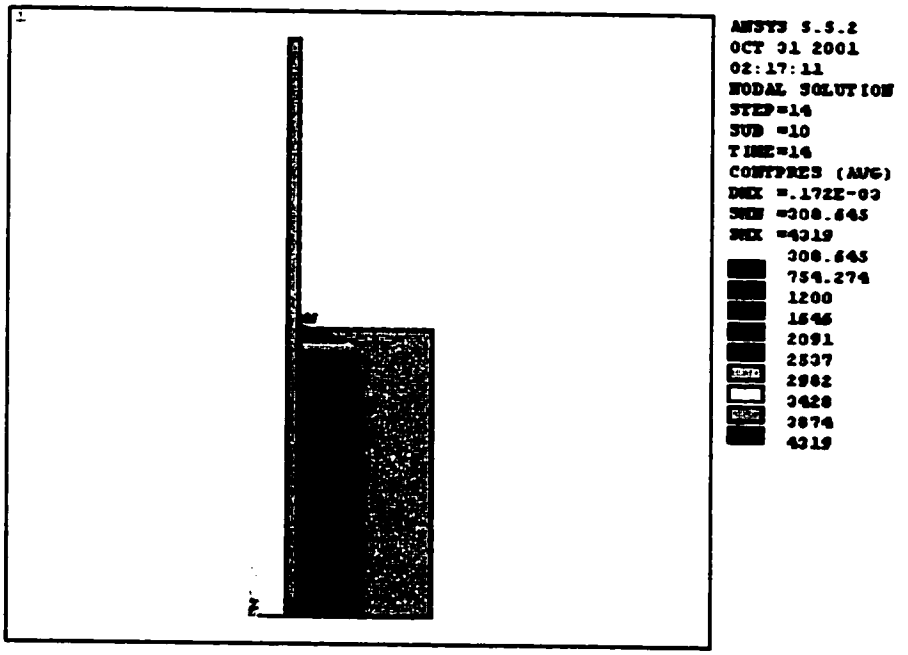

Fig. 4-5: Longitudinal Contact Pressure Distribution For The Case c = 0.0 in., E_{tt} = 500000 psi

The peak value of the residual contact pressure occurs below the secondary side in the cases where the initial radial clearance is not zero can be explained by noting that a smooth transition, like an S shape, will occur between the expanded and unexpanded portions of the tube. As a result, the tube surface in transition zone will

concave. The applied pressure will always act perpendicular to the line surface on which it is applied. So, the pressure will follow the curved tube surface and make the tube bow more and more until it comes in contact with the tubesheet. For demonstration, an axisymmetric model of the tube only (without tubesheet) having the same geometry and properties as that used in the analysis was generated. A pressure equal to 36000 psi was applied into the tube through a length of 2.5 in, just like what was done in the axisymmetric analysis of the tube-tubesheet assembly. Resultant nodal radial deformation was recorded and then plotted in Figure 4-6 to see the tube curvature resulting from the applied pressure.

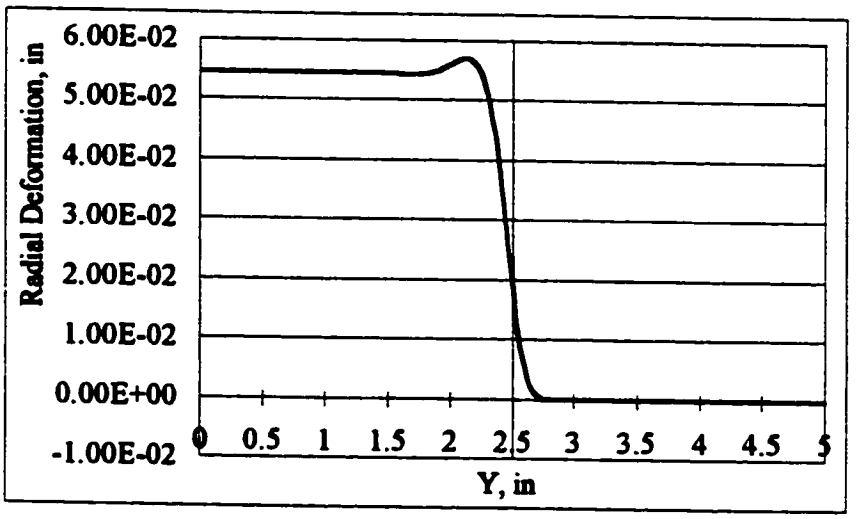

Fig. 4-6: Tube Only Outer Surface Curvature

After contact, the tubesheet will resist the concaved surface to flatten it back and thus more pressure will be exerted on the tubesheet hole surface in that location. When the pressure is released, residual contact pressure will be maximum in this location.

Furthermore, as the tube wall expands radially when the pressure is applied, it will retract axially, as will be seen later in Section 4.3.3, to conserve the material volume. As the initial clearance between the tube and tubesheet increases, tube retraction amount increases till the tube contacts the tubesheet. Recall that in the axisymmetric model defined in Chapter 3, the tube and tubesheet were restrained in the axial direction on the primary side. So, all the tube retraction will be on the free end. This retraction is responsible for the zero contact pressure occurrences at the secondary side.

For the case of zero initial radial clearance, the tube outer surface will immediately come in contact with the tubesheet once it stars to expand. As a result, there will be no concaved surface that would exert more pressure on the tubesheet. So, a peak contact pressure value was not observed at the secondary side. In addition, the frictional force between the tube and tubesheet, once they come in contact, will prevent the tube from moving axially through the expanded portion. The tube could move axially only at the free end beyond the tubesheet surface. In contrast with the case when clearance was present, for the case of zero initial radial clearance, the tube was elongated. This is due to the fact that extrusion takes place in the tube. Since the tube wall is reduced when a pressure is applied, as will be seen later in Section 5.3, some tube wall material flows axially which causes tube elongation. The tube elongation was not noticed when there is an initial radial clearance between the tube and tubesheet because the extrusion amount was less than the retraction amount resulting in an overall tube shortening.

On the other hand, the circumferential contact pressure distribution obtained from the planar model, discussed in Chapter 3, is uniform all around the tube-tubesheet joint. This is the case for both plane stress and plane strain analyses. Figure 4-7 shows a typical circumferential contact pressure distribution, with a value of 3450 psi, resulting from a plane stress analysis for the case of 0.002 in. initial radial clearance and tube's tangent modulus (E_t) of 500,000 psi.

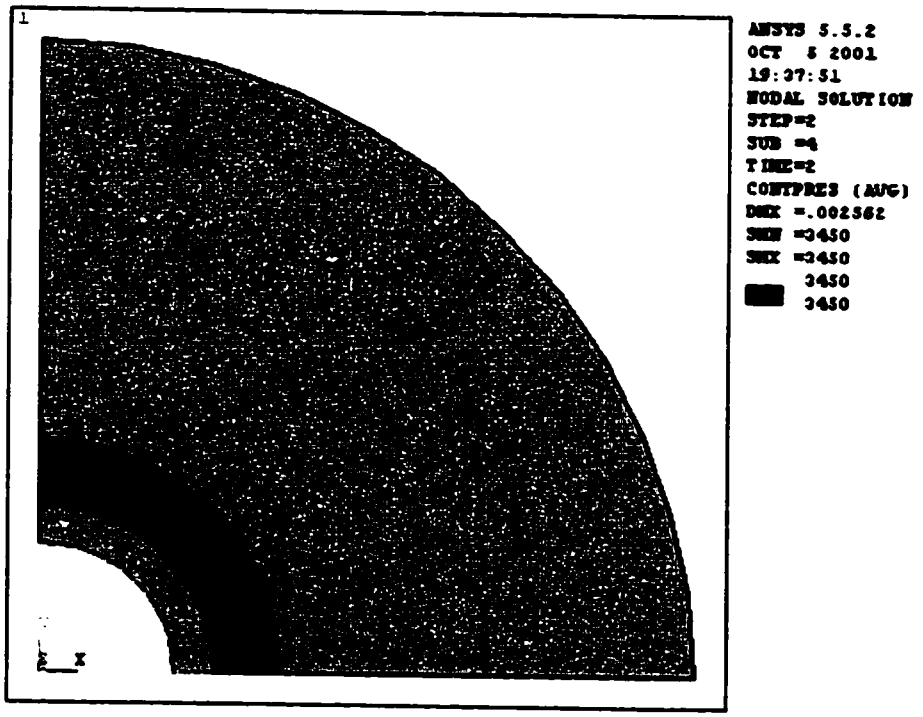

Fig. 4-7: Circumferential Contact Pressure Distribution For The Case c = 0.002 in., E_t = 500000 psi

The residual contact pressure for the range of initial radial clearance and tube's tangent modulus given in Chapter 3 is illustrated in Table 4-2. These results were computed using the axisymmetric, plane stress and plane strain models.

Table 4-2: Residual Contact Pressure (psi)

Radial Clearance (in)	AXISYMMETRIC			PLANE STRESS			PLANE STRAIN		
	Tube Tangent Modulus (psi)			Tube Tangent Modulus (psi)			Tube Tangent Modulus (psi)		
	0.1×10^6	0.5×10^6	1.0×10^6	0.1×10^6	0.5×10^6	1.0×10^6	0.1×10^6	0.5×10^6	1.0×10^6
0.0000	4458	4318	4152	5009	4753	4418	4439	4300	4134
0.0005	4399	4047	3625	4934	4372	3800	4397	4013	3553
0.0010	4350	3798	3135	4862	4060	3230	4348	3724	2975
0.0015	4302	3550	2650	4787	3757	2691	4292	3429	2393
0.0020	4250	3303	2169	4718	3463	2157	4234	3134	1813
0.0025	4201	3058	1692	4645	3177	1655	4175	2840	1236
0.0030	4153	2815	1217	4574	2898	1165	4116	2548	662
0.0035	4105	2575	744	4502	2626	683	4058	2258	88
0.0040	4056	2333		4432	2360	216	4000	1971	

To visualize the whole picture, the residual contact pressures shown in the above table for the three models and the three values of tube's tangent modulus are plotted versus initial radial clearance in Figure 4-8. As it can be see from the figure, a linear relationship exists between the residual contact pressure and the initial radial clearance for a given tangent modulus (E_t) value for the three models. This result is similar to that obtained by Allam et al [11] and discussed in Section 4.2.2 above. The decrease in the residual contact pressure is higher for the larger tube's tangent modulus. As E_t approaches zero, which is the case of elastic-perfectly-plastic material, the contact pressure will retain a constant value regardless of the radial clearance. In other words, the residual contact pressure will be independent of the initial radial clearance. This statement matches with the results published in literature.

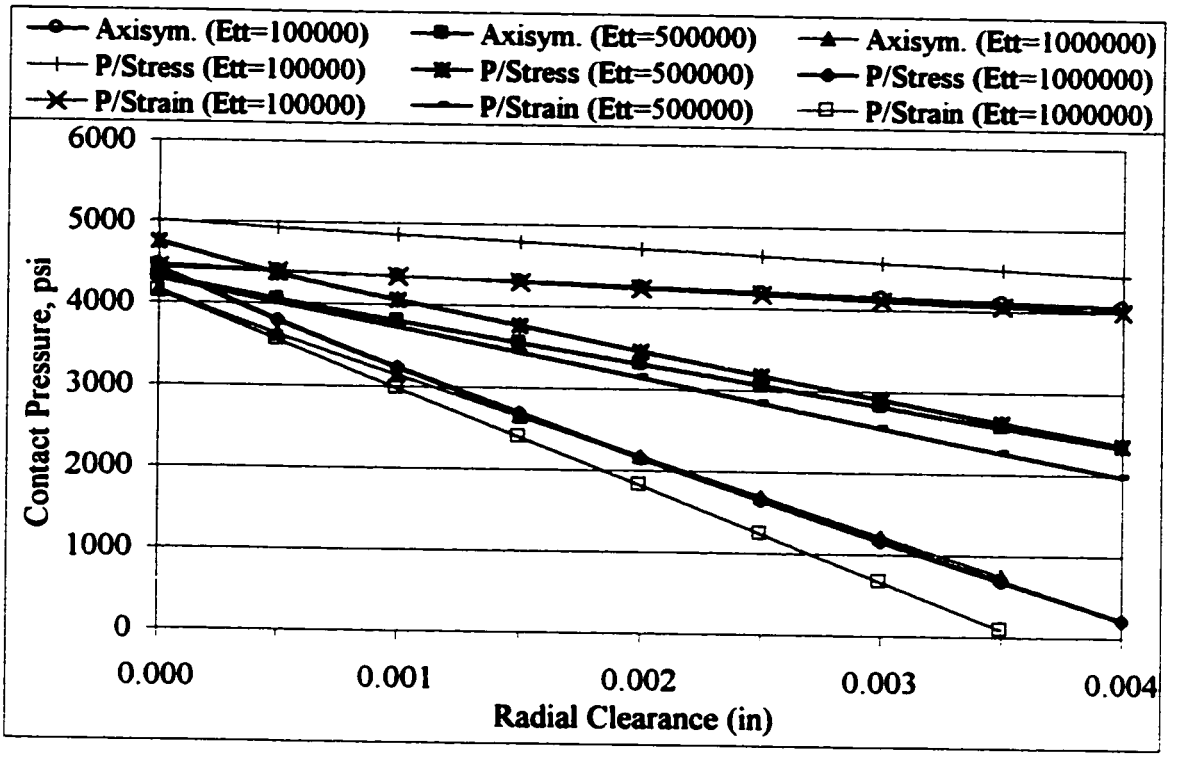

Fig. 4-8: Residual Contact Pressure

Since the axisymmetric model was validated and frequently used by a large number of researchers [5, 11, 15, 17], the residual contact pressure obtained from this model will primarily be used in the present study of the effect of initial radial clearance to be presented in Chapter 5. Nevertheless, it can be seen from Figure 4-8 that the values of residual contact pressure, for a given tangent modulus, obtained from the plane stress and plane strain models are close to that obtained from the axisymmetric model. Results from the axisymmetric model are closer to those from the plane stress model for the high level of tube's tangent modulus and they are closer to the results from plane strain model for the low level of tangent modulus. It should be mentioned

however that the axisymmetric model gives a more elaborate description of pressure distribution along radial and axial directions.

4.3.2 Radial Deformation

The radial deformations of the tube's inner and outer surfaces are recoded to be used later in calculating the tube wall reduction and tube thinning. These parameters are measures of the joint strength. The radial deformations of the tube's inner and outer surfaces after releasing the expansion pressure as computed from the axisymmetric, plane stress and plane strain models are listed in Table 4-3. The inner and outer surfaces radial deformation values are plotted against the initial radial clearance in Figures 4-9 and 4-10 respectively.

Results from the three models: axisymmetric, plane stress and plane strain, show that both the tube's inner and outer surfaces radial deformation increase linearly with the initial radial clearance for a given tube's tangent modulus. Plane strain results of the tube's inner surface radial deformation seems to deviate from those of the other two models, as the clearance gets large. The tube's inner surface radial deformation decreases as the tangent modulus increases for all models. This is expected since the harder the tube material is, the more resistance it will exert.

On the other hand, the tube's outer surface radial deformation resulting from the three models on the three levels of tube's tangent modulus seems to overlap. This leads to say that the tube's outer surface radial deformations is not influenced by the tube's

Table 4-3: Tube's Inner And Outer Surfaces Radial Deformations (in)

	Radial Clearance (in)	Tube's Inner Surface			Tube's Outer Surface		
		Tube Tangent Modulus (psi)			Tube Tangent Modulus (psi)		
		0.1×10^6	0.5×10^6	1.0×10^6	0.1×10^6	0.5×10^6	1.0×10^6
AXISYMMTRIC	0.0000	1.78E-04	1.72E-04	1.65E-04	1.06E-04	1.02E-04	9.82E-05
	0.0005	7.88E-04	7.72E-04	7.53E-04	6.05E-04	5.96E-04	5.85E-04
	0.0010	1.37E-03	1.35E-03	1.32E-03	1.10E-03	1.09E-03	1.07E-03
	0.0015	1.96E-03	1.93E-03	1.89E-03	1.60E-03	1.58E-03	1.56E-03
	0.0020	2.55E-03	2.51E-03	2.46E-03	2.10E-03	2.08E-03	2.05E-03
	0.0025	3.13E-03	3.08E-03	3.03E-03	2.60E-03	2.57E-03	2.54E-03
	0.0030	3.72E-03	3.66E-03	3.60E-03	3.10E-03	3.07E-03	3.02E-03
	0.0035	4.30E-03	4.24E-03	4.17E-03	3.60E-03	3.56E-03	3.51E-03
	0.0040	4.89E-03	4.82E-03		4.10E-03	4.05E-03	
PLANE STRESS	0.0000	2.75E-04	2.50E-04	2.24E-04	1.24E-04	1.16E-04	1.07E-04
	0.0005	8.87E-04	8.46E-04	8.08E-04	6.22E-04	6.07E-04	5.91E-04
	0.0010	1.47E-03	1.42E-03	1.37E-03	1.12E-03	1.10E-03	1.08E-03
	0.0015	2.06E-03	1.99E-03	1.93E-03	1.62E-03	1.59E-03	1.56E-03
	0.0020	2.65E-03	2.56E-03	2.48E-03	2.12E-03	2.08E-03	2.05E-03
	0.0025	3.23E-03	3.13E-03	3.05E-03	2.62E-03	2.58E-03	2.54E-03
	0.0030	3.82E-03	3.70E-03	3.62E-03	3.11E-03	3.07E-03	3.02E-03
	0.0035	4.41E-03	4.27E-03	4.19E-03	3.61E-03	3.56E-03	3.51E-03
	0.0040	4.99E-03	4.84E-03		4.11E-03	4.06E-03	
PLANE STRAIN	0.0000	1.76E-04	1.71E-04	1.64E-04	1.04E-04	1.01E-04	9.67E-05
	0.0005	8.27E-04	8.11E-04	7.92E-04	6.03E-04	5.94E-04	5.83E-04
	0.0010	1.48E-03	1.45E-03	1.42E-03	1.10E-03	1.09E-03	1.07E-03
	0.0015	2.13E-03	2.09E-03	2.05E-03	1.60E-03	1.58E-03	1.55E-03
	0.0020	2.78E-03	2.73E-03	2.68E-03	2.10E-03	2.07E-03	2.04E-03
	0.0025	3.43E-03	3.37E-03	3.30E-03	2.60E-03	2.57E-03	2.53E-03
	0.0030	4.08E-03	4.01E-03	3.93E-03	3.10E-03	3.06E-03	3.01E-03
	0.0035	4.72E-03	4.65E-03	4.56E-03	3.60E-03	3.55E-03	3.50E-03
	0.0040	5.37E-03	5.29E-03		4.10E-03	4.05E-03	

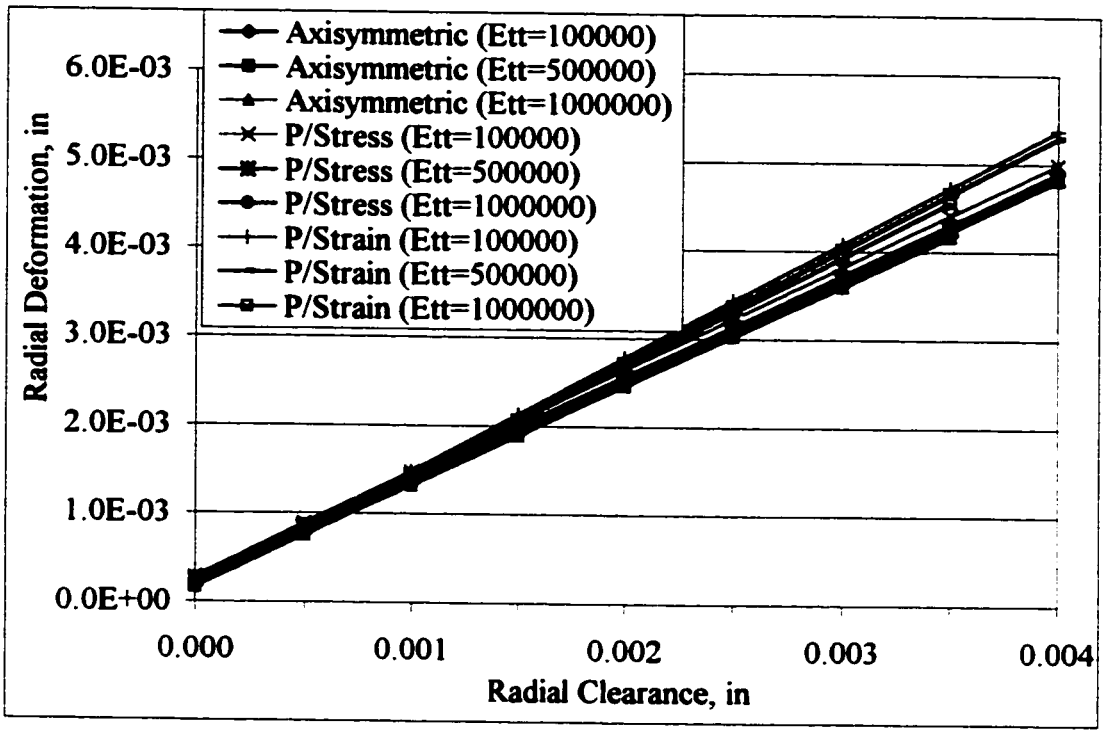

Fig. 4-9: Tube's Inner Surface Radial Deformation

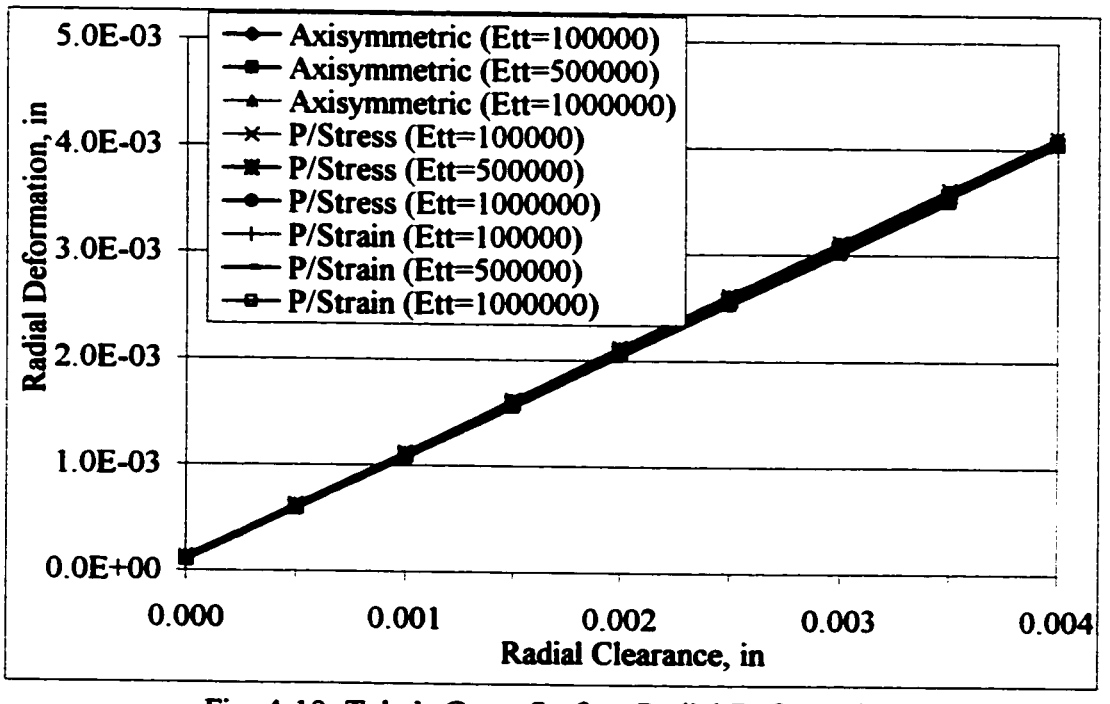

Fig. 4-10: Tube's Outer Surface Radial Deformation

tangent modulus. However, a close look at Table 4-3 shows that the tube's outer surface radial deformation is slightly affected by the tangent modulus. Yet, the effect of tube's tangent modulus on the inner surface deformation is more than that on the outer surface deformation. This is due to the fact that the tube's outer surface will follow the tubesheet hole surface deformations.

To examine this fact and to visualize the tube's curvature, an axisymmetric model is used to calculate the radial deformations of all the nodes on the tube's inner and outer surfaces with respect to their axial location. These values are plotted in Figure 4-11. This plot shows the curvature of the inner and outer surfaces of the tube when the full expanding pressure is applied and after releasing the pressure for the case of initial radial clearance of 0.001 in. and tangent modulus of 0.5×10^6 psi.

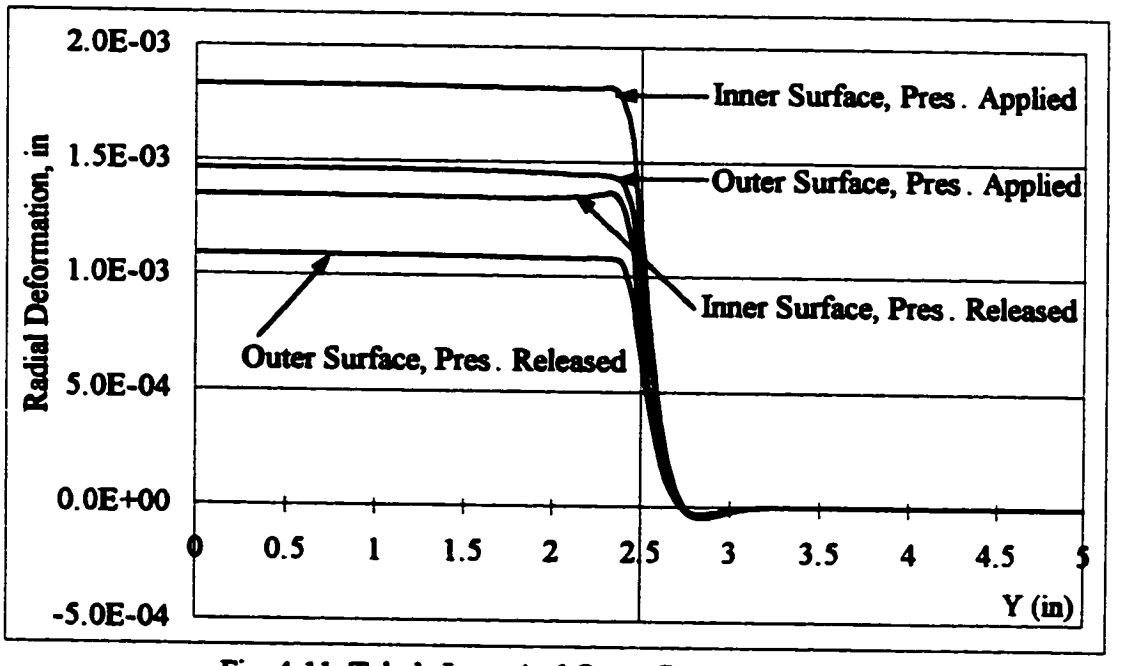

Fig. 4-11: Tube's Inner And Outer Curvatures For The Case c = 0.001 in., E_t = 500000 psi

Recall that the tubesheet thickness is 2.5 in and the expanding pressure is uniformly applied into the tube section embedded into the tubesheet. In Figure 4-11, the pressure is applied on the section extending from Y=0 in. to Y=2.5 in. For clarity, a line corresponding to Y=2.5 in. has been drawn in the figure. As it can be seen from these results, tube surfaces' radial deformations are uniform through out the section extending from the primary side (Y=0 in.) to about Y=2.375 in. This section accommodates 95% of the expanded tube length. A transition zone from the expanded to unexpanded tube sections then starts. For the above case, the transition zone extends from Y=2.375 in. on the expanded portion passing the secondary side (Y=2.5 in.) to about Y=3 in. on the unexpanded portion. Ahead of this point, the tube does not have any radial deformation. Just like the note mentioned in Section 4.3.1 in the illustration of the residual contact pressure, the tube radial deformations computed from the axisymmetric model and listed in table 4-3 above are the uniform deformations take place from the primary side to the point below the secondary side at which the transition zone starts.

Similarly, the axisymmetric model is used to calculate the radial deformations of all the nodes on the tubesheets' hole surface with respect to their axial location. These values are plotted in Figure 4-12. This plot shows the curvature of the tubesheets' hole surface when the full expanding pressure is applied and after releasing the pressure for the same case mentioned above.

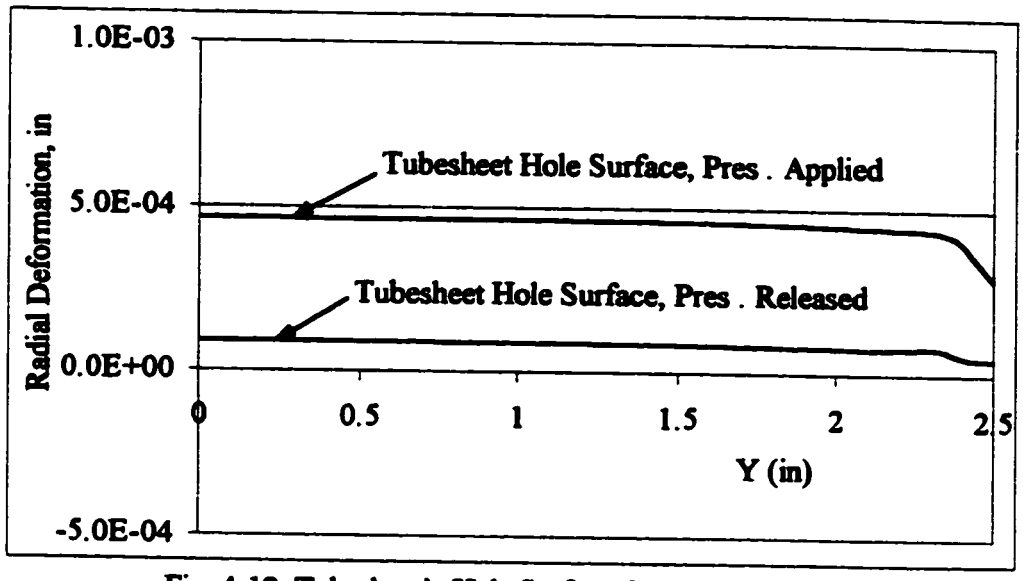

Fig. 4-12: Tubesheet's Hole Surface Curvatures For The Case c = 0.001 in., E_t = 500000 psi

As expected, tubesheet hole surface deformation is compatible with the tube's outer surface deformation, since both the surfaces are in contact. For the above case, tubesheet hole surface deformation is uniform through a length of 2.375 in., which corresponds to 95% of its thickness. However, because of the initial radial clearance, the radial deformation values of the tubesheet's hole surface are less than that of the tube's outer surface. The tube must deform an amount equal to the clearance first before any deformation happening in the tubesheet. After contact, the two surfaces will have the same radial deformation. So, the tubesheets' hole surface radial deformation will be equal to the tube's outer surface radial deformation minus the initial radial clearance. To illustrate this on the above mentioned case, the tube's outer surface radial deformation is found to be 0.00146 in. when the expanding pressure is applied and equal to 0.00109 in. after releasing the pressure. Similarly, tubesheets'

hole surface radial deformations when the pressure is applied and released are 0.000462 in. and 0.0000895 in. respectively. The tube's outer surface radial deformations are obtained by adding the value of the initial radial clearance (0.001 in.) to the tubesheets' hole surface radial deformations.

Table 4-4 illustrates the tubesheet hole surface radial deformations after releasing the expanding pressure. These values are obtained using the axisymmetric model for all the cases covered in the study. Again, the values recorded here are the uniform deformations extending from the primary side to a point below the secondary side (about 95% of the tubesheet thickness). Figure 4-13 is a plot of those deformations as a function of the initial radial clearance.

Table 4-4: Tubesheet Hole Surfaces Radial Deformations (in)

Radial Clearance (in)	Tube Tangent Modulus (psi)		
	0.1×10^6	0.5×10^6	1.0×10^6
0.0000	1.06E-04	1.02E-04	9.79E-05
0.0005	1.05E-04	9.56E-05	8.45E-05
0.0010	1.04E-04	8.95E-05	7.23E-05
0.0015	1.03E-04	8.34E-05	5.99E-05
0.0020	1.02E-04	7.72E-05	4.75E-05
0.0025	1.01E-04	7.10E-05	3.53E-05
0.0030	1.00E-04	6.50E-05	2.31E-05
0.0035	9.90E-05	5.90E-05	1.27E-05
0.0040	9.82E-05	5.30E-05	

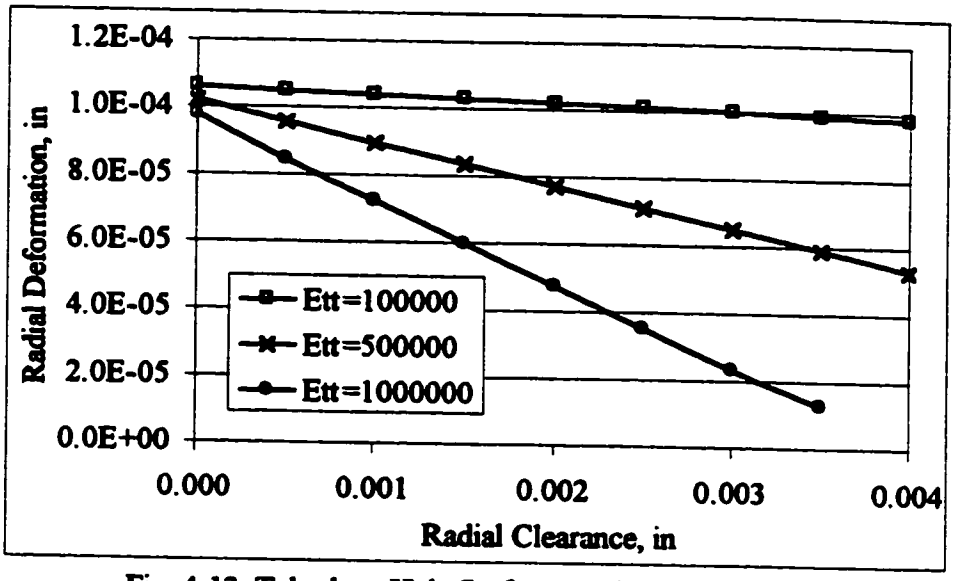

Fig. 4-13: Tubesheet Hole Surfaces Radial Deformations

These results show that the tubesheet hole surface radial deformations decrease linearly with the initial radial clearance for a given tube's tangent modulus. As the clearance increases, more pressure has to be applied into the tube for it to just come in contact with the tubesheet. This implies that less pressure will be exerted on the tubesheet hole surface, since the applied expansion pressure is fixed for all cases in the study. Consequently, less radial deformation occurs in the tubesheet hole surface for large clearance.

As illustrated in Figure 4-14, the radial deformations occurring in the tubesheet hole surfaces as a result of the expansion process are negligible when compared with those of the tube surfaces. This is why the strain hardening level of the tubesheet material was found to have negligible effect on the residual contact pressure. Thus, the

assumption of an elastic-perfectly-plastic material for the tubesheet material was valid.

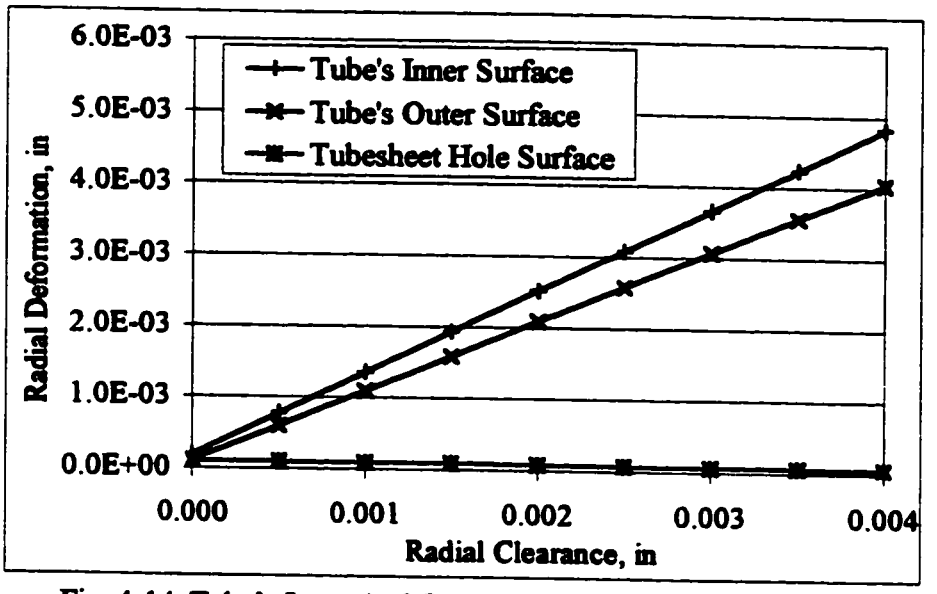

Fig. 4-14: Tube's Inner And Outer And Tubesheet Hole Surfaces Radial Deformations When $E_t = 500000$ psi

4.3.3 Tube Retraction

Tube retraction is the amount of axial deformation of the tube's free end. Because of the Poisson's effect, and as the tube circumference expands due to the applied pressure, tube length will be reduced. Since the tube material volume remains unchanged, therefore the length has to be shortened as the circumference gets larger. Obviously, tube retraction can be read from the axisymmetric model only. The tube retraction amounts, for all the cases covered in this study, are listed in Table 4-5 and plotted in Figure 4-15.

Table 4-5: Tube Retraction (in)

Radial Clearance (in)	Tube Tangent Modulus (psi)		
	0.1×10^6	0.5×10^6	1.0×10^6
0.0005	1.01E-03	1.02E-03	1.03E-03
0.0010	2.57E-03	2.60E-03	2.60E-03
0.0015	4.11E-03	4.14E-03	4.14E-03
0.0020	5.66E-03	5.69E-03	5.68E-03
0.0025	7.19E-03	7.21E-03	7.22E-03
0.0030	8.69E-03	8.73E-03	8.75E-03
0.0035	1.02E-02	1.02E-02	1.03E-02
0.0040	1.16E-02	1.18E-02	

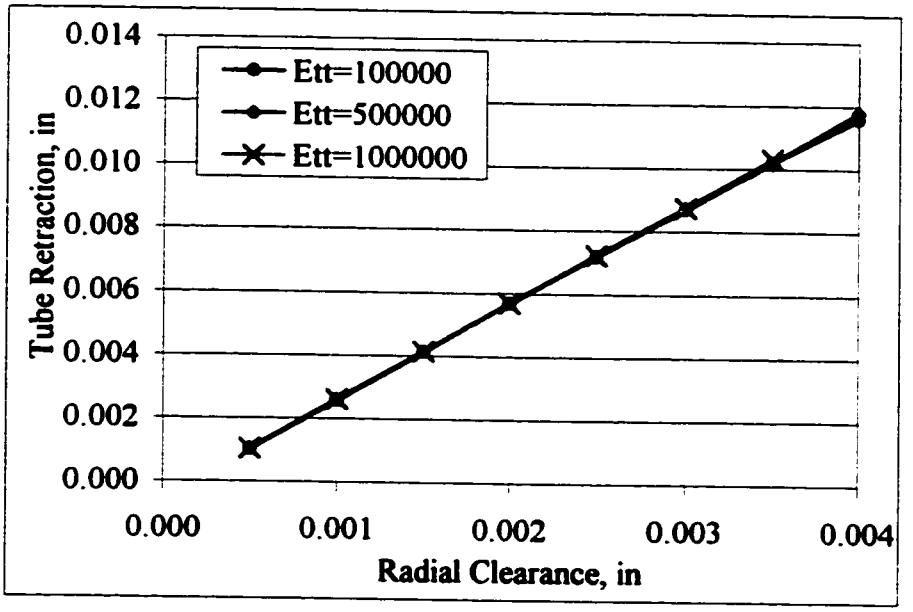

Fig. 4-15: Tube Retraction

It can be seen from Figure 4-15 that the tube retraction is independent of the tube's tangent modulus. For a given initial radial clearance, tube retraction is the same regardless of the tube material.

4.3.4 Frictional Coefficient Effect

The coefficient of friction between two materials is very difficult to be precisely determined. For any given two materials, it could fluctuate based on parameters, such as, surface roughness, humidity and temperature. To have a practical empirical equation, some researchers have assumed unity for the coefficient of friction [2]. Others have assumed some average value for the materials under study [7].

To study the effect of coefficient of friction on the tube-tubesheet joint residual contact pressure, the axisymmetric model for the case of 0.001 in. initial radial clearance and 500000 psi tangent modulus was analyzed using a coefficient of friction other than 0.74, which is the assumed coefficient between the tube and tubesheet materials as described in Chapter 3. The coefficient of friction was varied from 0.1 to 0.9. As far as the residual contact pressure is concerned, the results are all the same as that obtained by assuming 0.74 for the coefficient of friction. As explained by Reinhardt et al [15], this may lead to the conclusion that sticking occurs between the tube and tubesheet once they come in contact. There is no slipping between the two surfaces, so the frictional coefficient does not influence the analysis.

4.3.5 Multi Holes Model

As described in Chapter 3, the model under investigation in this study is a 4.5 × 4.5 in., $2\ ^{7}/_{16}$ in. thick square steel block containing nine holes, from which an equivalent single hole model was derived by estimating its equivalent sleeve diameter. To find how realistic the single hole model is, plane strain analysis on the nine holes model

was performed to compare the results with those presented earlier. However, due to symmetry, only one eighth of the nine hole model was analyzed. Only the results concerning the center hole will be considered; this hole is the joint of interest and the neighboring holes are included to take account of the ligament effect.

Contact pressure distribution as obtained from the plane strain analysis for the case of initial radial clearance of 0.001 in. and tube's tangent modulus of 500000 psi is shown in Figure 4-16.

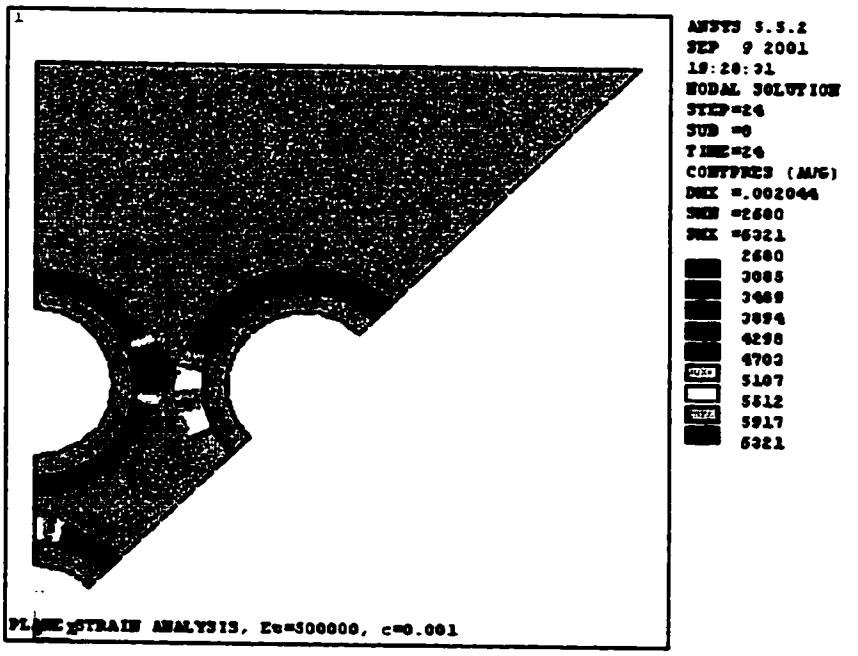

Fig. 4-16: Contact Pressure Distribution For The Case c=0.001 in., E_{tt}=500000 psi

Because of the difference in ligament width around the tube, the residual contact pressure is fluctuating around its circumference. This is one of the reasons why the

equivalent sleeve principle was introduced [11, 13, 15]. For the above case, the residual contact pressure is fluctuating from 5734 psi to 3574 psi with an average value of 4431 psi. The average values of the residual contact pressure and tube's inner and outer surfaces radial deformations obtained from plane strain analysis of the multi hole model having a tube's tangent modulus of 500000 psi are listed in Table 4-6 for selected initial radial clearance.

Table 4-6: Average Contact Pressure And Radial Deformation

Radial Clearance (in)	Contact Pressure (psi)	Tube Inner Surface Radial Deformation (in)	Tube Outer Surface Radial Deformation (in)
0.0005	4555	1.26E-03	9.42E-04
0.0010	4431	1.87E-03	1.41E-03
0.0015	4177	2.49E-03	1.88E-03

4.4 EXPERIMENTAL RESULTS

As stated earlier, an experimental program was conducted to study the tubesheet hole enlargement effect on the tube-to-tubesheet joints strength. The details of the model used in the experimental program are described in Chapter 3. The model is basically a square steel plate with nine holes. Two grooves were machined in each hole as per TEMA standard [1]. To obtain a range of clearances, each tubesheet hole is enlarged with different sizes. Tubes were roller-expanded into the nine holes but final measurements and pull out force were conducted on the center hole only.

Initial dimensions, including the tube inner radius (r_i), tube outer radius (r_o), original tube thickness (t), tubesheet hole radius (R_i), expansion length (L_e) and initial radial clearance (c), used in each experimental test are illustrated in Table 4-7 together with the results obtained from the tests. The results shown in the table are the final tube inner radius after rolling ($r_{i,f}$) and the pull out force (F). The data shown in the table is sorted by the initial radial clearance (c).

Table 4-7: Experimental Data And Results

Test No.	r_i (in)	r_o (in)	t (in)	R_i (in)	L_e (in)	c (in)	$r_{i,f}$ (in)	F (lb)
1	0.2860	0.3750	0.0890	0.3797	1.70	0.0047	0.2938	5938
2	0.2868	0.3745	0.0878	0.3793	1.65	0.0048	0.2942	6228
3	0.2858	0.3745	0.0888	0.3797	1.60	0.0052	0.2948	6108
4	0.2863	0.3745	0.0883	0.3801	1.60	0.0056	0.2952	6441
5	0.2868	0.3745	0.0878	0.3805	1.70	0.0060	0.2961	6248
6	0.2860	0.3750	0.0890	0.3813	1.60	0.0063	0.2967	6881
7	0.2863	0.3745	0.0883	0.3809	1.55	0.0064	0.2966	5863
8	0.2871	0.3744	0.0873	0.3819	1.65	0.0075	0.2970	7147
9	0.2869	0.3743	0.0874	0.3821	1.65	0.0078	0.2978	6782
10	0.2868	0.3743	0.0875	0.3825	1.65	0.0082	0.2998	5798
11	0.2872	0.3743	0.0871	0.3831	1.67	0.0088	0.2997	6099
12	0.2864	0.3743	0.0879	0.3844	1.66	0.0101	0.3001	7088
13	0.2853	0.3755	0.0903	0.3872	1.60	0.0117	0.3031	6537
14	0.2873	0.3743	0.0870	0.3862	1.64	0.0119	0.3035	7340
15	0.2871	0.3744	0.0873	0.3864	1.70	0.0120	0.3051	7973
16	0.2870	0.3741	0.0871	0.3864	1.70	0.0123	0.3052	6421
17	0.2865	0.3750	0.0885	0.3874	1.75	0.0124	0.3041	5947
18	0.2866	0.3743	0.0877	0.3874	1.43	0.0132	0.3049	6308

As shown from the finite element analysis, the higher the initial radial clearance, the weaker the tube-to-tubesheet joint strength, providing that all conditions are the same. However, Table 4-7 shows that the pull out force, which is a measure of the joint strength, does not confirm this fact. As the clearance increases, the force is fluctuating up and down. This is due to the possible variations in the conditions during roller expansion process, such as expanding tool, length and power. Nevertheless, the fact that the initial radial clearance is not affecting the measured pull out force is in agreement with that of Fisher et al [26] who stated that the oversize holes do not necessarily affect the roller expanded joints strength, that is, if the joints are rolled according to the enlarged and oversized tubesheet hole and can be rolled without damaging the tube metal.

CHAPTER 5

EFFECT OF INITIAL RADIAL CLEARANCE ON THE JOINT STRENGTH

5.1 INTRODUCTION

Recall that the main objective of this study is to investigate the effect of initial radial clearance on the expanded tube-to-tubesheet joint strength. For this purpose, the finite element code (ANSYS) has been used to compute the residual contact pressure between the tube and tubesheet at different levels of initial radial clearance and tube tangent modulus. All other parameters, such as dimensions, expansion pressure, expansion length, frictional coefficient, yield strength, modulus of elasticity and Poisson's ratio were fixed. Additional results including radial deformations and tube retraction were also computed at the different levels of clearance and tangent modulii. Computations were conducted using

axisymmetric, plane stress and plane strain models. Focus has been given to the axisymmetric model, since it has been widely used in the past. Planar models were given less attention. Planar models were brought here for the purpose of comparison with the axisymmetric model. Nevertheless, results computed from the three models are comparable. The same trend of linearly decreasing the residual contact pressure with the initial radial clearance for a given tube tangent modulus was observed in the three models with minor differences in the results. Similar observation was noticed on the radial deformation results. All the three models resulted the same trend of linearly increasing the inner and outer tube surfaces radial deformations with the clearance even if minor difference in the resulted values were observed.

5.2 RESIDUAL CONTACT PRESSURE

The results obtained from the axisymmetric, plane stress and plane strain models presented in Section 4.3.1 show that the residual contact pressure varies linearly with the initial radial clearance for any given tube tangent modulus. As the tangent modulus increases, the residual contact pressure becomes more sensitive to the initial radial clearance.

Following the parametric study conducted by Allam et al [11], the variables will be nondimensionlized to generalize the analysis. The pressure will be normalized by the yield strength, the clearance by the tube's outer radius and the tangent modulus by the modulus of elasticity. The residual contact pressure results for the range of initial radial

clearances and tangent modulii covered in this study obtained from the axisymmetric model and illustrated in Table 4-2 will be utilized to generate the nondimensionl parametric analysis.

Recall that the analytical calculation was based on the assumption of elastic-perfectly-plastic material ($E_t = 0$) and the initial radial clearance was neglected ($c = 0$). As seen from Figure 4-8, both E_t and c have a negative effect on the residual contact pressure. To account for their effect, a reduction factor has to be introduced into the analytical solution. As shown in Section 4.2.1, the calculated residual contact pressure for the dimensions and material used in this study is 4434 psi. The reduction factor for each case covered in this study can then be found by dividing the residual contact pressure obtained from the finite element analysis by 4434 psi. The reduction factors thus obtained, by using the results of the axisymmetric model illustrated in Table 4-2, are shown in Table 5-1.

Table 5-1: Reduction Factor

Radial Clearance (in)	Tube Tangent Modulus (psi)		
	0.1×10^6	0.5×10^6	1.0×10^6
0.0000	1.0054	0.9738	0.9364
0.0005	0.9921	0.9127	0.8175
0.0010	0.9811	0.8566	0.7070
0.0015	0.9702	0.8006	0.5977
0.0020	0.9585	0.7449	0.4892
0.0025	0.9475	0.6897	0.3816
0.0030	0.9366	0.6349	0.2745
0.0035	0.9258	0.5807	0.1678
0.0040	0.9147	0.5262	

The normalized clearance is then multiplied by the normalized tangent modulus to have a non-dimensional parameter ($\frac{c}{r_o} \times \frac{E_u}{E_t}$) that includes both variables under study (c & E_u). The reduction factor due to grouping c and E_u for each case is plotted with respect to this non-dimensional parameter in Figure 5-1.

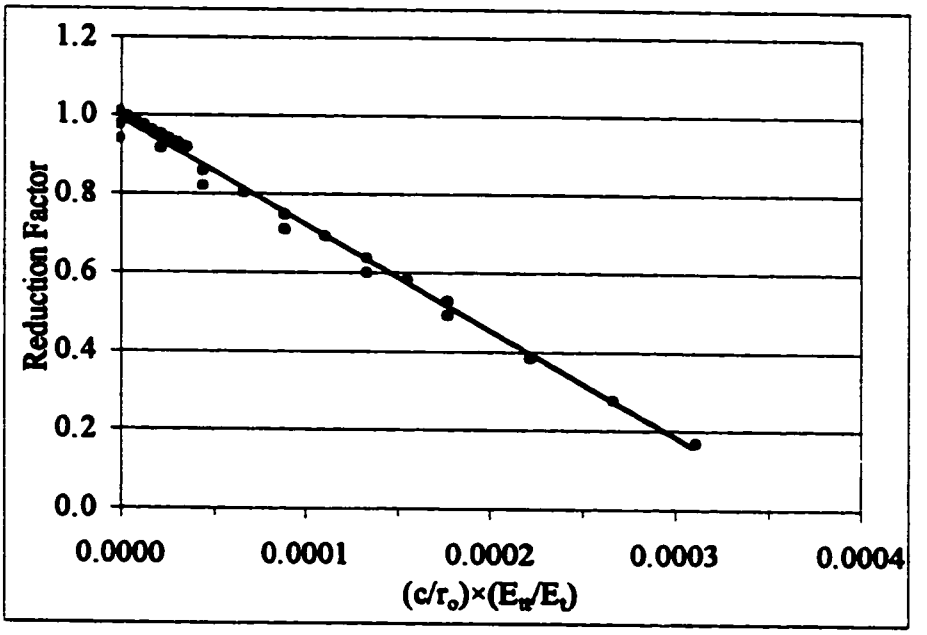

Fig. 5-1: Reduction Factor of Combined Clearance and Tangent Modulus Effect

The figure shows a linear relationship between the reduction factor and the non-dimensional parameter ($\frac{c}{r_o} \times \frac{E_u}{E_t}$). The line has a negative slope of 2770 and intersects the ordinate at the value of unity. The variation of the reduction factor with ($\frac{c}{r_o} \times \frac{E_u}{E_t}$) can be expressed by the following relationship:

$$z_{(c \& E_t)} = 1.0 - 2770 \frac{c}{r_o} \frac{E_t}{E_t} \qquad (5\text{-}1)$$

As explained earlier, the initial radial clearance value does not affect the residual contact pressure if an elastic-perfectly-plastic material is assumed. This means that the reduction factor will be equal to 1.0 for this case. Equation (5-1) will successfully give this result when E_t is set to zero. However, this equation will also give a unity reduction factor when the initial radial clearance is zero, regardless of the tangent modulus value. This is not true. As the tangent modulus level increases, the tube material becomes harder and exerts more resistance to the applied pressure. Since the applied pressure is fixed for all the cases in the study, resultant pressure on the tubesheet hole surface will be less because more pressure has been taken by the tube. As a result, the residual contact pressure will decrease as the level of tube tangent modulus increases.

To make the necessary correction in equation (5-1), the effect of the tangent modulus on the residual contact pressure was studied for the case of zero initial radial clearance. An axisymmetric model having zero clearance was generated and the tangent modulus was changed in the range of 0 to 10×10^6 psi. Resultant residual contact pressures for each case are shown in Table 5-2.

Again, The reduction factor is found by dividing the residual contact pressure obtained above by 4434 psi, and the tangent modulus (E_t) will be nondimensionlized by dividing it by the tube modulus of elasticity (E_t). The reduction factor for each case is tabulated and

plotted with respect to the non-dimensional parameter ($\frac{E_a}{E_t}$) in Table 5-3 and Figure 5-2 respectively.

Table 5-2: Residual Contact Pressure When Initial Clearance is Zero

E_a (psi)	0	0.1×10^6	0.5×10^6	1×10^6	2×10^6	5×10^6	10×10^6
Contact Pressure (psi)	4494	4458	4318	4152	3840	3060	2100

Table 5-3: Reduction Factor Due to Tangent Modulus Only

$\frac{E_a}{E_t}$	0.0000	0.0033	0.0167	0.0333	0.0667	0.1667	0.3333
Reduction Factor	1.0135	1.0054	0.9738	0.9364	0.8660	0.6901	0.4736

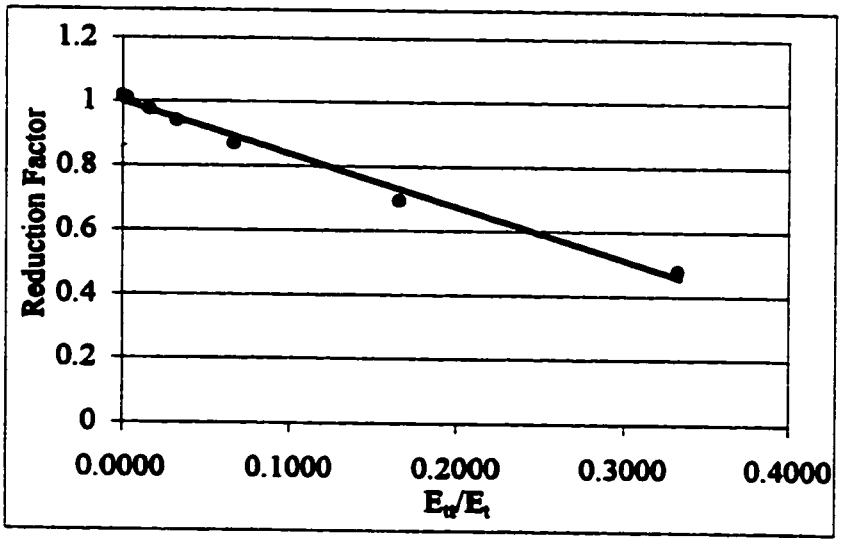

Fig. 5-2: Reduction Factor Due to Tangent Modulus Only

A linear relationship exists between the reduction factor and the non-dimensional parameter ($\frac{E_u}{E_t}$) and again the line intersects the ordinate at a value of 1.0. This line has a negative slope of 1.7, which means that the reduction factor on the residual contact pressure of a tube-tubesheet joint having zero initial radial clearance is given by:

$$z_{(E_u)} = 1.0 - 1.7\frac{E_u}{E_t} \tag{5-2}$$

To arrive at a single formula for estimating the reduction factor applicable for any combination of the initial radial clearance and tangent modulus, the reduction factor due to E_u alone is added to the reduction factor due to grouping c and E_u for each case. The resulting values are plotted with respect to the non-dimensional parameter ($\frac{c}{r_o}\times\frac{E_u}{E_t}$) in Figure 5-3.

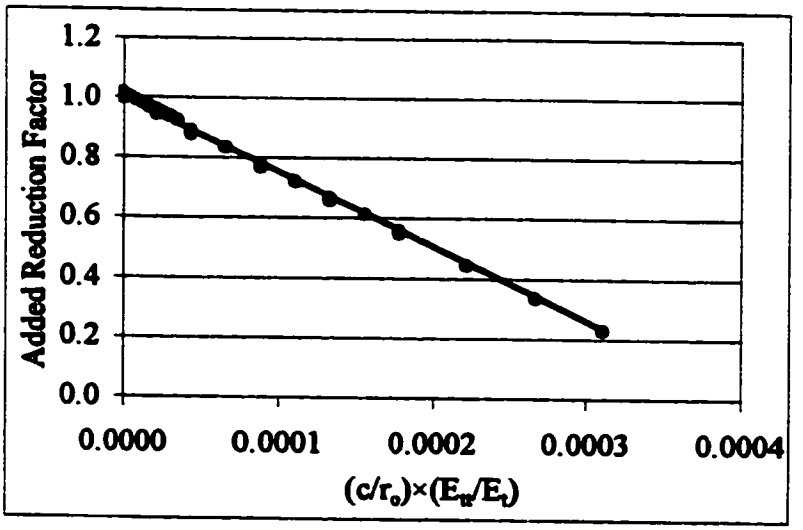

Fig. 5-3: Added Reduction Factor

This plot shows a linear relationship intersecting the ordinate at a value of 1.0 and having a negative slope of 2500. Consequently, the reduction factor (z) due to both the initial radial clearance (c) and tangent modulus (E_u) can be expressed as:

$$z = 1.0 - 2500\frac{c}{r_o}\frac{E_u}{E_t} - 1.7\frac{E_u}{E_t} \tag{5-3}$$

This relation is a more general one than equation (5-1). It would give the reduction factor for any given combination of initial radial clearance and tube's tangent modulus to be then multiplied with the calculated residual contact pressure explained in Section 4.2.1. When both c and E_u are equal to zero, equation (5-3) will yield a reduction factor of unity. Moreover, it will successfully give the reduction factor value for the case of zero clearance and any given tube's tangent modulus value, unlike the case of equation (5-1).

The reduction factor given by equation (5-3) is of a similar form as equation (2-13) proposed by Allam et al [11]. However, for an elastic-perfectly-plastic tube having zero clearance with the tubesheet hole, equation (2-13) will give a reduction factor of 0.91745, while it should be 1.0. The residual contact pressures as found from the finite element analysis on the axisymmetric model and the analytical calculations of the reduction factor, and thus the residual contact pressure, for all the cases covered in this study by the use of equation (2-13) are presented in Table 5-4. For comparison, the percentage difference between the finite element results and the values calculated from equation (2-13) is included in the table for each case. The difference becomes very large as the radial clearance increases especially with the higher tube's tangent modulus. This is possibly

Table 5-4: Comparison of FEM Results With Those Given by Available Model

Tube Tangent Modulus (psi)	Radial Clearance (in)	Contact Pres. From FEM (psi)	Equation (2-13)		% Diff. in Contact Pressure
			Reduction Factor	Resultant Contact Pressure (psi)	
$0.1x10^6$	0.0000	4458	0.9125	4046	9.24%
	0.0005	4399	0.9001	3991	9.27%
	0.0010	4350	0.8878	3936	9.51%
	0.0015	4302	0.8754	3881	9.77%
	0.0020	4250	0.8630	3827	9.96%
	0.0025	4201	0.8507	3772	10.22%
	0.0030	4153	0.8383	3717	10.50%
	0.0035	4105	0.8259	3662	10.79%
	0.0040	4056	0.8135	3607	11.06%
$0.5x10^6$	0.0000	4318	0.8927	3958	8.33%
	0.0005	4047	0.8309	3684	8.97%
	0.0010	3798	0.7690	3410	10.22%
	0.0015	3550	0.7072	3136	11.67%
	0.0020	3303	0.6453	2861	13.37%
	0.0025	3058	0.5835	2587	15.40%
	0.0030	2815	0.5216	2313	17.84%
	0.0035	2575	0.4598	2039	20.83%
	0.0040	2333	0.3979	1764	24.37%
$1.0x10^6$	0.0000	4152	0.8680	3849	7.31%
	0.0005	3625	0.7443	3300	8.96%
	0.0010	3135	0.6206	2752	12.23%
	0.0015	2650	0.4969	2203	16.86%
	0.0020	2169	0.3732	1655	23.71%
	0.0025	1692	0.2495	1106	34.62%
	0.0030	1217	0.1258	558	54.17%
	0.0035	744	0.0021	9	98.75%

because the reduction resulting from the tube tangent modulus alone was not added to that of the combined effect of clearance and tangent modulus in deriving the final factor of the non-dimensional parameter $(\frac{c}{r_o} \times \frac{E_a}{E_t})$ in Equation (2-13). If this was the case, it means that the effect of tangent modulus was counted twice. This explains the divergence of solution as the tube tangent modulus increases.

5.3 TUBE WALL REDUCTION

In the industry, tube wall reduction is a very important measure and it may be a basis for rejecting equipment if the tube wall has reduced more than a pre-specified value. Tube wall reduction amount is also used to specify the rolling torque or expansion pressure to be applied into the tube for a given tube-tubesheet joint geometry and material. The torque or pressure is determined by first running expansion tests each with different torque or pressure and measuring the tube wall reduction each time. The rolling torque or expansion pressure that will give the pre-specified tube wall reduction value is then fixed to perform expansion on the real tubesheet. Normally, tube wall reduction caused by roller expansion is 3 to 12%, whereas it is 1 to 3% when the expansion is performed by applying uniform pressure [2].

Since it is not practical to measure the wall thickness after expansion, tube wall reduction is calculated by the following formula:

$$WR = \frac{(r_{i,f} - r_i) - (R_i - r_o)}{(r_o - r_i)} \times 100 \qquad (5\text{-}4)$$

where, WR = Tube wall reduction (%)

r_i = Tube inner radius before expansion

$r_{i,f}$ = Tube inner radius after expansion

r_o = Tube outer radius before expansion

R_i = Tubesheet hole radius before expansion

The wall reduction calculated by equation (5-4) is named "apparent wall reduction" because it does not account for the radial ligament deformation. Only the inner tube radius after expansion needs to be measured. However, since the tube radius can not be read directly from the finite element code, it would be more practical to express equation (5-4) in terms of radial deformation. By doing so, tube wall reduction formula is re-written in the following form:

$$WR = \frac{U_{ri} - c}{t} \times 100 \qquad (5\text{-}5)$$

where, U_{ri} = Radial deformation of the tube's inner surface

c = Initial radial clearance

t = Initial tube wall thickness

By knowing the radial deformation of the tube's inner surface, the percentage tube wall reduction can then be easily calculated from equation (5-5). Making use of Table 4-3, which lists the tube's inner surface radial deformation for all the cases covered in this study, percentage tube wall reductions are calculated and listed in Table 5-5. Figure 5-4 is a plot of the percentage tube wall reduction for the three levels of tube's tangent modulus.

Table 5-5: Percentage Tube Wall Reduction

Radial Clearance (in)	AXISYMMETRIC			PLANE STRESS			PLANE STRAIN		
	Tube Tangent Modulus (psi)			Tube Tangent Modulus (psi)			Tube Tangent Modulus (psi)		
	$0.1x10^6$	$0.5x10^6$	$1.0x10^6$	$0.1x10^6$	$0.5x10^6$	$1.0x10^6$	$0.1x10^6$	$0.5x10^6$	$1.0x10^6$
0.0000	0.20%	0.20%	0.19%	0.31%	0.28%	0.25%	0.20%	0.19%	0.19%
0.0005	0.33%	0.31%	0.29%	0.44%	0.39%	0.35%	0.37%	0.35%	0.33%
0.0010	0.42%	0.40%	0.36%	0.53%	0.48%	0.42%	0.54%	0.51%	0.48%
0.0015	0.52%	0.49%	0.44%	0.63%	0.56%	0.49%	0.71%	0.67%	0.62%
0.0020	0.62%	0.58%	0.52%	0.74%	0.63%	0.54%	0.88%	0.83%	0.77%
0.0025	0.71%	0.66%	0.60%	0.83%	0.71%	0.62%	1.05%	0.99%	0.91%
0.0030	0.82%	0.75%	0.68%	0.93%	0.79%	0.70%	1.22%	1.15%	1.05%
0.0035	0.91%	0.84%	0.76%	1.03%	0.87%	0.78%	1.38%	1.30%	1.20%
0.0040	1.01%	0.93%		1.12%	0.95%		1.55%	1.46%	

It is noticeable from Figure 5-4 that the tube wall reduction resulting from the axisymmetric and plane stress models are close to each other, while that from plane strain model is deviating. A similar observation was noted on the tube's inner surface radial deformation results, Section 4.3.2. However, a higher degree of deviation between the plane strain model and the other two models is taking place on the wall reduction results

than it was on the tube's inner surface radial deformation, see Figure 4-9. This means that the tube wall reduction is highly sensitive to its surface's radial deformation.

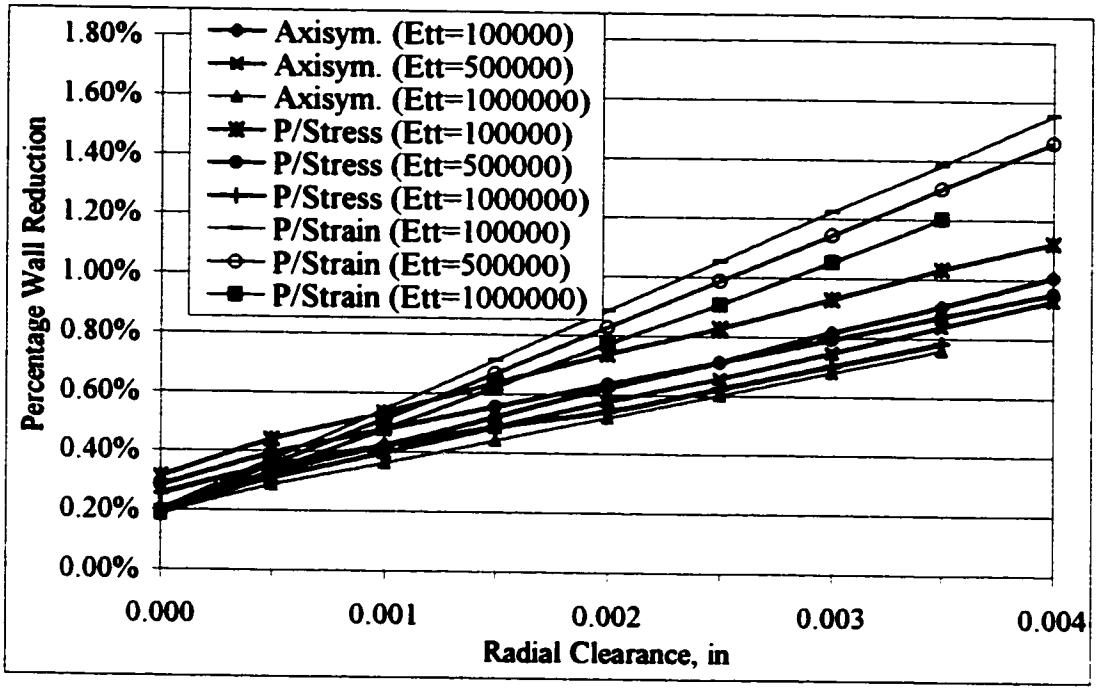

Fig. 5-4: Percentage Tube Wall Reduction

In addition, as it was noticed in the tube's surfaces radial deformation, the tube wall reduction decreases as the tangent modulus increases and, certainly, it increases as the initial radial clearance increases. In the range of initial radial clearances (c) and tube's tangent modulus (E_t) covered in this study, the maximum tube wall reduction, which will be for the case having the highest clearance and lowest tangent modulus, was 1.55% resulting from the plane strain analysis. An axisymmetric analysis of the same case resulted in a wall reduction of 1.01% only. This value is way below the normal maximum acceptable percentage wall reduction, which is 3% for uniformly expanded tube. This

means that more initial clearance could still be acceptable. Alternatively, higher expansion pressure, limited to the plastic limit of the tube ($(2/\sqrt{3})\sigma_{yt}$), may be applied to get a stronger joint while the percentage tube wall reduction will still be satisfactory.

To acquire a mathematical relation for estimating the percentage tube wall reduction, it may be more feasible to establish an equation for estimating the tube's inner surface radial deformation and then, by the help of equation (5-5), the wall reduction will be calculated. To achieve this goal, all variables involved were nondimesionalized for a more general form. Following the same procedure for the residual contact pressure above, the tube's inner surface radial deformation (U_{ri}) and the initial radial clearance (c) are normalized with the initial tube's inner radius (r_i) and the tangent modulus (E_α) with the modulus of elasticity (E_t). The axisymmetric results of the tube's inner surface deformation shown in Table 4-3 are used to generate the nondimensional values for this analysis; the results are listed in Table 5-6. When plotting $(\frac{U_{ri}}{r_i})$ with respect to $(\frac{c}{r_i})$ for all the values of $(\frac{E_\alpha}{E_t})$, result is a straight line. This relationship is represented by the curve marked (Total) in Figure 5-5. This may imply that U_{ri} is a function of c only. In other words, E_α value has no effect on U_{ri}. This statement is not true. In fact, the effect of c on U_{ri} is much bigger than the effect of E_α, which makes it very dominant.

To identify the effect of the tube's tangent modulus on the tube's inner surface radial deformation, it was separately studied for the case of zero initial radial clearance. Results were nondimesionalized and plotted in Figure 5-6.

Table 5-6: Normalized Tube's Inner Surface Radial Deformations (U_{ri}/r_i)

$\frac{c}{r_i}$	E_s/E_t		
	0.00333	0.01667	0.03333
0.00000	0.00062	0.00060	0.00058
0.00175	0.00275	0.00270	0.00263
0.00349	0.00479	0.00472	0.00461
0.00524	0.00685	0.00674	0.00660
0.00699	0.00891	0.00877	0.00859
0.00873	0.01093	0.01076	0.01058
0.01048	0.01299	0.01278	0.01257
0.01222	0.01502	0.01481	0.01457
0.01397	0.01708	0.01684	

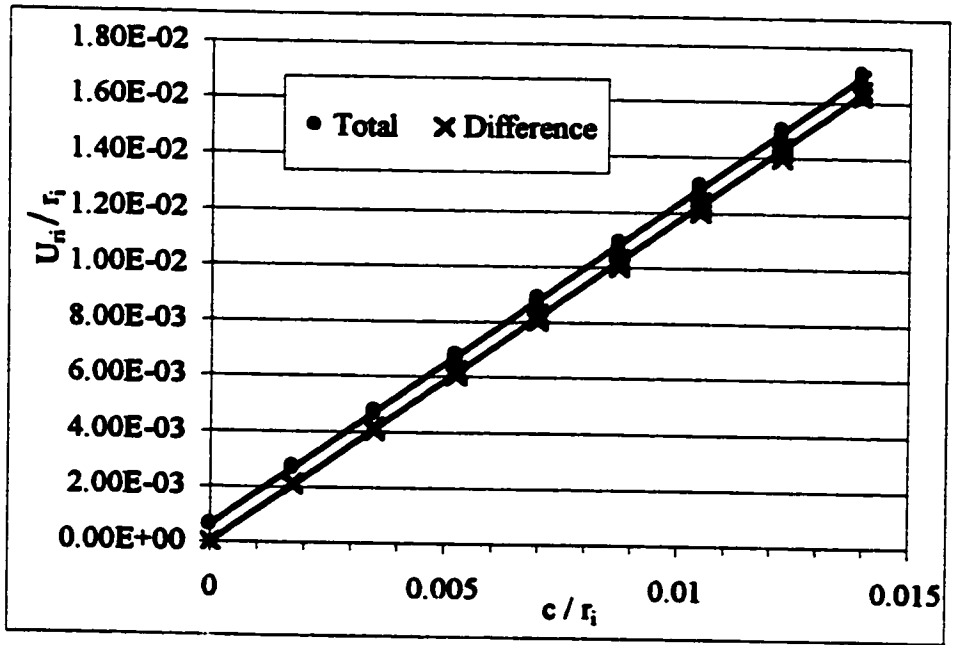

Fig. 5-5: Normalized Tube's Inner Surface Radial Deformations (U_{ri}/r_i) vs. Normalized Clearance (c/r_i)

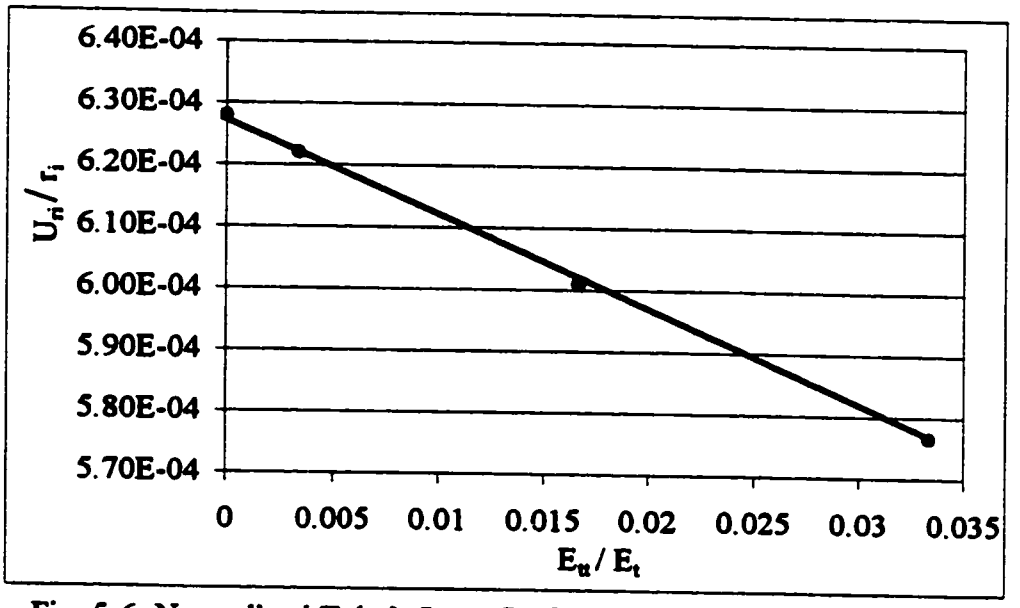

Fig. 5-6: Normalized Tube's Inner Surface Radial Deformations (U_{ri}/r_i) vs. Normalized Tangent Modulus (E_{tt}/E_t)

From Figure 5-6, one can deduce that the tube's inner surface radial deformation for the case of zero initial radial clearance is given by:

$$\left(\frac{U_{ri}}{r_i}\right)_{E_{tt}} = 0.000628 - 0.00156\frac{E_{tt}}{E_t} \qquad (5\text{-}6)$$

Now, the radial deformation due to E_{tt}, given by equation (5-6), is subtracted from the total deformation shown in Table 5-6. The results are illustrated by the curve titled "Difference" in Figure 5-5. This plot is a straight line intersecting the origin and has a slope of 1.18. Therefore, a practical equation for estimating the tube's inner surface radial deformation can be written as follows:

$$\frac{U_{ri}}{r_i} = 0.000628 - 0.00156\frac{E_s}{E_t} + 1.18\frac{c}{r_i} \qquad (5\text{-}7)$$

The combination of equations (5-5) and equations (5-7) allows the calculation of the percentage tube wall reduction for a given initial radial clearance (c) and tube tangent modulus (E_s).

5.4 TUBE THINNING

Tube thinning is another way to look at the reduction in the tube wall thickness due to the expansion process. It is the difference between the original tube wall thickness and that after expansion. The final tube wall thickness is the difference between the final outer and inner tube radii. Since, as stated earlier, tube radii can not be read directly from the finite element code, tube thinning calculation will be more handy if it is expressed in terms of the radial deformations. When subtracting the final tube wall thickness $\{(r_o + U_{ro}) - (r_i + U_{ri})\}$ from the original thickness $(r_o - r_i)$, result will be just $(U_{ri} - U_{ro})$. So, tube thinning is basically the difference between the tube inner and outer surfaces radial deformations. Using Table 4-3, tube thinning amounts for all the cases covered in this study are calculated and listed in Table 5-7. Figure 5-7 is a plot of the percentage tube thinning as calculated from the following formula:

$$TT = \frac{U_{ri} - U_{ro}}{t} \times 100 \qquad (5\text{-}8)$$

where, TT = Tube thinning (%)

U_{ri} = Tube's inner surface radial deformation

U_{ro} = Tube's outer surface radial deformation

t = Tube thickness

Table 5-7: Tube Thinning (in)

Radial Clearance (in)	AXISYMMETRIC			PLANE STRESS			PLANE STRAIN		
	Tube Tangent Modulus (psi)			Tube Tangent Modulus (psi)			Tube Tangent Modulus (psi)		
	$0.1x10^6$	$0.5x10^6$	$1.0x10^6$	$0.1x10^6$	$0.5x10^6$	$1.0x10^6$	$0.1x10^6$	$0.5x10^6$	$1.0x10^6$
0.0000	7.20E-05	6.95E-05	6.67E-05	1.51E-04	1.34E-04	1.17E-04	7.21E-05	6.98E-05	6.69E-05
0.0005	1.83E-04	1.76E-04	1.69E-04	2.65E-04	2.39E-04	2.16E-04	2.24E-04	2.17E-04	2.09E-04
0.0010	2.70E-04	2.59E-04	2.48E-04	3.49E-04	3.20E-04	2.90E-04	3.75E-04	3.64E-04	3.52E-04
0.0015	3.57E-04	3.44E-04	3.30E-04	4.38E-04	4.00E-04	3.62E-04	5.27E-04	5.11E-04	4.94E-04
0.0020	4.43E-04	4.28E-04	4.11E-04	5.29E-04	4.78E-04	4.34E-04	6.78E-04	6.58E-04	6.35E-04
0.0025	5.30E-04	5.12E-04	4.92E-04	6.18E-04	5.56E-04	5.11E-04	8.28E-04	8.05E-04	7.77E-04
0.0030	6.18E-04	5.97E-04	5.72E-04	7.06E-04	6.34E-04	5.95E-04	9.77E-04	9.50E-04	9.17E-04
0.0035	7.05E-04	6.81E-04	6.54E-04	7.94E-04	7.10E-04	6.76E-04	1.13E-03	1.10E-03	1.06E-03
0.0040	7.92E-04	7.65E-04		8.82E-04	7.86E-04		1.27E-03	1.24E-03	

Figure 5-7 shows that the tube thinning varies linearly with the initial radial clearance. Here again, the axisymmetric and plane stress results are very close while the plane strain results are different. Obviously, the effect of tube's tangent modulus and initial radial clearance on the tube thinning would be similar to their effect on the tube wall reduction. Tube wall thinning decreases as the tangent modulus increases and increases as the initial radial clearance increases.

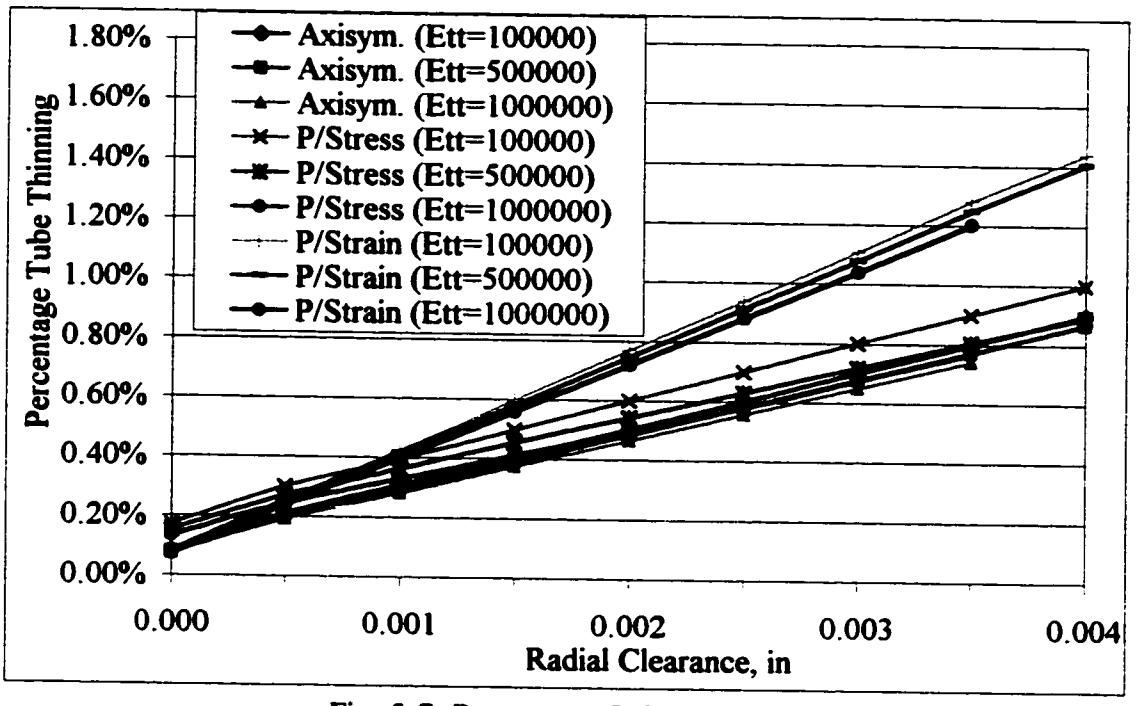

Fig. 5-7: Percentage Tube Thinning

The percentage tube wall thinning results given by equation (5-8) is always less than the calculated percentage tube wall reduction given by equation (5-5). This is because of the definition of each term. Tube wall thinning is defined by the difference between the tubes' inner and outer surfaces radial deformations. On the other hand, tube wall reduction is defined by the difference between the tube's inner surface radial deformation and the initial radial clearance. In the expansion process, tube's outer surface will always deform radialy an amount equal to the radial clearance to come in contact with the tubesheet hole surface. More deformation has to take place then to acquire tight joints, as discussed in Chapter 2. This means that the resultant tube's outer surface radial deformation will always be more than the radial clearance. Consequently, the calculated tube wall thinning is less than the tube wall reduction. For example, for the case of the highest clearance and

lowest tangent modulus, tube thinning resulting from the plane strain analysis is 1.44%, compared to 1.55% tube wall reduction. An axisymmetric analysis on the same case resulted a tube thinning of 0.90%, while the wall reduction is 1.01%.

Analytical estimation of the percentage tube wall thinning would require the knowledge of the tube's inner and outer surfaces radial deformation. A correlation for estimating the tube's inner surface radial deformation has been already established (equation 5-7). A similar equation for estimating the tube's outer surface radial deformation could be established by following the same procedure outlined above. This time, the tube's outer surface radial deformation (U_{ro}) and the initial radial clearance (c) are normalized with the initial tube's outer radius (r_o) and the tangent modulus (E_{tt}) with the modulus of elasticity (E_t). The axisymmetric results of the tube's outer surface deformation shown in Table 4-3 are nondimensionalized and listed in Table 5-8. The plot of $(\frac{U_{ro}}{r_o})$ with respect to $(\frac{c}{r_o})$ for all values of $(\frac{E_{tt}}{E_t})$ is a straight line (curve marked Total in Figure 5-8). The same explanation stated earlier is valid here, the effect of c on U_{ro} is much bigger than the effect of E_{tt}, which make it very dominant.

The tube's outer surface radial deformations for the case of zero initial radial clearance while varying E_{tt} are recorded, normalized and then plotted in Figure 5-9.

Table 5-8: Normalized Tube's Outer Surface Radial Deformations (U_{ro}/r_o)

$\frac{c}{r_o}$	E_o/E_t		
	0.00333	0.01667	0.03333
0.00000	0.00028	0.00027	0.00026
0.00134	0.00162	0.00159	0.00156
0.00267	0.00294	0.00291	0.00286
0.00401	0.00427	0.00422	0.00417
0.00534	0.00561	0.00555	0.00547
0.00668	0.00694	0.00686	0.00678
0.00801	0.00828	0.00820	0.00806
0.00935	0.00961	0.00951	0.00937
0.01068	0.01095	0.01081	

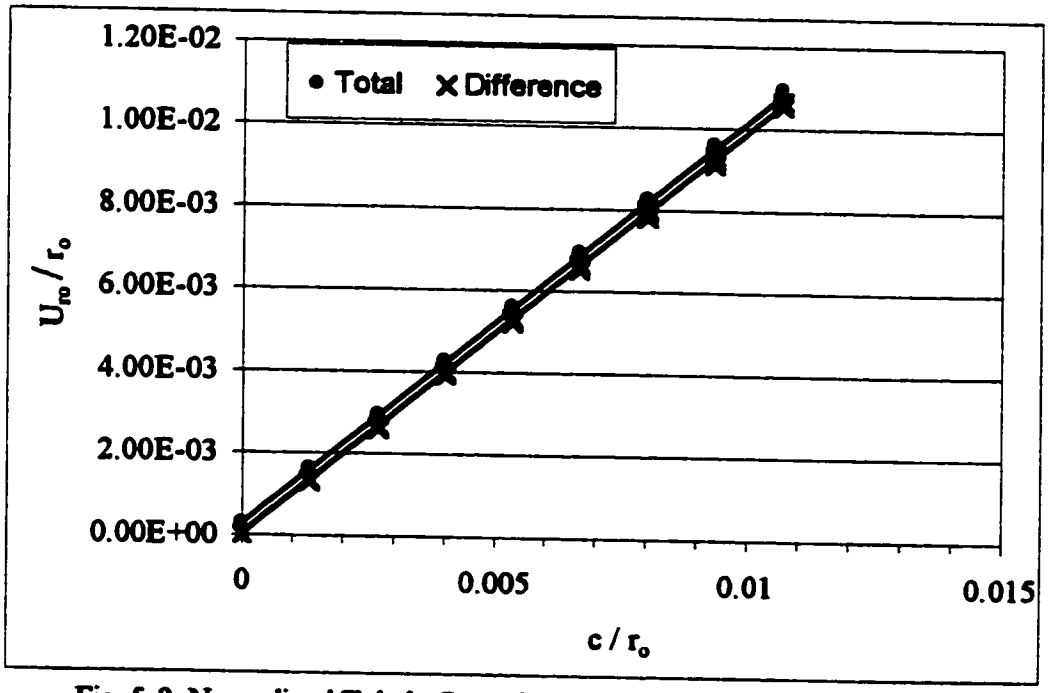

Fig. 5-8: Normalized Tube's Outer Surface Radial Deformations (U_{ro}/r_o) vs. Normalized Clearance (c/r_o)

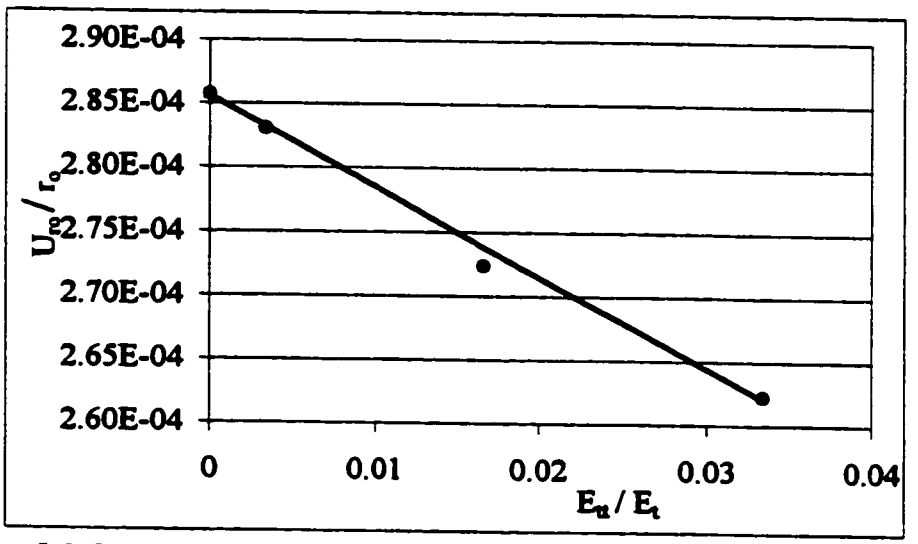

Fig. 5-9: Normalized Tube's Outer Surface Radial Deformations (U_{ro}/r_o) vs. Normalized Tangent Modulus (E_u/E_t)

From Figure 5-9, the tube's outer surface radial deformation can be expressed as:

$$\left(\frac{U_{ro}}{r_o}\right)_{E_u} = 0.000286 - 0.00072\frac{E_u}{E_t} \tag{5-9}$$

The resultant $(\frac{U_{ro}}{r_i})$ values after subtracting their values due to E_u, given by equation (5-9), are plotted with respect to $(\frac{c}{r_i})$ in Figure 5-8 (curve marked Difference). This plot is a straight line intersecting the origin and has a slope of 0.9863. Therefore, a practical equation for estimating the tube's outer surface radial deformation will be the following:

$$\frac{U_{ro}}{r_o} = 0.000286 - 0.00072\frac{E_u}{E_t} + 0.9863\frac{c}{r_o} \tag{5-10}$$

Now, the percentage tube wall thinning can be calculated from equation (5-8) after estimating the tube's inner and outer surfaces radial deformations through the use of equations (5-7) and (5-10) respectively.

5.5 TUBE RETRACTION

As was seen in Section 4.3.3, tube retraction is independent of the tube's tangent modulus but highly dependent on the initial radial clearance. Because of the applied pressure, tube circumference will expand until it comes in contact with the tubesheet hole surface. For a given clearance, the circumferential expansion is the same regardless of the tube tangent modulus. As a result, and since the Poisson's ratio is the same for all the cases, tube retraction will be independent of the tube's tangent modulus.

Tube retraction is linearly related with the clearance as seen in Figure 4-15. This linear relationship has a slope of about 3. This means that the increase in the tube retraction is three times the increase in the radial clearance. For example, an increase of clearance from 0.002 in. to 0.0035 in. would result an increase in the tube retraction equal to 3×(0.0035-0.002) in., which is 0.0045 in. From Table 4-5, tube retraction amount for the case of $E_t = 0.5\times10^6$ psi and c = 0.002 in. is 0.00569 in. and that when c = 0.0035 in. is 0.0102 in. The difference in the tube retraction is (0.0102-0.00569) which is equal to 0.00451 in. This is the same amount as was calculated from the line slope above.

5.6 MULTI-HOLES MODEL

Recalling that the main objective of this study is to investigate the effect of initial radial clearance on the joint strength of the tube-to-tubesheet assembly on the heat exchanger equipments. The real tubesheet assemblies have multi holes that each affects the other. However, for simplification, the study was performed on an equivalent single hole model. For comparison purposes, a few selected cases were analyzed on the multi hole model and results are presented in Table 4-6. Those results were compared with the respective results obtained from the equivalent axisymmetric model on the same cases. Treating the results of the multi hole model as the baseline, the percentage difference between the multi hole and axisymmetric models on each result is listed in Table 5-9.

Table 5-9: Percentage Difference in Results of Multi Holes And Axisymmetric Models

Radial Clearance (in)	Contact Pressure	Tube Inner Surface Radial Deformation	Tube Outer Surface Radial Deformation
0.0005	11.15%	38.73%	36.73%
0.0010	14.29%	27.81%	22.70%
0.0015	15.01%	22.49%	15.96%

The differences in the contact pressure results obtained from the multi holes and axisymmetric models are acceptable, but those of the tube radial deformations are fairly high. This depends on the approach used in finding the equivalent sleeve diameter. Recall

from Chapter 2 that Kohlpaintner approach [12] is equating the radial deformation of the center hole exhibit under any applied pressure to that resulted in the equivalent sleeve under the application of the same pressure, while Chaaban et al [13] is equating the residual contact pressure around the centered hole instead. Since the later approach was utilized in this study to find the equivalent sleeve diameter, contact pressure results of the axisymmetric model came out to be comparable with the results from the multi holes model while those of the radial deformations are not.

5.7 EXPERIMENTAL RESULTS

Experimental results listed in Table 4-7 are utilized to find the residual contact pressure, tube's inner surface radial deformation and the percentage tube wall reduction. Equation (2-8) of Jawad et al [7] is applied to back calculate the residual contact pressure from the measured pull out force. A coefficient of friction of 0.74 is assumed in the calculation. Furthermore, the tube's inner surface radial deformation (U_{ri}) is simply the difference between the tube inner radii after and before rolling ($r_{i,f}$) and (r_i) respectively. The percentage tube wall reduction is then calculated by either equation (5-4) or (5-5). Calculation results are listed in Table 5-10.

The residual contact pressure is plotted with respect to the initial radial clearance in Figure 5-10. Just like the observation noted on the pull out force in Section 4.4, the contact pressure is fluctuating up and down with the initial clearance. Most of the data points are scattered between 2000 and 2500 psi. Generally, the data points seem to be in a

Table 5-10: Experimental Results

Test No.	c (in)	Contact Pressure (psi)	U_{ri} (in)	%WR
1	0.0047	2003	0.0078	3.46%
2	0.0048	2167	0.0075	2.98%
3	0.0052	2192	0.0090	4.25%
4	0.0056	2311	0.0090	3.78%
5	0.0060	2110	0.0094	3.80%
6	0.0063	2466	0.0107	4.89%
7	0.0064	2171	0.0103	4.41%
8	0.0075	2487	0.0099	2.80%
9	0.0078	2361	0.0109	3.49%
10	0.0082	2019	0.0130	5.46%
11	0.0088	2098	0.0125	4.23%
12	0.0101	2453	0.0137	4.06%
13	0.0117	2339	0.0179	6.81%
14	0.0119	2571	0.0162	4.94%
15	0.0120	2693	0.0180	6.88%
16	0.0123	2170	0.0182	6.83%
17	0.0124	1948	0.0176	5.82%
18	0.0132	2534	0.0183	5.87%

horizontal line, which indicate that the clearance is not affecting the contact pressure. This is contradicting the results obtained from the finite element analysis.

The contradiction in the residual contact pressure results obtained from the finite element analysis and those obtained from the experiment can be attributed to a number of reasons. First, a uniform expanding pressure was assumed on the finite element analysis, while

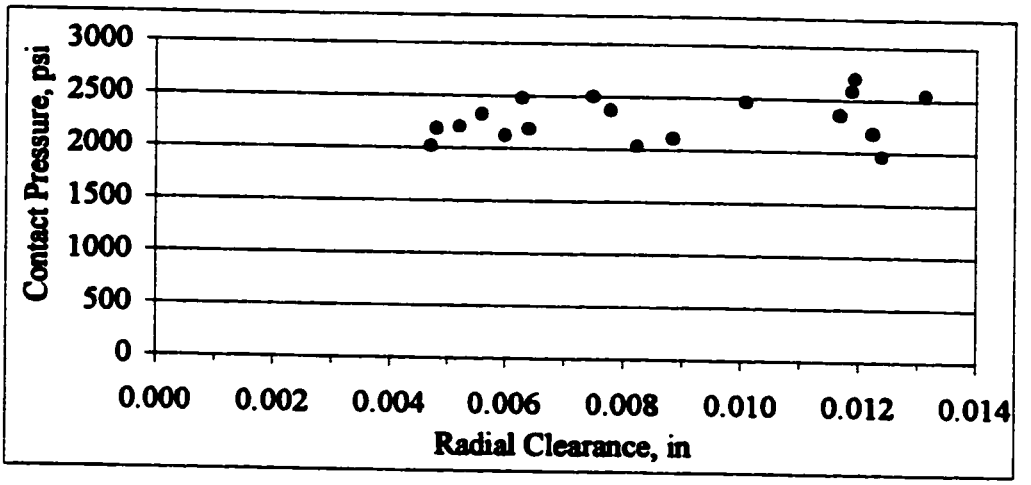

Fig. 5-10: Residual Contact Pressure

rolling expansion is actually executed in making the joints used in the experiment. As stated in Section 4.4, the roller expanded joint strength is not necessarily affected by the radial clearance [26]. Secondly, two grooves were machined on each hole used in the experiment, but the model used in the finite element analysis does not have any groove. As were discussed in Chapter 2, grooves give additional locking mechanism enhancing the joint strength. This is especially true when the joints are made by rolling, since the rollers apply a highly localized force that squeeze the tube wall material into the grooves. This has a big influence on the pull out force rather than the residual contact pressure; and since the residual contact pressure was back calculated from the measured pull out force, grooves effect has influenced the calculated results. In addition, the variations in the surface finish of the tubesheet's holes used in the experiment may contribute to this result.

According to Yokell [6], increasing the roughness of the hole's surface in the roller expanded joints may increase its strength by as much as 35%.

Moreover, the tubes used in the experiment have a low level of tangent modulus. As was shown in Section 3.4, tube's tangent modulus was approximated by 127,000 psi. The finite element analysis results show a minimal effect of initial radial clearance on the residual contact pressure for the cases of low tube's tangent modulus. For the case of 100,000 psi tube's tangent modulus, residual contact pressure falls from 4458 psi to 4056 psi when the clearance was increased from 0.0 in to 0.004 in. On the other hand, the residual contact pressures computed from the finite element analysis are generally higher than those calculated from the experimentally measured pull out forces. This is due to the assumed frictional coefficient. A lower coefficient would yield higher contact pressure. For instance, if the frictional coefficient is assumed to be 0.42, the calculated residual contact pressure will then fluctuate around the value of 4000 psi. This indicates that the average steel-to-steel coefficient of friction could be way below 0.74 that was reported by Jawad et al [7].

The tube's inner surface radial deformation is also plotted against the initial radial clearance in Figure 5-11. The data points seem to fall in a straight line having a positive slope. This means that the radial deformation increases as the clearance increases. The best fitted line through the tube's inner surface radial deformation data points is drawn in Figure 5-11. This line has a slope of 1.315 and, when extending, it intersect the ordinate at

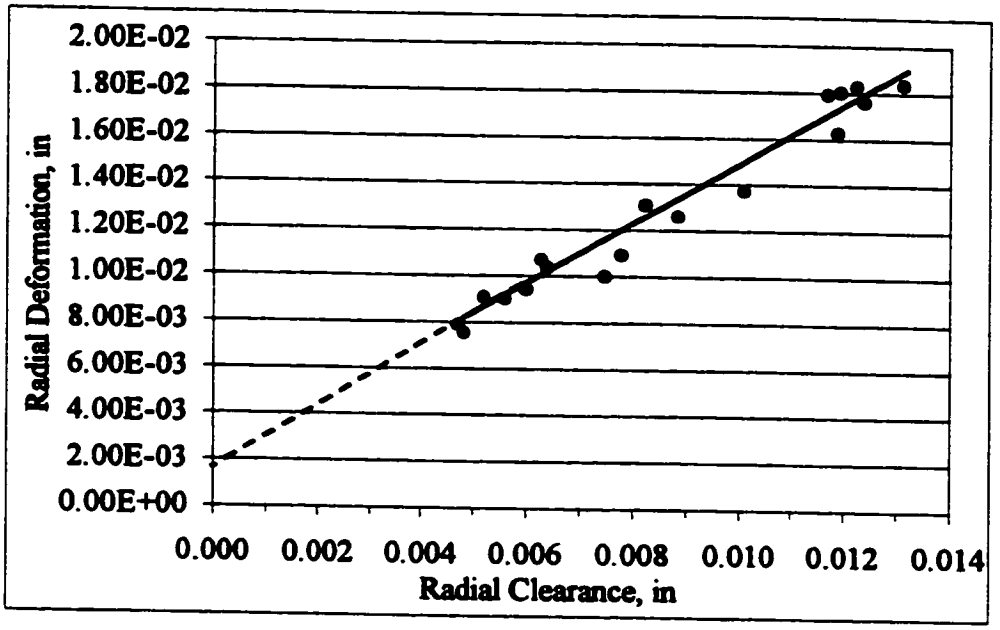

Fig. 5-11: Tube's Inner Surface Radial Deformation

the point 0.0015 in. Consequently, for the specified conditions applied in the experimental parameters, the tube's inner surface radial deformation (U_{ri}) can be estimated by the following equation:

$$U_{ri} = 0.0015 + 1.315c \tag{5-11}$$

The fact that the tube's inner surface radial deformation increases with the initial radial clearance observed in the experimental results agrees with that obtained from the finite element analysis. However, experimentally measured radial deformations are generally more than those calculated by the finite element code. This is because of the different

expansion technique. Roller expansion normally produces more deformation than uniform expansion.

Finally, the percentage tube wall reduction is plotted with respect to the initial radial clearance in Figure 5-12. The data points in this figure are scattered, but they have a general trend of increasing the percentage wall reduction value as the clearance increases. The best fitted line through the data points drawn in Figure 5-12 has a lot of diverging points. So, as was suggested earlier, it would be easier to estimate the tube's inner surface radial deformation first by equation (5-11) and then the percentage tube wall thickness is calculated using either equation (5-4) or (5-5).

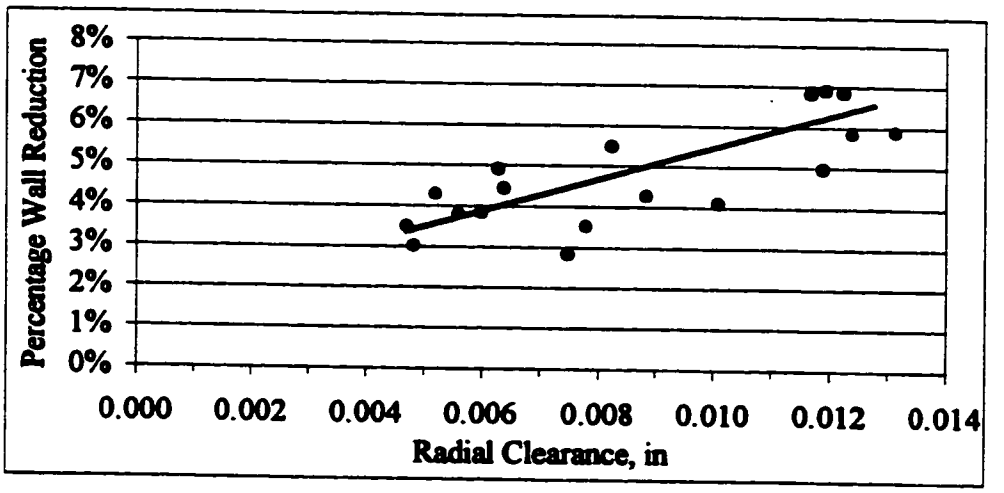

Fig. 5-12: Percentage Tube Wall Reduction

Similar to the note on the tube's inner surface radial deformation results, since both are directly related, the percentage tube wall reduction created from the roller expansion is

generally more than that obtained from the uniform expansion. As explained earlier, tube wall reduction caused by roller expansion is normally between 3 to 12%, whereas uniform pressure expansion causes 1 to 3% wall reduction [2]. This fact is clearly noticed in this study. For example, the first test point listed in Table 5-10 shows a tube's inner surface radial deformation of 0.0078 in. and a wall reduction of 3.46% after rolling the tube into a tubesheet having an initial radial clearance of 0.0047 in. For the same data point, the maximum possible tube's inner surface radial deformation is 0.005726 in. as calculated from equation (5-7) by ignoring the tube's tangent modulus. Using this value into equation (5-5), the maximum tube wall reduction as a result of uniform expansion is found to be 1.15%.

CHAPTER 6

CONCLUSIONS AND RECOMMENDATIONS

6.1 CONCLUSIONS

A test block with nine holes simulating the tubesheet hole design configuration of the stabilizer feed/bottom exchanger was used in the experimental program conducted by the Faculty of the Mechanical Engineering Department in King Fahd University of Petroleum and Minerals to study the effect of initial radial clearance on the expanded tube-to-tubesheet joint strength. For the same purpose, equivalent single-hole planar and axisymmetric models were generated and analyzed using the finite element code (ANSYS). A multi-hole model having the same configuration as the test block used in the experiment was also analyzed by ANSYS to validate the use of the simplified single-hole

models. Based on the results obtained from the finite element analysis, a reduction factor that accounts for the initial radial clearance and tube strain hardening was introduced into the analytical formulations, available in the open literature, for calculating the joint strength, which were neglecting these two parameters. In addition, formulations for estimating the tube's inner and outer surfaces radial deformation, necessary for calculating the tube wall reduction and tube thinning, were developed. The findings may be summarized as follows:

1. The residual contact pressure between the uniformly expanded tube-to-tubesheet joint decreases linearly with the initial radial clearance. As the tube's tangent modulus increases, the contact pressure becomes more sensitive to the clearance.

2. The available closed-form solutions of the residual contact pressure that ignore the initial radial clearance and tube strain hardening can be corrected by introducing a reduction factor accounting for these two parameters. A correlation for calculating the reduction factor was developed from the results of the finite element analyses.

3. The tube's inner and outer surfaces radial deformations at the end of the expansion process increase linearly with the initial radial clearance. The tube's tangent modulus has a minimal effect on the tube's radial deformation. Correlations for estimating the tube surfaces radial deformations for the cases covered in this study were developed. By knowing the tube surfaces radial deformations, tube wall reduction and tube thinning can then be calculated.

4. Tube retraction increases linearly with the initial radial clearance and it is independent on the tube's tangent modulus. The increase in the tube retraction was found to be three times the increase in the radial clearance for the cases covered in this study.

5. The residual contact pressures obtained from the simplified axisymmetric model and those from the original multi-holes model were comparable. Percentage difference between the average results of the models was 11% to 15%. However, due to the method used in calculating the equivalent sleeve radius, the tube's inner and outer surfaces radial deformation results from the axisymmetric and multi-holes models were not comparable.

6. The planar model results of the residual contact pressure and the tube's inner and outer surfaces redial deformations show the same trend of linear relationship with the initial radial clearance as the results of the axisymmetric model. The results obtained from the plane stress analysis were very similar to the axisymmetric results, while those obtained from plane strain analysis were deviating.

7. The pull out force, and thus the residual contact pressure, measured in the experimental program is fluctuating up and down with the initial radial clearance. The joint strength seems to be independent of the clearance in the roller-expanded joints tested during the experimental work. One of the reasons is that two grooves were machined in each hole, which give additional locking mechanism enhancing the joint

resistance to the pull out force. The effect of the clearance may be overshadowed by the locking mechanism and other factors such as the surface roughness.

8. Results of the experimentally measured tube's inner surface radial deformation show that they increase linearly with the clearance. The measured radial deformations, and thus the wall reduction, are generally higher than those calculated by the finite element code. This is expected because of the different expansion technique. Roller expansion normally produces more deformation than the expansion performed by applying uniform pressure.

6.2 RECOMMENDATIONS

Researchers have looked at the expanded tube-to-tubesheet joints from different angles. However, some issues related to this joint have not been addressed adequately. Some of the subjects that need attention in this field of research are as follows:

1. Analytical investigation of the effect of the initial radial clearance and material strain hardening on the expanded tube-to-tubesheet joint strength.

2. Experimental measurements of joint strength of tubes that are roller or uniformly expanded into ungrooved tubesheet holes with different clearances. This could be compared with the results obtained from the finite element analysis performed in this and other published studies.

3. Experimental measurements of the joint strength of tubes that are roller or uniformly expanded into a single-hole tubesheet. Again, this could be compared with the results obtained from the finite element analysis performed in this and other published studies.

4. More work on the simulation of the roller expanded tubes into tubesheet holes using a finite element code.

LIST OF REFERENCES

[1] Standards of the Tubular Exchanger Manufacturer Association 'TEMA', Seventh Edition, 1988

[2] Yokell, S., *'Expanded, and Welded-and-Expanded Tube-to-Tubesheet Joints'*, Journal of Pressure Vessel Technology, Vol. 114, May 1992, pp. 157-165.

[3] ANSYS, Version 5.5, Swanson Analysis System, Inc.

[4] ME2203 Final Report, *Investigation of Heat Exchanger Tube Sheet Hole Enlargement'*, King Fahd University of Petroleum & Minerals, Dhahran, February 2001.

[5] Scott, D. A.; Wolgemuth, G. A.; Aikin, J. A., *'Hydraulically Expanded Tube-to-Tubesheet Joints'*, Transactions of the ASME, Vol. 106, February 1984, pp. 104-109.

[6] Yokell, S., *'Expanded, and Welded-and-Expanded Tube-to-Tubesheet Joints'*, TEMA Technical Committee Meeting, San Francisco, 1991.

[7] Jawad, M. H.; Clarkin, E. J.; Schuessler, R. E., *'Evaluation of Tube-to-Tubesheet Junctions'*, Journal of Pressure Vessel Technology, Vol. 109, February 1987, pp. 19-26.

[8] Kasraie, B; Porowski, J. S.; O'Donnell, W. J.; Selz, A., *'Elastic-Plastic Analysis of Tube Expansion in Tubesheet'*, ASME Paper no. 83, PVP-71, Pressure Vessel and Piping Conference, Portland, 1983.

[9] Goodier, J. N.; Schoessow, G. J., *'The Holding Power and Hydraulic Tightness of Expanded Tube Joints: Analysis of the Stress and Deformation'*, Transactions of the ASME, Vol. 65, July 1943, pp. 489-496.

[10] Allam, M.; Chaaban, A.; Bazergui, A., *'Estimation of Residual Stresses in Hydraulically Expanded Tube-to-Tubesheet Joints'*, Journal of Pressure Vessel Technology, Vol. 120, May 1998, pp. 129-137.

[11] Allam, M.; Bazergui, A.; Chaaban, A., *'The Effect of Tube Strain Hardening Level on the Residual Contact Pressure and Residual Stresses of Hydraulically Expanded Tube-to-Tubesheet Joint'*, PVP-373, Fatigue, Fracture and Residual Stresses, ASME 1998, pp. 447-455.

[12] Kohlpaintner, W. R., *'Calculation of Hydraulically Expanded Tube-to-Tubesheet Joints'*, Journal of Pressure Vessel Technology, Vol. 117, February 1995, pp. 24-30.

[13] Chaaban, A.; Ma, H.; Bazergui, A., *'Tube-Tubesheet Joint: A Proposed Equation for the Equivalent Sleeve Diameter Used in the Single-Tube Model'*, Journal of Pressure Vessel Technology, Vol. 114, February 1992, pp. 19-22.

[14] Porowski, J. S.; O'Donnell, W. J., *'Plastic Strain Concentrations in Ligament'*, Transactions of the ASME, May 1977, pp. 328-336.

[15] Reinhardt, W.; McGregor, R.; Mou, Y., *'Simulation of the Hydraulic Expansion of Steam Generator Tubes in a Tubesheet'*, PVP-385, Computer Technology, ASME 1999, pp. 165-173.

[16] ABAQUS, Version 5.3, Hibbitt, Karlsson & Sorensen, Inc., 1995.

[17] Thiel, F.; Sok, K.; Chabrerie, J., *'Evaluation of the Residual Stress Field in a Steam Generator End Tube After Hydraulic Expansion'*, PVP-280, Fatigue, Flaw Evaluation and Leak-Before-Break Assessments, ASME 1994, pp. 51-56.

[18] SYSTUS Finite Element Code, Version 231.1, Framatome, Tour Fiat, France.

[19] Nadai, A., *'Theory of the Expanding of Boiler and Condenser Tube Joints Through Rolling'*, Transactions of the ASME, Vol. 65, 1943, pp. 865-880.

[20] Saches, G., *'Note on the Tightness of Expanded Joints'*, Journal of Applied Mechanics, 1947, pp. A285-A286.

[21] Krips, H.; Podhorsky, M., *'Hydraulic Expansion – A New Method for the Anchoring of Tubes'*, VGB KRAFTWERKSTECHNIK, No. 7, 1976, pp. 418-426.

[22] Sang, Z. F.; Zhu, Y. Z.; Widera, G. E. O., *'Reliability Factors and Tightness of Tube-to-Tubesheet Joints'*, Journal of Pressure Vessel Technology, Vol. 118, May 1996, pp. 137-141.

[23] Updike, D. P.; Kalnins, A.; Caldwell, S. M., *'Residual Stresses in Transition Zones of Heat Exchanger Tubes'*, Journal of Pressure Vessel Technology, Vol. 114, May 1992, pp. 149-156.

[24] Appendix A, ASME Boiler and Pressure Vessel Code (1986), Section VIII, Division 1, pp. 575-580.

[25] Calladine, C. R., *'Plasticity for Engineers'*, Ellis Horwood Limited, England, 1985.

[26] Fisher, F. F.; Brown, G. J., *'Tube Expanding and Related Subjects'*, Transaction of the ASME, May 1954, pp. 563-575.

APPENDIX A

Example of Subroutine Written For ANSYS

```
/PREP7
ET,1,PLANE82
KEYOPT,1,3,1
UIMP,1,EX, , ,30e6,
UIMP,1,NUXY, , ,0.3,
UIMP,1,MU, , ,0.74,
UIMP,2,EX, , ,30e6,
UIMP,2,NUXY, , ,0.3,
UIMP,2,MU, , ,0.74,
TB,BISO,1, , , ,
TBMODIF,2,1,36000
TBMODIF,3,1,500000
TB,BISO,2, , , ,
TBMODIF,2,1,36000
TBMODIF,3,1,0
RECTNG,0.3755,1.4165,0,2.5,
RECTNG,0.2863,0.3745,0,5,
FLST,2,2,4,ORDE,2
FITEM,2,6
FITEM,2,8
LDIV,P51X,0.5, ,2,0
CM,_Y,AREA
ASEL, , , ,2
CM,_Y1,AREA
CMSEL,S,_Y
CMSEL,S,_Y1
AATT,1, ,1,0
CMSEL,S,_Y
CMDELE,_Y
CMDELE,_Y1
CM,_Y,AREA
ASEL, , , ,1
CM,_Y1,AREA
CMSEL,S,_Y
CMSEL,S,_Y1
AATT,2, ,1,0
CMSEL,S,_Y
CMDELE,_Y
CMDELE,_Y1
SAVE
ESIZE,0.11,0,
MSHAPE,0,2D
MSHKEY,0
FLST,5,2,5,ORDE,2
FITEM,5,1
FITEM,5,-2
CM,_Y,AREA
ASEL, , , ,P51X
CM,_Y1,AREA
CHKMSH,'AREA'
CMSEL,S,_Y
AMESH,_Y1
```

```
CMDEL,_Y
CMDEL,_Y1
CMDEL,_Y2
/UI,MESH,OFF
/COM, CONTACT PAIR CREATION - START
CM,_NODECM,NODE
CM,_ELEMCM,ELEM
CM,_LINECM,LINE
CM,_AREACM,AREA
/GSAV,cwz,gsav,,temp
MP,MU,1,0.74
MAT,1
R,3
REAL,3
ET,2,169
ET,3,172
KEYOPT,3,9,0
LSEL,S,,,4
CM,_TARGET,LINE
TYPE,2
NSLL,S,1
ESLN,S,0
ESURF,ALL
LSEL,S,,,6
CM,_CONTACT,LINE
TYPE,3
NSLL,S,1
ESLN,S,0
ESURF,ALL
ALLSEL
ESEL,ALL
ESEL,S,TYPE,,2
ESEL,A,TYPE,,3
ESEL,R,REAL,,3
/PSYMB,ESYS,1
/PNUM,TYPE,1
/NUM,1
EPLOT
ESEL,ALL
ESEL,S,TYPE,,2
ESEL,A,TYPE,,3
ESEL,R,REAL,,3
CMSEL,A,_NODECM
CMDEL,_NODECM
CMSEL,A,_ELEMCM
CMDEL,_ELEMCM
CMSEL,S,_LINECM
CMDEL,_LINECM
CMSEL,S,_AREACM
CMDEL,_AREACM
/GRES,cwz,gsav
CMDEL,_TARGET
CMDEL,_CONTACT
```

```
/COM, CONTACT PAIR CREATION - END
R,3,0,0,300,0,-1E-6,0,
RMORE,0,0,0,0,0,
LPLOT
FINISH
/SOLU
ANTYPE,0
NLGEOM,1
NROPT,FULL, ,
LUMPM,0
EQSLV, , ,0,
PREC,0
PIVCHECK,0
SSTIF,ON
TOFFST,0,
FLST,2,2,4,ORDE,2
FITEM,2,1
FITEM,2,5
/GO
DL,P51X, ,UY,0
FLST,2,1,4,ORDE,1
FITEM,2,10
/GO
NEQIT,75,
TIME,0
AUTOTS,1
NSUBST,100,10000,1,1
KBC,0
TSRES,ERASE
SAVE
FLST,2,1,4,ORDE,1
FITEM,2,10
/GO
SFL,P51X,PRES,10000,
SOLVE
FINISH
/SOLU
ANTYPE,,REST
FLST,2,1,4,ORDE,1
FITEM,2,10
/GO
SFL,P51X,PRES,10450,
SOLVE
FINISH
/SOLU
ANTYPE,,REST
FLST,2,1,4,ORDE,1
FITEM,2,10
/GO
SFL,P51X,PRES,10500,
SOLVE
FINISH
/SOLU
```

```
ANTYPE,,REST
FLST,2,1,4,ORDE,1
FITEM,2,10
/GO
SFL,P51X,PRES,10530,
SOLVE
FINISH
/SOLU
ANTYPE,,REST
FLST,2,1,4,ORDE,1
FITEM,2,10
/GO
SFL,P51X,PRES,10560,
SOLVE
FINISH
/SOLU
ANTYPE,,REST
FLST,2,1,4,ORDE,1
FITEM,2,10
/GO
SFL,P51X,PRES,10600,
SOLVE
FINISH
/SOLU
ANTYPE,,REST
FLST,2,1,4,ORDE,1
FITEM,2,10
/GO
SFL,P51X,PRES,10700,
SOLVE
FINISH
/SOLU
ANTYPE,,REST
FLST,2,1,4,ORDE,1
FITEM,2,10
/GO
SFL,P51X,PRES,11000,
SOLVE
FINISH
/SOLU
ANTYPE,,REST
FLST,2,1,4,ORDE,1
FITEM,2,10
/GO
SFL,P51X,PRES,12000,
SOLVE
FINISH
/SOLU
ANTYPE,,REST
FLST,2,1,4,ORDE,1
FITEM,2,10
/GO
SFL,P51X,PRES,14000,
```

```
SOLVE
FINISH
/SOLU
ANTYPE,,REST
FLST,2,1,4,ORDE,1
FITEM,2,10
/GO
SFL,P51X,PRES,18000,
SOLVE
FINISH
/SOLU
ANTYPE,,REST
FLST,2,1,4,ORDE,1
FITEM,2,10
/GO
SFL,P51X,PRES,26000,
SOLVE
FINISH
/SOLU
ANTYPE,,REST
FLST,2,1,4,ORDE,1
FITEM,2,10
/GO
SFL,P51X,PRES,36000,
SOLVE
FINISH
/SOLU
ANTYPE,,REST
FLST,2,10,4,ORDE,2
FITEM,2,1
FITEM,2,-10
SFLDELE,P51X,PRES
SOLVE
FINISH
/POST1
*SET,_ZF,1
AVPRIN,0,0,
/EFACE,_ZF
PLNSOL,CONT,PRES,0,1
AVPRIN,0,0,
PRNSOL,CONT,
```